AUTOMOTIVE ENGINE CONTROL: A LINEAR QUADRATIC APPROACH

by

James Brian Lewis

B.M.E., General Motors Institute
(1978)

SUBMITTED IN PARTIAL FULFILLMENT
OF THE REQUIREMENTS FOR THE
DEGREE OF

MASTER OF SCIENCE

at the

MASSACHUSETTS INSTITUTE OF TECHNOLOGY

April 1980

Signature of Author .....
Department of Electrical Engineering
and Computer Science

Certified by .....
Thesis Supervisor

Accepted by .....
Chairman, Departmental Committee
on Graduate Students

AUTOMOTIVE ENGINE CONTROL: A LINEAR QUADRATIC APPROACH

by

James B. Lewis

Submitted to the Department of Electrical Engineering and Computer Science on April 9, 1980 in partial fulfillment of the requirements for the Degree of Master of Science

ABSTRACT

The design of an observer based linear quadratic control algorithm for automotive engine control about a single operating point is considered. Nonlinear numerical simulations are used to compare the transient response of a conventionally controlled engine-vehicle system with this linear quadratic approach.

A linearized 18 state engine model, complete with actuators and sensors, which is to a large extent based upon the physical principles of kinematics and thermodynamics is summarized. An eigenanalysis is included which exhibits the physical controllability and observability properties expected from this engine system while graphically demonstrating the extreme coupling inherent in internal combustion engine models. A decoupled Kalman filtering scheme is used to develop the state estimates required for the linear quadratic controller. A "washout" control algorithm is designed around these state estimates which permits the conventional nominal control algorithm to schedule the steady state engine inputs in a hierarchical fashion. Nonlinear numerical Monte Carlo simulation results are presented which clearly demonstrate the ability of the linear quadratic control approach to improve the transient brake torque and air/fuel ratio engine responses to small step throttle commands.

A singular value robustness of stability analysis is included which reveals "large" singular values, indicative of a robust design, in the 4 - 10 Hz frequency range where the greatest modelling errors are expected. Small low frequency singular values are attributed to an implausible modelling error direction. A brief discussion is included on the intrinsic shortcomings of the singular value theory as it exists today.

Thesis Supervisor: Michael Athans

Title: Professor of Electrical Engineering and Computer Science
Director, Laboratory for Information and Decision Systems

ACKNOWLEDGEMENTS

I would like first to thank Michael Athans for his support, leadership, and guidance as my thesis advisor. His direction, suggestions, and insight during the entire course of this research were fundamental to the successful culmination of this work.

I would also like to thank John Cassidy of the General Motors Research Laboratories for his helpful comments throughout this effort. His influence was instrumental in delineating directions for this research. In addition, Ed Weller, the director, and the entire Electronics Department at the General Motors Research Laboratories deserve special recognition for working with me this past summer and truly introducing me to the engine control field.

Although this thesis represents my own work, and was written by myself exclusively, there are portions where I should elucidate and gratefully acknowledge other individual contributions. In particular I would like to acknowledge the help of John Cassidy, Al Kotwicki, Wolf Kohn, and Man Feng Chang in the model development described in Chapter II. Discussions with Norm Lehtomaki and Ricky Lee contributed to the development of the robustness analysis included in Chapter IV, and Appendix G represents a joint effort by all three of us. The dynamic programming solution to the discrete time tracking problem presented in Appendix E is a joint effort by Wolf Kohn and myself.

This research has also benefitted immeasurably from the countless discussions with my fellow students in room 35-312 here at MIT including Howard Chizeck, Marcel Coderch, Peter Thompson, Ricky Lee, and Eric Helfenbein.

I would be amiss not to personally thank Mr. G.W. Griffith, General Manager, Hydra-matic Division and Mr. R.A. Yutendale, Manager Employee Development, for their unfailing support and encouragement throughout the course of my graduate educational experience.

Finally, I would like to thank the Art Department, General Motors Research Laboratories, for the preparation of the illustrations contained in the main text of this thesis, Fifa Monserrate for her diligent typing of this manuscript, and Barbara Peacock Coady for her personal interest and supervision in the manuscript preparation.

This research was conducted at the Massachusetts Institute of Technology Laboratory for Information and Decision Systems with partial support provided by a research grant from the General Motors Research Laboratories.

James B. Lewis
April 9, 1980

TABLE OF CONTENTS

PAGE

Appendices

LIST OF ILLUSTRATIONS

I. INTRODUCTION

"Any customer can have a car painted any color that he wants so long as it is black." Henry Ford, 1909

1.1 Introduction and Motivation

Automotive engine control had its American beginnings in September of 1893 in Springfield, Massachusetts when Frank Duryea adjusted the carburetor and contacts, started the engine, and became the first American to drive an American built automobile. The car, which he had helped build himself, was appropriately named the Duryea and traveled about one hundred yards on that fateful day. It was powered by a four horsepower one cylinder water cooled engine with make-and-break electric ignition. This original car, predecessor to the US automobile industry can still be seen in the Smithsonian Institution in Washington D.C.

In October of 1908 Henry Ford introduced the now famous Model T Ford. Its 22 horsepower four cylinder gasoline engine was one of the first production engines to incorporate magneto ignition. The throttle was controlled by a hand lever on the steering wheel while fuel metering was accomplished with a rather crude, but effective, carburetor. Spark advance was simple - there was no control (some later cars used a manual spark advance lever). The concept of exhaust gas recirculation (EGR) was not to surface until many years later.

In the four decades since this inception of the American automobile industry the engineering challenges have become no less demanding. Instead of the problems Duryea faced in his one hundred yard run, or Heany's 1908 electric car light difficulties, or the electric starter

problems faced by Kettering on the 1912 Cadillacs, modern day automotive engineers must (among other things) maximize fuel economy and maintain a reasonably responsive car (maintain driveability) while meeting increasingly stringent Federally mandated emission constraints.

There are, of course, many aspects to this difficult and complex problem. Included are: the whole area of weight reduction, catalysis, alternative fuels, and alternate power plants, to name but a few. Yet even a lightweight converter equipped efficient car might be improved, in this fuel economy-driveability-emissions sense, by an appropriate dynamic engine control policy.

This engine control concept, being the focal point of this thesis, bears further explanation. Basically the problem is one of scheduling the engine system inputs in response to the driver's commands such that some cost function, or optimization criterion, is minimized as the desired closed loop system response is obtained. Feedback control is chosen because of its inherent robustness properties. The optimization criterion is, in a heuristic sense, a weighting of the fuel economy and driveability variables to obtain this desired closed loop system response. Thus even a well designed engine-vehicle system might be improved, from this point of view, with an appropriate engine control policy.

A short discussion of the specific problem at hand might prove elucidative. The automotive engine considered in this work is a gasoline powered four cycle V-8 internal combustion engine equipped with a

standard cast iron divided intake manifold, throttle body fuel injection, exhaust gas recirculation, and solid state electronic ignition. This is representable by a dynamical system which maps the four input control functions, throttle position (or inlet air rate control), fuel command, EGR valve pintle position (or inlet EGR rate control), and spark advance into the three pertinent output functions, brake torque, engine speed, and emissions. Even a well designed engine will respond poorly to the driver's acceleration commands if these four inputs are not coordinated in some reasonable fashion.

On most typical production automobiles available today this reasonable input scheduling, or "nominal control" as it is called, is achieved through the use of mechanical contrivances such as carburetors for fuel rate control, direct accelerator cables for throttle positioning, and centrifugal weights and vacuum modules for spark advance and EGR control. For fear of being too simplistic it should be mentioned that these nominal controls are often, by design, temperature dependent and can be fairly complex systems. The modern carburetors are classic examples of the degree of this complexity. Further, considering the job they have to do and the information they have to do it with, they work quite well.

When an industry is spending two billion dollars per mile-per-gallon improvement in the fleet average fuel economy [44], however, no single part of the complete vehicle system can go without scrutiny. These

nominal controls are no exception. Especially since the recent advances in microcomputer technology make possible the realization of moderately complex control policies the question must be asked, "For a fixed engine vehicle system can a different control algorithm improve this fuel economy-driveability-emissions response of the nominally controlled system?"

This question has been the center of much recent research (see references [2]-[12]) in several degrees of complexity. Cassidy in [2] and Athans in [10] present overviews of the problem in a general control context. Dobner in [4] presents a general nonlinear engine model for simulation and control studies. Hazell and Flowers in [6] present a discrete model for four cycle internal combustion engines with spark ignition and a single cylinder. Rubin in [7] develops highly theoretical optimal operating conditions for idealized reversible working fluid finite cycling time heat engines. Cassidy in [11] applies nonlinear programming techniques to obtain static optimal engine calibrations from regression models. Cassidy in [9] again solves this static calibration problem using an on-line optimization algorithm in a test cell environment. Rao et.al. in [8] use static regression engine models to obtain optimal engine control calibrations for the warmed up EPA urban cycle using nonlinear programming techniques.

Dohner in [5] incorporated driveability constraints and used empirical perturbational gradient information to apply the Maximum Principle to the hot and cold start engine calibration problem. Dohner's technique essentially uses the best model available - the engine-vehicle system

itself - to obtain optimal control calibrations at each operating condition encountered in the EPA cycles.

From a completely transient perspective Cassidy in [12] presents a state variable model used by Cassidy et.al. in [3] to apply linear quadratic control theory to the transient optimization problem.

In reviewing this literature it is important to note that one can easily pose this problem in such an extensive framework that even the most elaborate control techniques will fail to produce a solution. Similarly, one can readily impose enough simplifying assumptions that any resulting "simple" solution is hardly applicable to the real engine control problem. The question is quite complex and there is no single correct answer; rather the technique is to make enough simplifying assumptions to reasonably obtain a solution while retaining the significant aspects of the original process.

The approach taken here is to follow up on the original linear quadratic (LQ) work done by Cassidy, Athans, and Lee in [3]. Cassidy et.al. in [3] used the extensive LQ theory to obtain promising transient simulation performance improvements at a 45 mile-per-hour road load operating point. Their study, however, assumed full state feedback, i.e. no state reconstructors were designed. This thesis expands upon their earlier work in that state reconstructors are designed, a different operating point is chosen (30 miles-per-hour road load) and complete nonlinear Monte Carlo simulations are used to obtain similar improvements

in transient performance. Emission response is not considered explicitly in this thesis, however, whereas Cassidy et.al. used regression models to characterize the transient emission performance.

The problem addressed here is not to design a control system to accelerate the vehicle from 0 to 60 miles per hour in record time, but to dynamically coordinate the input variables such that a smooth torque response is obtained (corresponding to an improvement in driveability) and large air/fuel ratio deviations from stoichiometry are eliminated (corresponding to better 3-way catalytic converter efficiency).

It will be assumed that some static optimization, similar to that presented by Dohner in [5], has been run to obtain the optimal static control values and that this "nominal controller," in a hierarchical fashion, schedules these values. Thus, at steady state, the LQ controller should be a "washout" controller in the sense that there is no steady state LQ control action.

The time frames of interest do not include individual cylinder control for this work. Rather the average torque response and average air/fuel ratio response over all eight cylinders are the quantities of interest. This approach is historically what has been taken in the engine control field (there are not eight separate carburetors on normal V-8 engines, and even ported fuel injectors are typically not individually controlled). Cylinder control is a complex and challenging problem in its own right, deserving of a separate treatise, and will not be addressed here.

This LQ controller is also motivated by the inherently coupled nature of this engine system. The EGR valve position, for example, affects engine torque and manifold pressure with a resultant nominal control effect on fuel rate and spark advance. This coupling, visible in all four engine inputs, will be graphically demonstrated in the development of a mathematical engine model in Chapter II. It is just this type of tightly coupled system which renders the classical multivariable control techniques of sequential loop closing or diagonal dominance ineffective, while the linear quadratic controllers can quite naturally handle a dynamically coupled system.

The work done in [3] will be extended here in that full state feedback will not be assumed; state reconstructors will be designed. This results in the so called linear quadratic gaussian (LQG) control scheme. In addition the engine model itself, around which this controller is to be designed, will be extensively based upon physical principles. This has the added advantage of affording much insight into the actual processes of the complete engine system and enhances the controller synthesis.

The general non-linear dynamical engine map will be linearized about a nominal operating point to obtain this linear model required of the LQ controller. In any final implementation multiple linear models may be required covering the entire range of operating points and some multiple model control scheduling scheme may have to be developed. This work focuses on only a single operating point, however, and multiple

models with controller scheduling is left as an area of future research.

The operating point chosen here corresponds to a 48 kph (30 mph) road load point, a typical urban operating point and the one at which the greatest amount of time is spent in the Federal Test Procedure certification runs (see Vora [13]).

The specific objective of this research was, therefore, to design a linear quadratic gaussian controller, capable of test cell implementation, around a single engine-vehicle operating point to improve the dynamic torque and air/fuel ratio response to the driver's throttle commands. The purpose of this thesis is to present the major results of this research.

1.2 Controller Structure

It is only with the introduction of the microprocessor that the concept of implementing elaborate LQG control policies has firmly taken shape. Discrete state reconstructors and feedback gains are easily realized within the numerical capabilities of even simple microcomputer systems. In fact, within the next few years many production automobiles may already have an on-board computer system (used for other functions) which will be capable of implementing these LQG control algorithms.

The central idea is pictured in Figure 1.1. The microcomputer system is being used to control engine inputs in response to the driver's requested throttle command. Notice that this "drive-by-wire" approach (after the aerospace "fly-by-wire" control jargon) is fundamentally different than the nominal controller in that the driver has no direct link to the throttle position in the LQG control system. Recall that

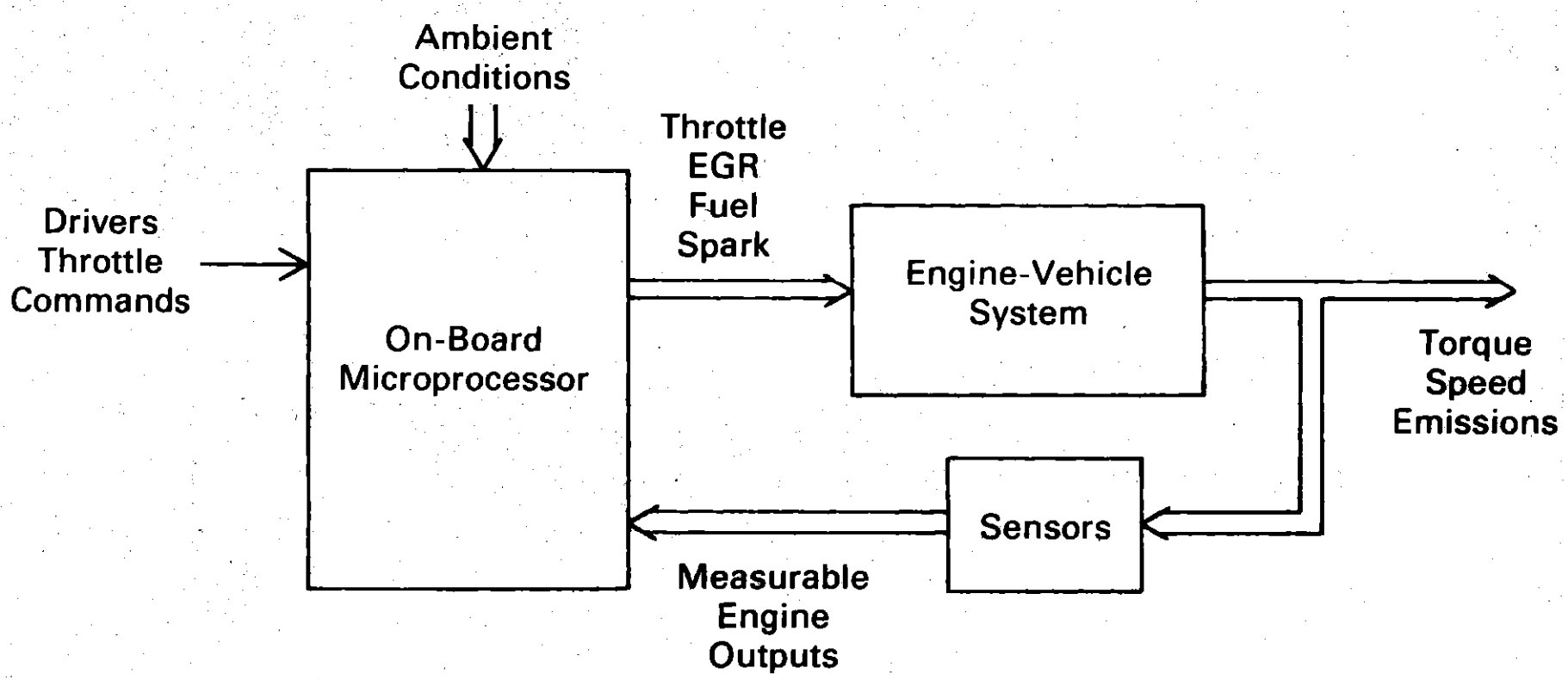

Figure 1.1: Controller Structure Block Diagram

the nominal controller had a direct mechanical cable link to the throttle blades from the accelerator pedal. In this LQG scheme the control system exercises complete control over all four engine inputs and can dynamically coordinate them to achieve the desired transient response.

It should be noted that in practice the hardware used to implement this control would most likely be arranged in some fail-safe type of strategy, such as adding or subtracting control perturbations around nominally controlled mechanical connections so a microprocessor failure would not incapacitate the vehicle or result in a catastrophic system failure. These implementation details are best addressed at a later stage of the research, e.g. after multiple controllers have been tested, and will be omitted in the ensuing discussions.

For the purpose of this work the nominal control scheme is assumed to be implemented in the microprocessor along with the LQG controller. In order to achieve the steady state nominal control values discrete integrators will be appended to the inputs on the LQG controller so that the washout effect is achieved, i.e. no steady state LQG control action (see Stein and Sandell [19]).

As with all microcomputer systems only discrete control algorithms can be implemented. In this research the original continuous time engine-vehicle model will be discretized and a discrete LQG problem will be solved from the start. The discrete sampling rate was selected as 50 Hz in a subjective fachion. This rate must be fast enough to avoid

aliasing on analog to digital conversion and adequately control the engine inputs while permitting enough time to allow for the numerical computations required of the control algorithm. It is straightforward to select a different rate, if desired, for the controller design.

1.3 Thesis Outline

Immediately following this outline will be a brief summary of the major results of this research. Chapter II will present, in moderate detail, the development of the linear model used for the controller design. The physical bases for the model development will be stressed while the tedious numerical details and specific state space realization will be relegated to various appendices. Nominally controlled nonlinear Monte Carlo simulation results are presented which demonstrate a noticeable torque hesitation and large air/fuel ratio deviations from stoichiometry in response to a step throttle command.

Chapter III presents the discrete LQG control algorithm design. The internal controller structure will be specified, the state reconstructors designed, and the feedback gain selected to improve the transient step response performance described in the nominal simulations in Chapter II. Again a complete set of nonlinear simulations is included to demonstrate the improvements due to this LQG dynamic input coordination.

Chapter IV presents a robustness of stability analysis for the previous chapters' model and control design. A singular value approach to robustness is outlined and applied to this specific engine problem

to afford at least some indication of the probable success, in terms of closed loop stability, of this control algorithm. This chapter hedges on the fringes of current research in the field of multivariable system robustness and some indication as to the drawbacks, advantages, and potentials of this singular value approach are included.

Chapter V briefly summarizes the major findings, conclusions, and recommendations of this research. A selected bibliography, acknowledgements, and complete appendices are included at the end of this work.

1.4 Major Contributions of this Research

A brief review of the major results of this research should help focus attention on the important aspects while the reader pours over the necessary but tedious details of the next three chapters.

Basically there are three major points to be made. The first should come as no surprise to the seasoned veterans of the engine control field, it is simply that dynamic engine modelling is a difficult task. The frequency range of the engine system, the nonlinearities, the severe cross coupling, the inherent sampling nature of the four cycle internal combustion engine, and the limited output sensor dynamic capabilities all contribute to make this modelling step a most arduous assignment. The model presented in Chapter II represents the author's "best" tractable dynamic linear approximation to the engine-vehicle system for the purposes of this LQG control project. The nonlinear Monte Carlo simulations are as accurate as practicable, using empirical

relationships for air-fuel-torque curves and matching physical data to the linearized parameters. These simulation results exhibit the type of system response one might expect, on intuitive grounds, from this engine operating under these conditions. This is, to some extent at least, gratifying since the intent of the model was to capture the essential engine system dynamics. Chapter II should not be construed, nor is it presented, as the final answer to the dynamic engine modelling problem. The work presented in this chapter should contribute, if even slightly, to this task while proving adequate for the controller design and evaluation described in this thesis.

The second major result is that the simulations indicate again (see Cassidy, Athans, and Lee [3]) that this LQ dynamic coordination of all four inputs can lead to an improvement in the torque and air/fuel ratio deviation from stoichiometry response to a driver's accelerator commands. This air/fuel ratio improvement should translate into improved tailpipe emissions since the conversion efficiency of the three way catalyst is a strong function of this air/fuel ratio. The torque sag seen in [3] and the torque hesitation seen here can be eliminated by this LQ control scheme. Further, the LQ controller accomplishes the kind of dynamic coordination, in response to the step commands tested, that seems intuitively pleasing upon close examination. The throttle blades are opened in a reasonably slow fashion, the fuel is increased immediately then regulated for maintaining a stoichiometric air/fuel

ratio (approximately 14.6:1), and EGR and spark advance are decreased and increased, respectively, to obtain the desired torque response.

The third major result concerns Chapter IV's robustness analysis. Although the singular values of the LQG system are, at each frequency, equal to or better than the "yardstick" nominal controller this does not lead directly to the conclusion that the LQG controller is as robust as the nominal system. This results from the fact that either controller may be sensitive to a slightly larger, yet more plausible, model perturbation. At least at the high frequencies (4 Hz and above), where the greatest modelling errors are expected, the LQG singular values become large very rapidly, indicating a robust design in the face of high frequency modelling errors.

The two basic pitfalls of a general multivariable singular value robustness analysis were highlighted by this example. They are that;

- small singular values, indicative of a nearly unstable design, can occur in modelling error directions which can be deemed (in an engineering sense) "implausible". When this occurs the singular value analysis does not yield much useful information because modelling errors in different directions, which might be deemed "plausible", and having slightly larger singular values might be destabilizing. The singular value analysis does not quantify this alternate yet plausible directional perturbation.

- results for this analysis are only in terms of the forward path gain, or loop transfer gain, perturbations, i.e. the plant-controller conbination. The item of interest is really destabilizing plant modelling error perturbations exclusive of the hand built and accurate controller. Translating the forward path gain changes resulting from this singular value analysis into a meaningful class of destabilizing plant modelling errors is, in general, a difficult task.

A complete collection of the detailed findings, conclusions, and recommendations of this work is included as Chapter V. Chapter II is now presented which describes the linear model development.

II. MODEL

"If you have $1,000 to spend on a control project spend at least $900 on model development"

an old control adage

2.1 Introduction

The ultimate success of any applications oriented control project hinges, to a great degree, upon the integrity of the underlying mathematical system model. A well developed and sophisticated control algorithm designed around a plant model that poorly reflects reality will often lead to undesirable, and perhaps even dangerous, results. Unfortunately, there are no set rules governing just how accurate this plant model must be to assure project success. A judgement decision must be made in light of the engineering tasks and control objectives at hand.

In a similar vein the type and scope of model chosen will depend upon the specific project objective under consideration. A model that is too detailed and too complex runs the risk of obscuring important phenomena during the control algorithm synthesis. Conversely, an overly simplified model may not capture the essential dynamics associated with the physical processes.

Perhaps no application highlights these inherent tradeoffs better than this engine control example. What is desired is a map, G, which takes the vector of input functions, $\underline{u}$, into the output functions, $\underline{y}$, as demonstrated in Figure 2.1. In state variable form this map becomes,

$$\underline{u} = \begin{bmatrix} \alpha_c \\ E_c \\ F_c \\ S_c \end{bmatrix}$$

α_c Throttle Position Command
E_c EGR Value Position Command
F_c Fuel Command
S_c Spark Command

$$\underline{y} = \begin{bmatrix} T_b \\ N \\ P_m \\ \alpha_p \\ E_p \\ T_f \\ P_f \end{bmatrix}$$

T_b Brake Torque
N Engine Speed
P_m Manifold Pressure
α_p Throttle Position
E_p EGR Position
T_f Filtered Torque
P_f Filtered Manifold Pressure

Figure 2.1: Engine Map

$$\dot{\underline{x}} = f(\underline{x},\underline{u}) \tag{2.1a}$$

$$\underline{y} = g(\underline{x},\underline{u}) \tag{2.1b}$$

$$\underline{u} \in R^m \qquad \underline{x} \in R^n \qquad \underline{y} \in R^p$$

As with all physical processes, and particularly for this engine example, the functions f and g are nonlinear. Further, the inclusion in exacting detail of the engine's distributed phenomena and the time delay associated with the induction process would necessitate the use of an infinite dimensional system. Even if the distributed phenomena are aggregated and the time delay approximated the system dimension can be prohibitively large since there is such a wide variety of events occuring in a broad frequency range. An accurate description of the "instantaneous" manifold pressure in an eight cylinder engine, for example, would require an analysis of the individual effects due to each of the eight intake values in addition to the more global effects of throttle angle and EGR pintle position.

Continuing with this example; an average manifold pressure appears to be a more meaningful quantity than this "instantaneous" pressure since, in keeping with the stated control objectives of Chapter I, individual cylinder control is not an issue here. For this four cycle engine each cylinder inducts a new charge every other engine revolution, indicating that dynamic effects on the order of half engine speed and above can essentially be averaged out in the model derivation. This

effectively imposes an upper frequency limit on events of interest in the map, G,

$$0 \leq \omega \leq \frac{N}{2} \tag{2.2}$$

N - engine speed

ω - frequency of interest

Equation (2.2) is not a hard constraint, rather it represents a guideline to be used when considering which phenomena should be described by G. This in turn imposes restrictions upon the control bandwidth and the required system robustness properties since G is - by design - inaccurate in the half engine speed and above frequency range, an important fact that must not be overlooked in the controller synthesis process.

This map, G, can be even further simplified since the control objectives state that a linear quadratic controller is to be designed. The nonlinear functions, f and g, can be linearized about the nominal operating point, χ, to obtain the perturbational equations,

$\chi = \{x^\circ, u^\circ\}$ the set of nominal conditions

$$\underline{x} = \underline{x}^\circ + \delta\underline{x}$$

$$\underline{u} = \underline{u}^\circ + \delta\underline{u}$$

$$\underline{y} = \underline{y}^\circ + \delta\underline{y}$$

$$f(\underline{x}^\circ, \underline{u}^\circ) \equiv 0$$

$$\underline{y}^\circ = g(\underline{x}^\circ, \underline{u}^\circ)$$

$$\delta\dot{\underline{x}} = \underline{A}\delta\underline{x} + \underline{B}\delta\underline{u} \tag{2.3a}$$

$$\delta \underline{y} = \underline{C}\delta\underline{x} + \underline{D}\delta\underline{u} \tag{2.3b}$$

where

$$\underline{A} \triangleq \left.\frac{\partial \underline{f}}{\partial \underline{x}}\right|_{\chi} \qquad \underline{B} \triangleq \left.\frac{\partial \underline{f}}{\partial \underline{u}}\right|_{\chi}$$

$$\underline{C} \triangleq \left.\frac{\partial \underline{g}}{\partial \underline{x}}\right|_{\chi} \qquad \underline{D} \triangleq \left.\frac{\partial \underline{g}}{\partial \underline{u}}\right|_{\chi}$$

Again, the process of linearization, although a requirement for the development of an LQ controller, introduces even further excursions of the math model from the real engine. How large these errors are depends upon how nonlinear the original system is and upon the size of the perturbations around the nominal operating point. They will be present, however, and a successful control design must be robust with respect to these linearization errors.

In addition to the bandwidth and linearization requirement it can also be important, where possible, to develop a model based upon first principle physical laws. This offers the distinct advantage of affording opportunities for intuition into the control process and its limitations (a collection of force-acceleration data for one mass is not as valuable as a basic understanding of Newton's second law). In addition, the use of physical principles in the model development can save time and expense when a linearized model is desired about

different operating points.

The desired model, therefore, is a linear map, G, accurate for frequencies from dc to half engine speed, based- as much as possible- on physical principles. The complete development of this model is covered in detail by Lewis and Cassidy in [15]. Only an overview of the salient points with sufficient depth to facilitate an understanding of the processes involved and a grasp of the more complicated issues is included here.

The engine separates naturally into six major categories,

1. manifold pressure
2. mass transport
3. brake torque
4. engine speed
5. actuators
6. sensors

each of which will be individually discussed. In addition, the concept of a global nominal controller will be introduced and developed, followed by a brief discussion of the model's eigenstructure and time response. A short summary will conclude this chapter.

2.2 Continuous Time Model Derivation

2.2.1 Manifold Pressure

The manifold pressure dynamics, in the frequency range of interest, are described using an ideal gas law analysis for a constant volume cavity - the intake manifold. Figure 2.2 illustrates the conceptual

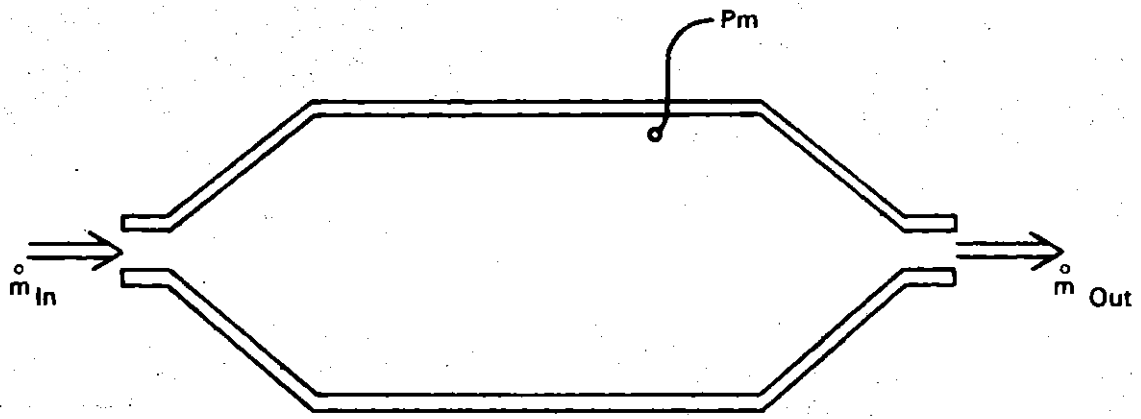

$$\dot{m}_{In} = \dot{m}_{Air} + \dot{m}_{EGR} + \beta\dot{m}_{Fuel}$$

$$\dot{m}_{Out} = \left|\frac{\eta ND}{2}\right| P_m = \left|\frac{\eta ND}{2}\right| \frac{P_m}{RT_m}$$

Figure 2.2: Manifold Pressure Model

process. Air enters the manifold through the throttle body, fuel is injected at the throttle body, and recirculated exhaust gas enters at the EGR value. The inlet air rate is, in general, a flow function of throttle angle, manifold and ambient pressure,

$$\dot{m}_{\substack{air \\ in}} = f_1(\alpha_p, P_m, P_0) \tag{2.4}$$

The fuel rate, due to the nature of the fuel injection logic used, is a function of the fuel command voltage and engine speed,

$$\dot{m}_{fuel} = f_2(F_c, N) \tag{2.5}$$

In a manner entirely analogous to air flow the EGR rate is given by a function of the EGR valve pintle position, manifold and exhaust pressure,

$$\dot{m}_{EGR} = f_3(E_p, P_m, P_e) \tag{2.6}$$

The outlet mass flow rate is defined by the volumetric efficiency as,

$$\dot{m}_{out} = \frac{\eta ND}{2} \frac{P_m}{RT_m} \tag{2.7}$$

where η, the volumetric efficiency, is given by Taylor and Taylor in [43] as,

$$\eta = \eta^* \left[\frac{k-1}{k} + \frac{r - P_e/P_m}{k(r-1)} \right] \tag{2.8}$$

η^* - wide open throttle volumetric efficiency

k - ratio of specific heats

r - compression ratio

D - engine displacement

T_m - manifold gasseous bulk temperature

R - ideal gas constant

Differentiating the ideal gas law for the manifold mixture at constant bulk temperature results in,

$$\dot{P}_m = \frac{RT_m}{V_m}\left[\dot{m}_{in} - \dot{m}_{out}\right] \tag{2.9}$$

V_m = manifold volume

Finally, substituting (2.4)-(2.8) in (2.9) and linearizing about the nominal operating point yields the governing differential equation for perturbed manifold pressure,

$$\begin{aligned}\delta\dot{P}_m = {} & \frac{-\eta^*[(k-1)(r-1) + r - C']ND}{2(r-1)kV_m}\Bigg|_\chi \delta P_m \\ & - \frac{\eta^* D\{[(k-1)(r-1)+r]P_m - P_e\}}{2k(r-1)V_m}\Bigg|_\chi \delta N \\ & + \frac{RT_m}{V_m}\Bigg|_\chi \left[\delta\dot{m}_{air} + \beta\delta\dot{m}_{fuel} + \delta\dot{m}_{EGR}\right]\end{aligned} \tag{2.10}$$

β - fraction of fuel in "ideal gas" form

$$C' - \left.\frac{\partial P_e}{\partial P_m}\right|_{\chi}$$

Actual frequency and time domain experiments have verified the predicted first order behavior, while the experimental pole position and gain values are generally within 10% of those predicted by equation (2.10).

2.2.2 Mass Transport

The air flow transport dynamics are given by the manifold pressure equation (2.10). The mass flow at the cylinders was given by equation (2.7) and represent the sum of the air flow, EGR and fuel flow resulting in,

$$\delta\dot{m}_{\substack{air \\ cylinders}} = \left.\frac{\eta ND}{2RT_m}\right|_{\chi} \delta P_m + \left.\frac{\eta DP_m}{2RT_m}\right|_{\chi} \delta N - \beta\delta\dot{m}_{\substack{fuel \\ cyl}} - \delta\dot{m}_{\substack{EGR \\ cyl}} \qquad (2.11)$$

which is a deterministic equation in the fuel and EGR flows at the cylinders and the manifold pressure.

The fuel and EGR transport dynamics are more complicated. Tanaka and Durbin in [16] present experimental data and a physical analysis of the fuel evaporation to describe the manifold transport dynamics for fuel perturbations. Research is currently in progress to extend their

work to include the convective and diffusive effects of non-liquid fuel transport and EGR. Preliminary experimental data tends to support that presented in [16] as a first approximation, however, and their first order dynamic fuel model will be used. In the Laplace transform variable, s,

$$\delta\dot{m}_{\substack{\text{fuel} \\ \text{cylinders}}}(s) = \frac{\alpha}{s+\alpha}\,\delta\dot{m}_{\substack{\text{fuel} \\ \text{inlet}}}(s) \tag{2.12}$$

where the time constant, $1/\alpha$, in some sense increases with a characteristic manifold length and decreases with liquid fuel film velocity,

$$\frac{1}{\alpha} \simeq \frac{kz_o}{V_f} \tag{2.13}$$

k - constant

z_0 - characteristic manifold length

V_f - fuel velocity (liquid film)

The EGR transport dynamics are complicated by the extreme temperature variation between the recirculated exhaust gas and the bulk manifold flow as well as the pressure resonances between the exhaust and intake manifold cavities. Coupling between perturbations in the high temperature EGR flow and the rate of evaporation of liquid fuel necessitates an even more detailed analysis, research which - at the time of this writing - is currently in progress. For the purposes of

this linear quadratic control design study the empirical data will be used which suggests that these dynamics can best be approximated by a third order linear system.

2.2.3 Brake Torque

The engine torque analysis presented here closely parallels that given by Taylor in [43] and begins with the definition of engine efficiency, η_e,

$$\eta_e = \frac{P_{out}}{P_{in}} \tag{2.14}$$

P_{out} - power out of the engine system

P_{in} - power in to the engine system

Assuming that all energy transfers of interest across the system boundary are associated inward with the fuel flow and outward with the output shaft power then (2.14) can be written as,

$$\eta_e = k \frac{T_b N}{Q \dot{m}_{fuel}} \tag{2.15}$$

Q - higher heating value of the fuel

T_b - engine brake torque

N - engine speed

k - conversion constant

Rearranging (2.15) and absorbing the constant into one term yields,

$$T_b = \frac{k' \eta_e \dot{m}_{fuel}}{N} \tag{2.16}$$

The efficiency variable in this equation is, in general, a function of the dilution factor, manifold pressure, spark advance, and engine speed,

$$\eta_e = f_4(DF, P_m, S, N) \tag{2.17}$$

$$DF \triangleq \left. \frac{\dot{m}_{air} + \dot{m}_{EGR}}{\dot{m}_{fuel}} \right|_{cylinders}$$

Equation (2.16) and (2.17) can be linearized about the operating point to obtain the steady state gains,

$$\delta T_{b_{SS}} = k_{11}\delta\dot{m}_{air} + k_{12}\delta\dot{m}_{EGR} + k_{13}\delta\dot{m}_{fuel} + k_{14}\delta P_m + k_{15}\delta S + k_{16}\delta N \tag{2.18}$$

The variation of steady state brake torque with perturbations in EGR rate, manifold pressure, spark advance, and engine speed is fairly linear at the operating point of interest. In that respect, therefore, (2.18) is a good approximation to reality. Around this stoichiometric point, however, torque is a highly nonlinear function of air and fuel flows, as the experimental data presented in Figure 2.3 illustrates.

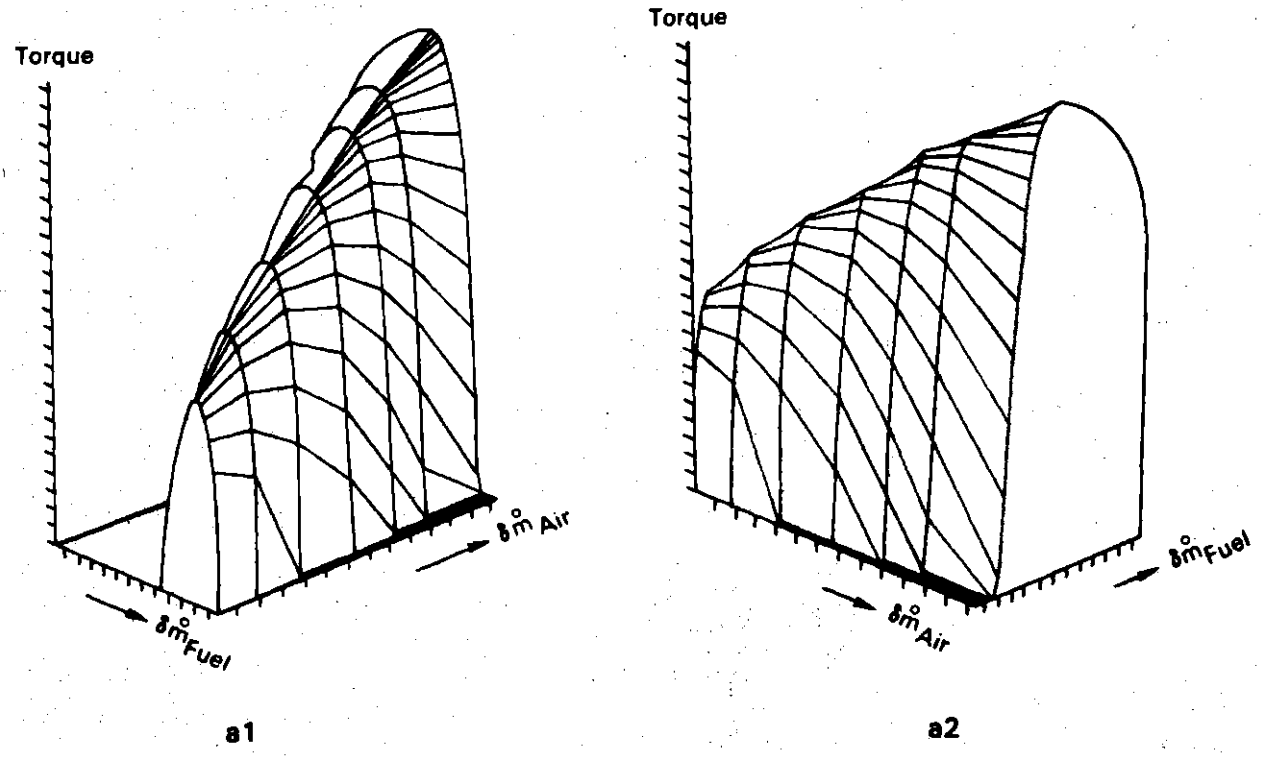

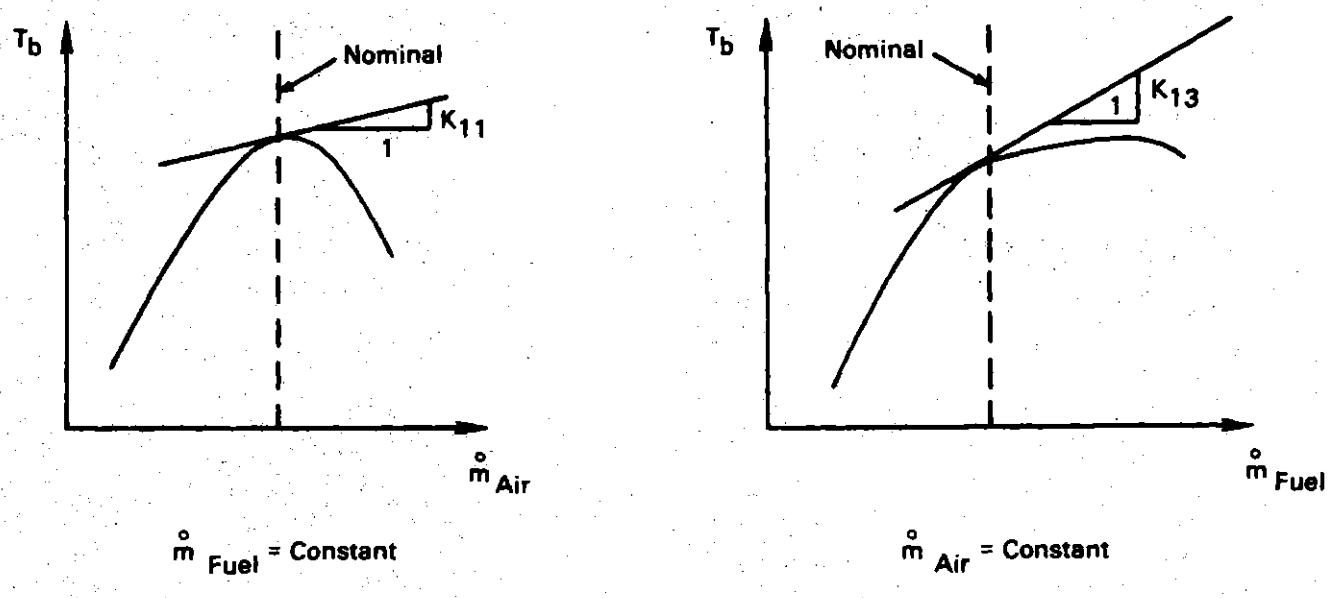

Figure 2.3: Air-Fuel-Torque Curves

For this linear model the curves can be linearized about the nominal operating point to obtain the nominal gains. For simulation studies the actual nonlinear curves must be used to obtain reasonably accurate results. A successful control design must first attempt to maintain the stoichiometric operating conditions (thus preventing large deviations in the values of k_{11} and k_{13}) and second be robust to the remaining persistent air-torque and fuel-torque gain changes.

The dynamics associated with the brake torque equation are due to the inherent sampling nature of a four cycle engine. An instantaneous perturbation in fuel rate at the cylinders, for example, must first be inducted, compressed, and then ignited before any perceptible change in brake torque will occur. This introduces a time delay in equation (2.18) for the air, EGR, fuel, and pressure terms (spark and speed effects on torque are assumed to be instantaneous),

$$\begin{aligned}\delta T_b(t) = {} & k_{11}\delta\dot{m}_{air}(t-\tau) + k_{12}\delta\dot{m}_{EGR}(t-\tau) + k_{13}\delta\dot{m}_{fuel}(t-\tau) \\ & + k_{14}\delta P_m(t-\tau) + k_{15}\delta S(t) + k_{16}\delta N(t)\end{aligned} \tag{2.19}$$

where the limits on the time delay, τ, are

$$\frac{60}{2N} < \tau < \frac{60}{N} \tag{2.20}$$

The lower limit corresponds to a perturbation just at the end of an intake stroke, the upper limit corresponds to perturbations at the

beginning of an intake stroke. Of course, for a multicylinder engine these regions are not sharply defined, and a good approximation to this sampling phenomenon is an averaged time delay,

$$\tau = \frac{3 \cdot 60}{4N} \tag{2.21}$$

2.2.4 Engine Speed

The speed dynamics chosen here are intended to reflect the behavior of an engine in a car equipped with an automatic transmission. The two important physical factors which map the perturbed engine brake torque, δT_b, to a perturbed engine speed, δN, for this case are the reflected vehicle inertia and the torque converter. Kotwicki in [14] presents a physical argument and experimental data to suggest that these factors can be dynamically represented as a second order linear system with one pole representing the vehicle inertia (approximately a 20 second time constant) and a pole-zero combination to handle slippage in the torque converter, in the Laplace transform variable s,

$$\delta N(s) = \frac{k(s+z)}{(s+p_1)(s+p_2)} \delta T_b(s) \tag{2.22}$$

2.2.5 Actuators

The actuators modelled are those typically found in a dynamometer-engine test cell environment. The throttle actuator is assumed to be of the dc motor type and is modelled as a second order linear system.

The EGR actuator is a pulse width modulated vacuum type with a position control loop and is also modelled as a second order linear system. The injector logic for the throttle body fuel injection system schedules the width of fuel pulses (four every engine revolution) with a fuel command voltage. The response of the fuel rate at the injectors to a change in this command voltage is instantaneous (in the frequency range of interest) and no dynamics are assumed here. Similarly, the spark responds instantaneously in this time frame to perturbed spark commands.

2.2.6 Sensors

The brake torque sensor is of the strain gauge type and has a cutoff frequency in the 2 kHz region. In practice this results in a torque signal which reflects each cylinder firing and some filtering must be done to obtain an average torque signal for the half engine speed and below frequency range. In addition, this filtering is required to prevent aliasing of the sampled signal. A third order filter was found acceptable for these purposes.

The engine speed signal is obtained from a tachometer coupled to the output shaft. Its associated electrical poles are assumed to be much higher than the half engine speed of interest and no dynamics are included here.

The manifold pressure transducer is of the semiconductor type and reacts to every opening intake value. Just as in the case of the torque sensor this signal must be filtered and a second order filter model was employed for this purpose.

The throttle angle and EGR pintle position feedback signals are obtained from linear potentiometers and no dynamics are used.

2.2.7 Block Diagram

A block diagram for the engine model, complete with actuators and sensors, is included as Figure 2.4. Numerical values for the constants are included in Appendix B. Appendix A contains the derivation of the state equations used to develop the system matrices, [A,B,C,D] referenced in the remainder of this report. Finally, for completeness, the numerical values for these matrices are presented in Appendix C.

The engine model, using a second order Padé approximant for the engine time delay, is a nine state model. The actuators add four states while the sensors add five for a total system dimension of 18.

2.3 Discrete Time Model

Since the final implementation for a control algorithm of this type is envisioned as a microprocessor based system a discrete time control law will be developed. Two approaches are possible. First,

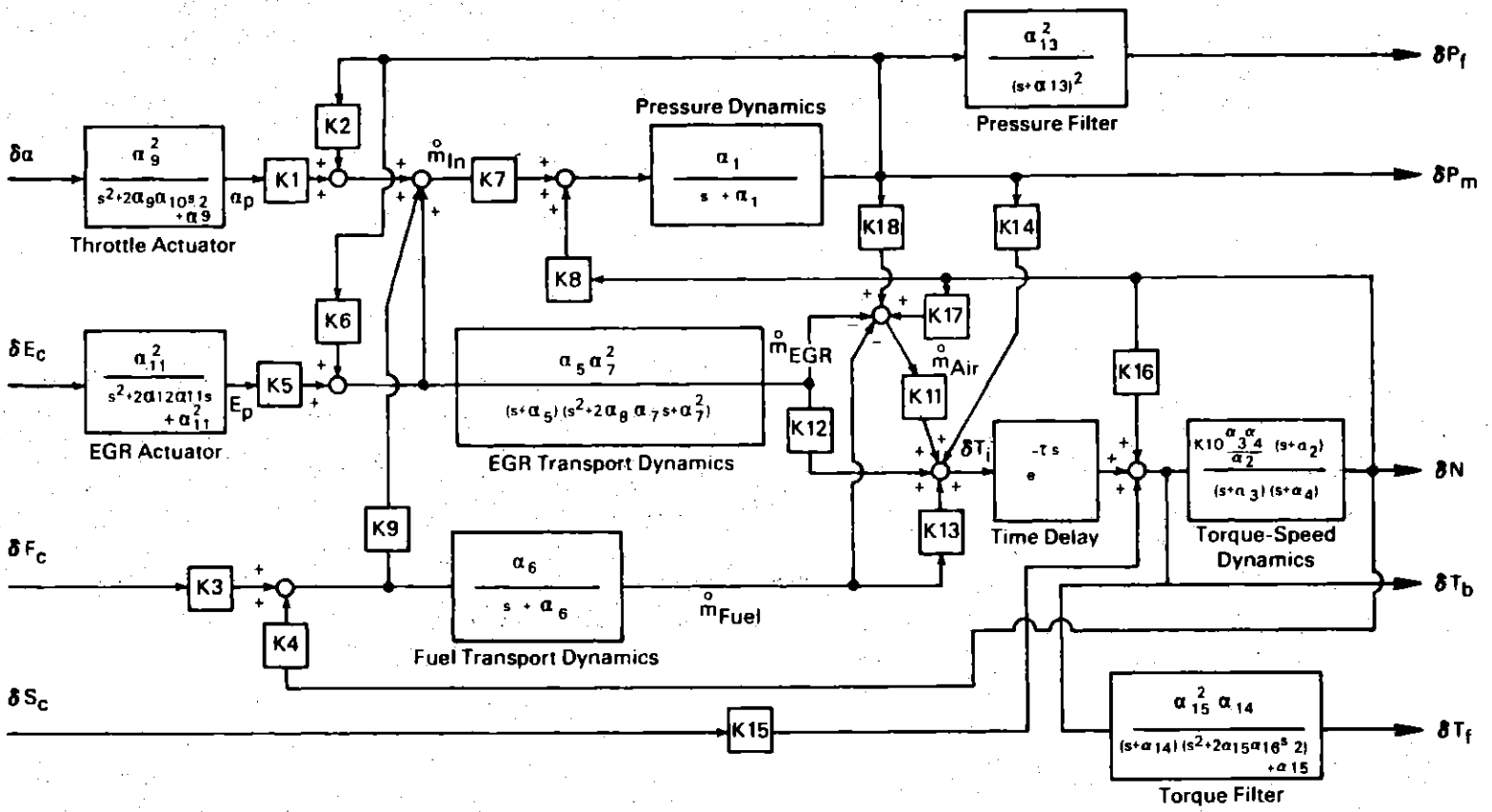

Figure 2.4: A Block Diagram For The Linearized Engine Model

a continuous time control law can be designed, then discretized for implementation. Second, the original continuous time plant model can be discretized and a discrete time controller designed from the start. There appears to be no hard and fast rule governing which is best for any specific application, and the later approach is adopted here.

The discrete model derivation follows. Using a standard procedure for matching the continuous time sampling interval step response to the piecewise constant inputs from a zero order hold digital to analog device the discrete model becomes,

$$\delta\underline{x}(k+1) = \hat{\underline{A}}\delta\underline{x}(k) + \hat{\underline{B}}\delta\underline{u}(k) \tag{2.23a}$$

$$\delta\underline{y}(k) = \underline{C}\delta\underline{x}(k) + \underline{D}\delta\underline{u}(k) \tag{2.23b}$$

where, from the variation of constants formula for this linear time invariant system,

$$\hat{\underline{A}} = e^{\underline{A}\Delta} \; ; \qquad \hat{\underline{B}} = \int_0^{\Delta} e^{\underline{A}(\Delta-\tau)}\underline{B}d\tau$$

Both the continuous and discrete systems will be referenced in the ensuing work and the circumflex (^) distinction for the discrete time dynamic and input matrices will be carried throughout.

2.4 Nominal Controls

Automotive engines in current production include some type of global nominal control law (mechanically implemented in the past, often microprocessor based today) which schedules spark advance and

EGR with engine speed and manifold pressure. In addition, since throttle body fuel injection completely decouples the air and fuel flows, the fuel command must be scheduled with manifold pressure to maintain stoichiometry. Representing these global nominal laws in vector form,

$$\underline{\tilde{u}} = h(y)$$

$$\underline{\tilde{u}} \text{ - nominal control action} \tag{2.24}$$

which can be linearized about the nominal operating point (the functions h are typically piecewise linear so this is a good approximation) to obtain,

$$\delta\underline{\tilde{u}} = \underline{P}\delta\underline{y} \tag{2.25}$$

$$\underline{P} = \begin{bmatrix} 0 & 0 & 0 & 0 & 0 & 0 & 0 \\ 0 & c_1 & 0 & 0 & 0 & 0 & c_2 \\ 0 & 0 & 0 & 0 & 0 & 0 & c_7 \\ 0 & c_3 & 0 & 0 & 0 & 0 & c_4 \end{bmatrix}$$

where the numerical values for c_1 - c_7 are included Appendix B.

Figure 2.5 illustrates this typical nominal control approach as implemented in a microprocessor based system. The driver moves the accelerator which is mechanically linked to the throttle blades. This in turn affects the engine outputs which the nominal controller uses to schedule the perturbed EGR, fuel, and spark commands. In

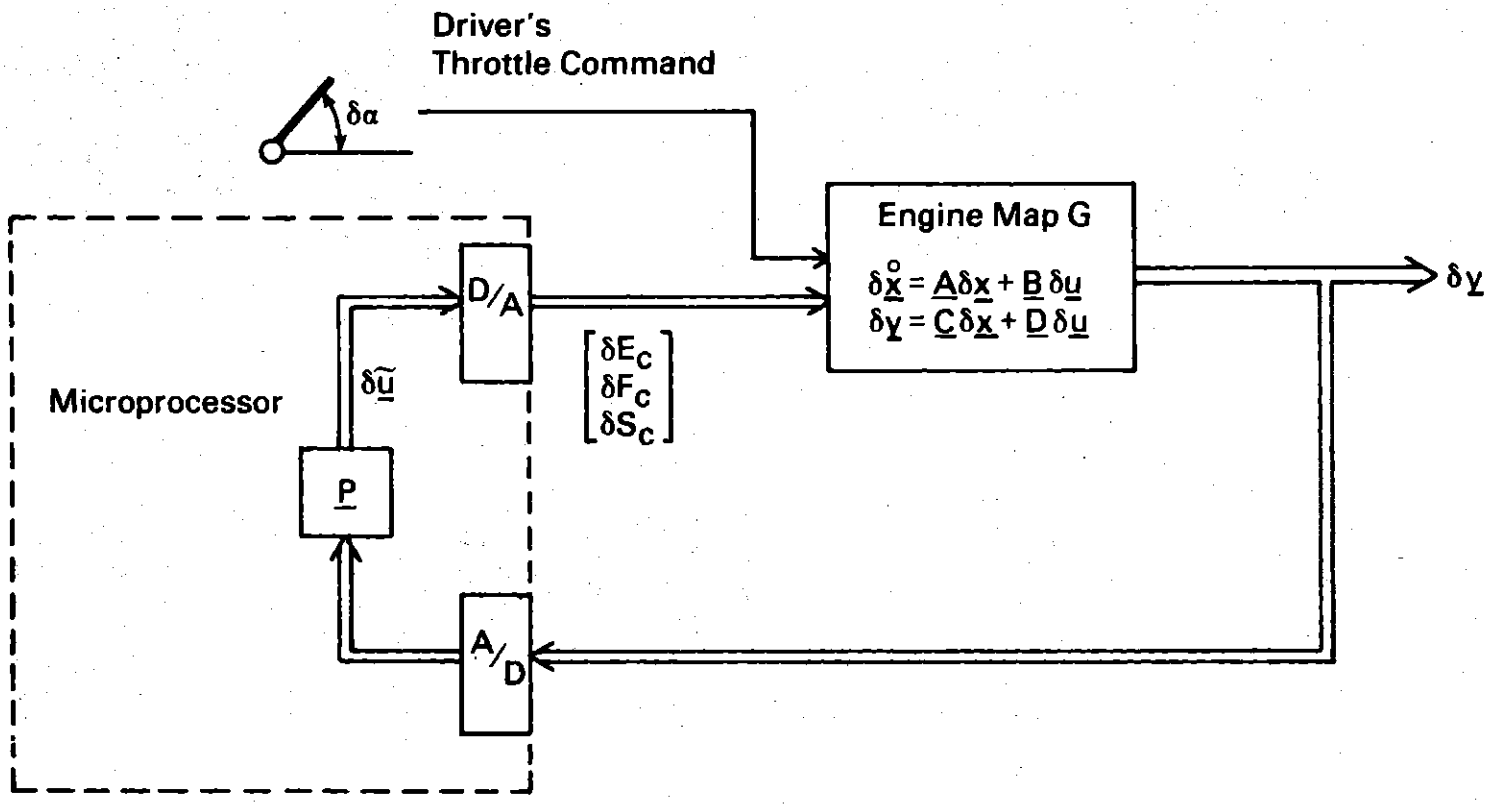

Figure 2.5: Microprocessor Based Nominal Controls

practice other systems, such as a zirconium sensor based air/fuel ratio control, may be present but will not be considered in this work. The nominal controller defined in equation (2.25) and illustrated in Figure 2.5 represents the baseline control scheme against which the LQ design will be compared from both a time response and robustness perspective.

2.5 Eigenstructure

The high system dimension (18 states) in this example precludes all but the most cursory eigenstructure analysis. A polar plot of the eigenvalues for both the original uncontrolled model and the nominally controlled model is included as Figure 2.6 where, for the uncontrolled plant the eigenvalues, λ, are defined by,

$$\underline{A}\,\underline{x} = \lambda\underline{x} \tag{2.26}$$

and, for nominal control,

$$(\underline{A} + \underline{B}\,\underline{P}\,\underline{C})\underline{x} = \lambda\underline{x} \tag{2.27}$$

These eigenvalues range in speed from the slow (20 second time constant) torque-speed pole representing the vehicle inertia to the 14.6 Hz Pade approximant used to represent the engine time delay.

The model is, by design, both completely controllable and completely observable as confirmed by a standard eigenvector analysis

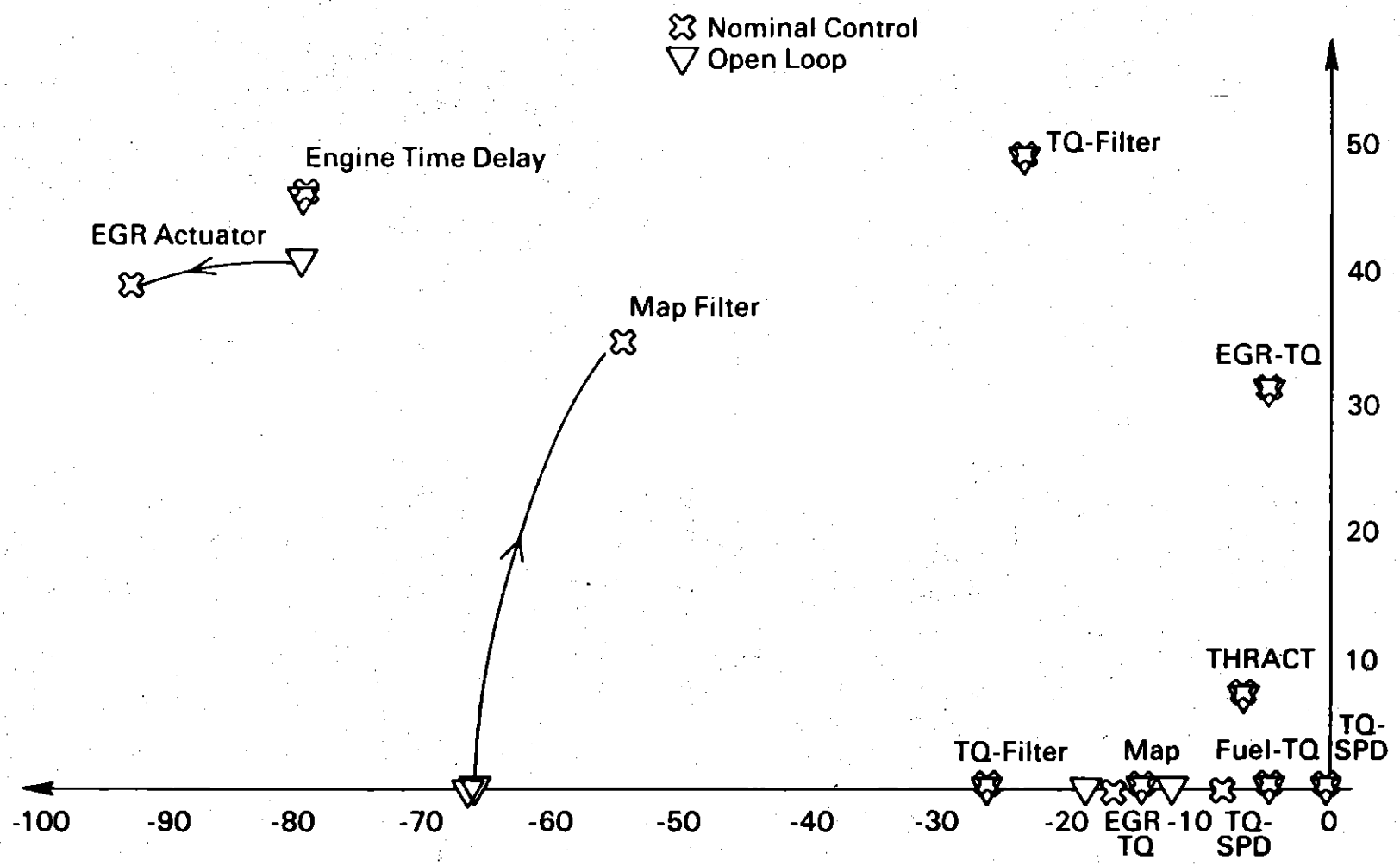

Figure 2.6: Continuous Time Eigenvalues - Nominally Controlled

(see Stein and Sandell [19]). Some interesting system theoretic results for the nominally controlled system are,

- all 18 modes are controllable from the throttle input and (of course) the throttle actuator modes are only controllable from the throttle input.
- The three torque filter modes are observable only in the filtered torque signal. This is not surprising since that signal is the only one not fed back by the nominal controller and not coupled in the block diagram. All 18 modes are observable in the filtered torque signal.
- With the exception of the above mentioned torque filter modes the remaining 15 modes are equally observable in the torque or speed signals.
- The manifold pressure signal may also be used to observe these 15 modes, with the exception of the two modes associated with the engine time delay which are only weakly observable in the pressure signal.

The above statements result from inspection of the controllability and observability matrices defined here as,

$$\text{Controllability Matrix} \triangleq \underline{Y}\ \underline{B} \tag{2.28}$$

$$\text{Observability Matrix} \triangleq \underline{C}\ \underline{X} \tag{2.29}$$

where $\underline{Y}$ and $\underline{X}$ are the suitably normalized left and right eigenvectors given by,

$$\underline{Y}(\underline{A} + \underline{B}\,\underline{P}\,\underline{C}) = \underline{\Lambda}\,\underline{Y} \tag{2.30}$$

$$(\underline{A} + \underline{B}\,\underline{P}\,\underline{C})\underline{X} = \underline{X}\,\underline{\Lambda} \tag{2.31}$$

$$\underline{Y}\,\underline{X} = \underline{I} \tag{2.32}$$

$$\underline{\Lambda} = \text{diag}(\lambda_1, \lambda_2, \ldots, \lambda_{18})$$

Equations (2.28) and (2.29) are subject to scaling, a fact which must be considered when interpreting the results.

2.6 Simulations

Since one of the objectives is to improve the torque and air fuel ratio transient response to step throttle changes it seems appropriate at this time to briefly discuss the computer simulation technique used in this analysis.

Basically the approach has been to discretize the differential equations presented in section 2.2 to propagate the perturbed inputs, throttle, EGR, fuel, and spark commands, into the manifold pressure and the air rate, fuel rate, and EGR rate at the cylinders. The cylinder rates are then used with the nonlinear air-fuel-torque relationships pictured in Figure 2.3 and linearized EGR-torque and manifold

pressure-torque relationships to obtain an indicated torque value. This indicated torque is then delayed by τ seconds and added to the spark-torque and speed-torque values to obtain the combined engine brake torque. Finally, this brake torque value is used with the discretized torque-speed relationship to obtain the engine speed. Actuators and sensors are augmented to the model where appropriate.

The entire one step simulation process is repeated every 0.010 seconds, twice as fast as the expected controller scan time, with brake torque averaging to minimize errors which naturally occur when a looped continuous system is discretized with a break in the forward path (engine speed, for example, is an input to the manifold pressure and fuel rate models used to determine brake torque which is required to calculate the engine speed). The 20 second torque-speed time constant, however, prohibits any major speed changes in these 0.010 second steps, and an examination of the engine speed time response confirms the belief that these errors are indeed negligible.

Figure 2.7 presents the nominally controlled engine response to a 3% step throttle perturbation (from 17% to 20%) corresponding to a speed change from 48 km/hr (30 mph) to 56 km/hr (35 mph), a mild city driving acceleration maneuver.

These time responses are typical of what might be expected from an engine operating under these conditions. There is a characteristic delay (hesitation) prior to any significant increase in brake torque

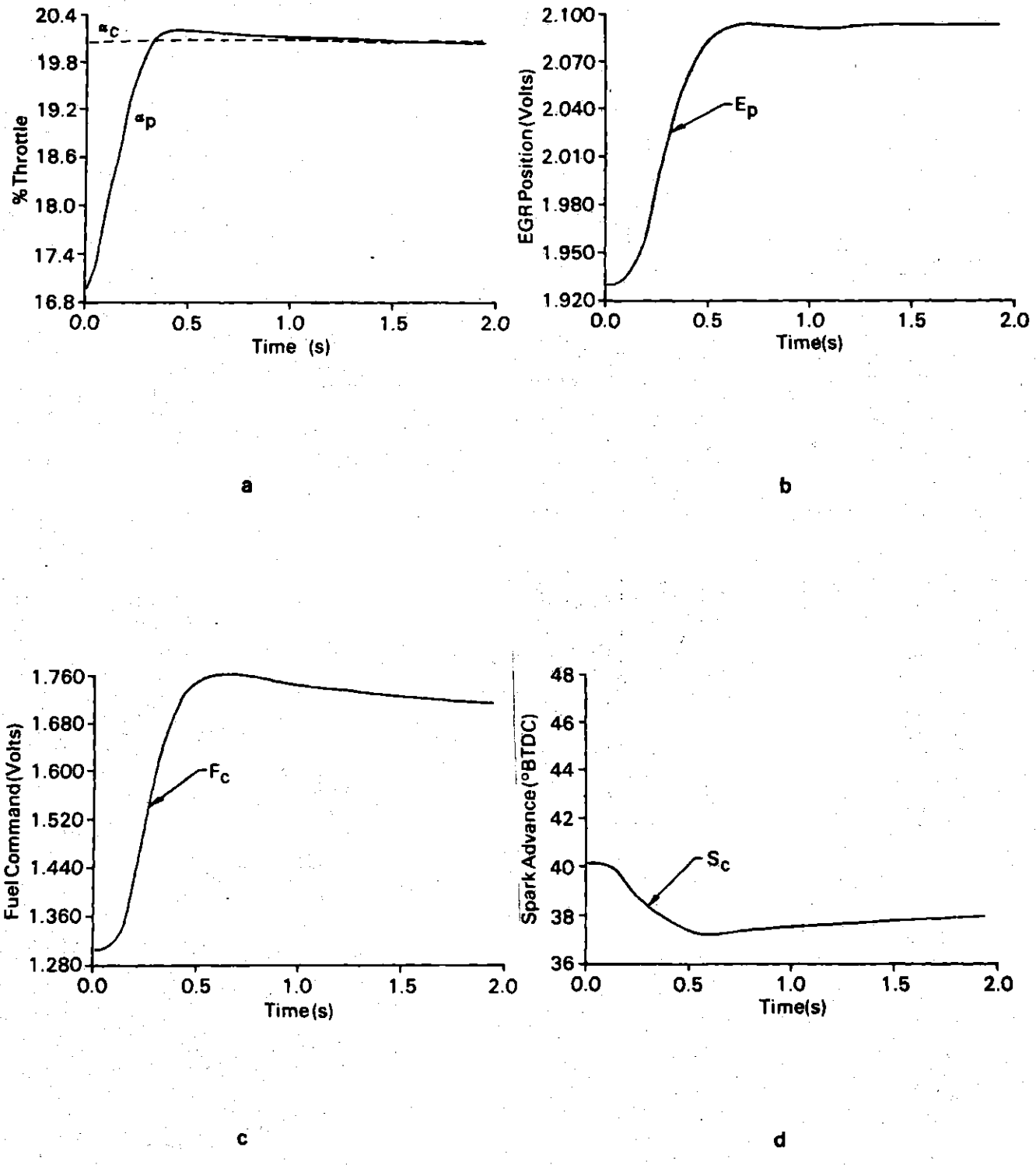

Figure 2.7: Nominally Controlled Time Histories

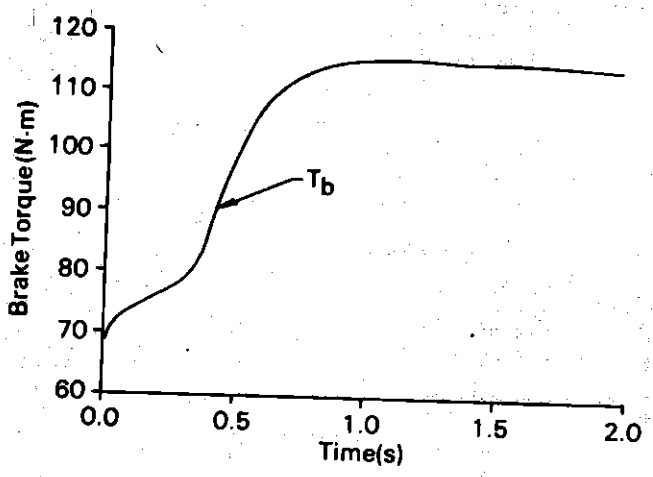
Brake Torque (N·m)
120
110
100
90
80
70
60
T_b
0.0
0.5
1.0
1.5
2.0
Time(s)

e

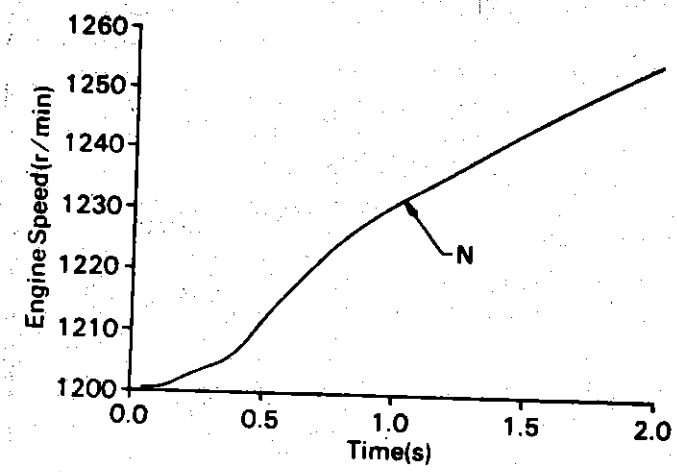
Engine Speed (r/min)
1260
1250
1240
1230
1220
1210
1200
N
0.0
0.5
1.0
1.5
2.0
Time(s)

f

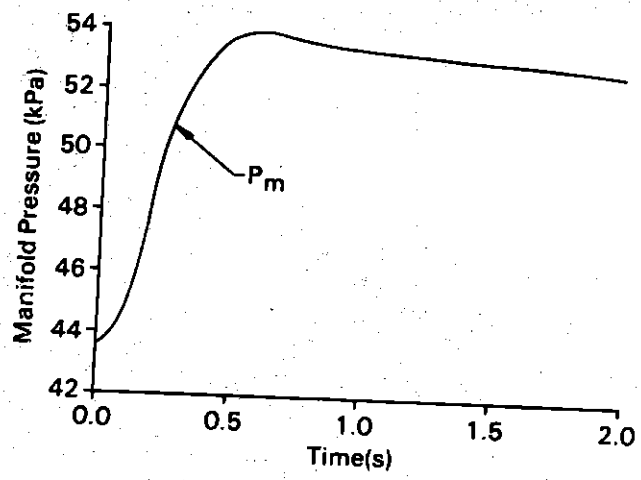
Manifold Pressure (kPa)
54
52
50
48
46
44
42
P_m
0.0
0.5
1.0
1.5
2.0
Time(s)

g

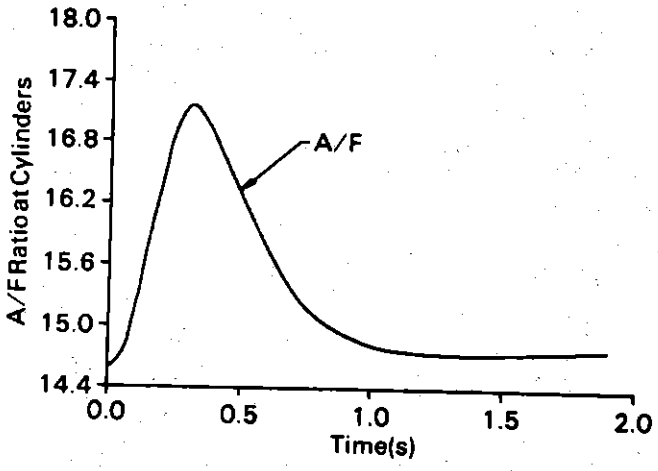
A/F Ratio at Cylinders
18.0
17.4
16.8
16.2
15.6
15.0
14.4
A/F
0.0
0.5
1.0
1.5
2.0
Time(s)

h

due to the lean air fuel ratios resulting from the air surge at the cylinders (the fuel transport dynamics are slower than those of air). In fact, for throttle perturbations larger than 3% a "torque sag" is typically seen.

The nominal controller schedules the EGR valve pintle position, fuel command, and spark advance in response to engine speed and manifold pressure as designed. The cylinder fuel rate lags behind the cylinder air rate, however, because of the slow fuel transport dynamics. This leans the air/fuel ratio out to 17:1 and is a major contributor to the hesitation seen in the transient brake torque response.

Eliminating this torque delay and minimizing the air/fuel ratio deviations will be the principal objectives of the linear quadratic controller to be designed in Chapter III.

2.7 Summary

This chapter first presented a brief motivation for the type of model selected for this research. The upper frequency of interest was limited to half engine speed and the general nonlinear equations were linearized about the chosen operating point, resulting in a linear time invariant model.

Much emphasis was placed on the development of physically based models since this generally tends to increase the intuitive feel

for the process while greatly aiding model development at other operating points. Physical models were described for the manifold pressure, air and fuel transport, brake torque, actuators, and sensors. A reference was cited for the physical development of the torque speed model. The exhaust gas recirculation transport dynamics stand alone as the only totally empirically based part of this engine model and a brief discussion was included on some of the complicating factors.

The continuous time model was discretized and a nominal controller designed to schedule EGR, fuel, and spark advance with engine speed and manifold pressure in response to the driver's external throttle input. A modest analysis of the system eigenvalues as well as the nominally controlled observability and controllability properties was included. Finally, a comprehensive discussion of the simulation technique used to obtain transient responses preceeded Figure 2.7 depicting the system's response to a commanded speed change.

Many sections of this engine model- the manifold pressure, air flow, actuators, and sensors - are judged to be generally accepted in the dynamic engine modelling field for the specified modelling objectives. The transport dynamics and engine time delay, however, are not as generally agreed upon. It is important to understand that the processes are complicated, the required simplifications ill-defined, and the field relatively poorly understood from an engineering outlook. It is hoped that the analysis presented here (and referenced

in [15]) will capture the essential dynamics from this control perspective while, in some small way at least, contributing to the general body of knowledge concerned with dynamic engine modelling.

The main thrust of this work is still, however, the development and evaluation of a linear quadratic controller, as presented in the next two chapters.

III. CONTROLLER DESIGN

"There is no such thing as an optimal design process since it depends very strongly on the specific application, designer experience, and *time available to do the job*" (emphasis added)

Michael Athans, 1971

3.1 Introduction and Motivation

The purpose of this chapter is to present the LQ controller which has been designed to meet the broad objectives outlined in Chapter I. Specifically, this controller is intended to improve the transient torque response and decrease the large air/fuel ratio deviations which were seen in the nominal controller simulation results of Chapter II.

The use of a linear quadratic controller is especially motivated in this application by three desirable properties. First, under some relatively weak controllability and observability conditions, easily satisfied in this engine example, the closed loop system is guaranteed to be exponentially stable. Second, the inherent robustness properties of linear quadratic controllers in the continuous time full state feedback case are well known, see Anderson and Moore [40], Safonov and Athans [27], that is at least a 6db gain reduction margin, an infinite gain margin, and at least $\pm$ 60 degrees phase margin in all channels. Safonov in [24] presents the discrete time robustness results for the full state feedback case. His work shows that the discrete time results approach the continuous time ones as the sampling interval gets smaller.

As a final note on this topic, there are no robustness guarantees for linear quadratic controllers with state estimators (Doyle [25]), though current research has shown (Stein and Doyle [26]) that, for minimum phase plants, one can get arbitrarily close to these robustness guarantees by sacrificing noise performance. In fact, it is entirely possible that the addition of the state reconstructor dynamics might add robustness to the system without sacrificing transient response (see Appendix G). Suffice it to say that this linear quadratic control concept offers a potentially robust solution to this complex engine control problem. In practice robustness properties must be checked for each specific design, a task detailed in Chapter IV of this report for the LQG design presented here.

The third and final motivating property for the LQ approach is its appeal from an implementation perspective. The design and construction of linear time invariant model reference state reconstructors is well understood. Further, these reconstructors are readily realized in microcomputers, as is the feedback gain scheme resulting from the LQ problem formulation.

Thus this linear quadratic control approach with state reconstructors appears to be a viable candidate for the engine control problem about a nominal operating point. The remainder of this chapter will focus on the design of a single controller at a specific

operating point, multiple operating points and controller scheduling is an area of future research.

The controller will be detailed as succinctly as possible while providing sufficient information to allow for a critical review of its major functions. Some general remarks regarding the controller structure will preceed the final state reconstructor, feedback gain, and input shaping filter designs. A presentation of the closed loop nonlinear simulation results will be included, followed by a brief chapter summary.

Essentially this chapter presents the complete design of a dynamic engine controller about a single operating point that is ready for test cell implementation. It represents an extension of Cassidy, Athans, and Lee's work in the sense that state reconstructors have been designed and nonlinear Monte Carlo simulations conducted. Both designs are based on an LQ controller with "washout" integral LQ control action designed around a heirarchical global nominal control law. Both designs give promising simulation results. Chapter V contains the recommendation that the design presented here be implemented in a test cell environment. An outline of the specific control concept for this thesis follows.

3.2 Control Concept

Recall that in the nominal control scheme the driver had direct mechanical control over the throttle position while the nominal

controller scheduled EGR, fuel rate, and spark advance with engine speed and manifold pressure to maintain a quasi steady state optimal operating condition. In this linear quadratic control concept the driver's throttle command is an input to a microprocessor based control system which dynamically schedules all four inputs in order to obtain an improved transient response. In addition, an integral type controller is used to preserve the steady state optimal nominally controlled input values.

This concept is illustrated graphically in Figure 3.1. Command shaping is done on the throttle request input to provide the steady state bias required for integral control. This bias is chosen to preserve the nominal controller's steady state values, i.e.

$$\delta\underline{u}^*_{ss} = \begin{bmatrix} \delta\alpha_r \\ 0 \\ 0 \\ 0 \end{bmatrix} \begin{matrix} \text{LQ throttle command} \\ \text{LQ EGR command} \\ \text{LQ fuel command} \\ \text{LQ speed command} \end{matrix} \tag{3.1}$$

The controller itself is in state feedback form,

$$\delta\underline{u}^* = -\underline{G}\delta\underline{\hat{x}} \tag{3.2}$$

where $\underline{G}$ is chosen to minimize a quadratic cost function subject to linear state dynamics and $\delta\underline{\hat{x}}$ represents the augmented estimated perturbational state vector, an output of the state reconstructor.

The design of each of these three control components will be discussed in the ensuing sections.

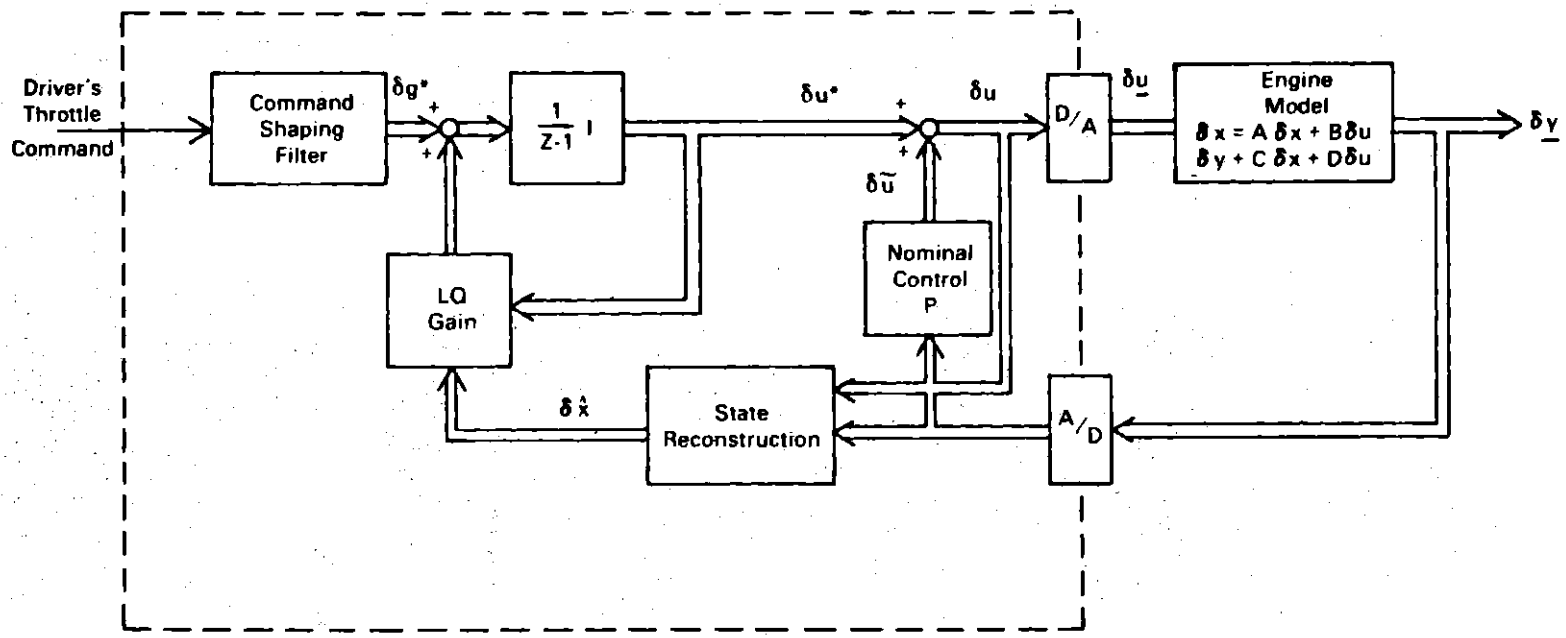

Figure 3.1: LQ Control Concept

3.3 State Reconstructor Design

This section will outline the design of a linear system which maps the five measurable engine outputs into the state estimates required for the LQ controller. The traditional Kalman filtering scheme will first be reviewed, followed by a description of a standard slightly sub-optimal decoupling approach which saves on numerical computations. The numerical details for these decoupled filter designs are included as Appendix D of this report.

3.3.1 Kalman Filtering Algorithm

A Kalman filter provides the minimum mean square error state estimate for a linear system corrupted by white gaussian plant and measurement noise with specific statistics. Let the state equation be given by,

$$\underline{x}(k+1) = \underline{A}\,\underline{x}(k) + \underline{B}\,\underline{u}(k) + \underline{\xi}(k) \tag{3.3a}$$

$$\underline{y}(k) = \underline{C}\,\underline{x}(k) + \underline{\theta}(k) \tag{3.3b}$$

$\underline{x} \in R^n \quad \underline{u} \in R^m \quad \underline{y} \in R^p \quad \underline{\xi} \in R^n \quad \underline{\theta} \in R^p$

$E\{\underline{\xi}(k)\}=\underline{0} \qquad E\{\underline{\xi}(k)\underline{\xi}(\ell)^T\} = \underline{\Xi}\delta(k-\ell)$

$E\{\underline{\theta}(k)\}=\underline{0} \qquad E\{\underline{\theta}(k)\underline{\theta}(\ell)^T = \underline{\Theta}\delta(k-\ell)$

$\underline{\Xi} \geq 0 \qquad \underline{\Theta} > 0 \qquad \delta(\cdot)$ - dirac delta function

$\underline{\xi}(k)$ and $\underline{\theta}(\ell)$ are statistically independent random variables (discrete white noise) for all k and ℓ.

The minimum mean square error optimization criterion now becomes,

$$\hat{\underline{x}}(k) = \min_{\hat{\underline{x}}(k)} \left\{ E[(\underline{x}(k)-\hat{\underline{x}}(k))^T(\underline{x}(k)-\hat{\underline{x}}(k)) \,|\, \underline{y}(k)] \right\} \tag{3.4}$$

The steady state solution to this problem can be written as (see, for example, Astrom [41]),

$$\hat{\underline{x}}(k) = (\underline{A}-\underline{H}\,\underline{C}\,\underline{A})\hat{\underline{x}}(k-1) + (\underline{B}-\underline{H}\,\underline{C}\,\underline{B})\underline{u}(k-1) + \underline{H}\,\underline{y}(k) \tag{3.5}$$

with the initial condition,

$$\hat{\underline{x}}(0) = E\{\underline{x}(0)\}$$

and the filter gain, $\underline{H}$, given by,

$$\underline{H} = \underline{\Sigma}\,\underline{C}^T[\underline{C}\,\underline{\Sigma}\,\underline{C}^T + \underline{\Theta}]^{-1} \tag{3.6}$$

where $\underline{\Sigma}$ is the unique positive definite matrix solution to the algebraic Riccati equation,

$$\underline{\Sigma} = \underline{A}\,\underline{\Sigma}\,\underline{A}^T - \underline{A}\,\underline{\Sigma}\,\underline{C}^T[\underline{C}\,\underline{\Sigma}\,\underline{C}^T + \underline{\Theta}]^{-1}\,\underline{C}\,\underline{\Sigma}\,\underline{A} + \underline{\Xi} \tag{3.7}$$

Equation (3.5) represents a linear system which maps the measurements, $\underline{y}$, and the known inputs, $\underline{u}$, into an optimum state estimate, $\hat{\underline{x}}$. If the actual noise parameters, $\underline{\Xi}$ and $\underline{\Theta}$, are known with certainty then (3.5) is indeed an optimal estimate. In practice $\underline{\Xi}$ and $\underline{\Theta}$ are often used as design parameters to determine the filter eigenstructure

(Stein [30]), the eigenvalues and eigenvectors of ($\underline{A}$-$\underline{H}$ $\underline{C}$ $\underline{A}$). In a strictly heuristic sense, filter poles slower than the closed loop control poles deteriorate system performance, while a fast filter becomes noise sensitive. In each application the designer must choose $\underline{\Xi}$ and $\underline{\Theta}$ to achieve a satisfactory tradeoff between system response and noise sensitivity.

The dimension of the filter described in (3.5) is the dimension of the state, n. This results in the number of multiplications, M, being,

$$M = n^2 + nm + np \tag{3.8}$$

For the discrete engine model (equation (2.23)),

n=18
m=4
p=5

resulting in 486 multiplications (recall that the form of the discretization procedure used almost guarantees dense matrices). A slightly sub-optimal decoupling scheme will now be discussed which can greatly reduce this computational burden.

3.3.2 Decoupling Scheme

The standard decoupling scheme discussed here is applicable where individual components with measurable outputs combine to form a larger system. It will be presented through an illustrative example.

For the engine control problem an important parameter is the perturbed throttle angle, $\delta\alpha_p$. In practice the actual throttle position is determined by a perturbed voltage command, $\delta\alpha_c$, to a dc motor servo system. In state variable form this throttle actuator adds two states to the engine model, necessitating an 18 state Kalman filter in contrast to the 16 required without an actuator model.

Since the actual throttle position is readily measurable the two actuator states can be sub-optimally estimated independent of the 16 state engine model. This is accomplished by a two state Kalman filter with input $\delta\alpha_c$ and measurement $\delta\alpha_p$. The two state filter is sub-optimal only in that knowledge of the engine outputs downstream of the throttle actuator contains some information about the actual throttle states. Knowledge of the perturbed manifold pressure and engine speed, for example, gives some indication of the throttle position, $\delta\alpha_p$; information the 18 state filter uses but the two state filter does not. In practice, however, the throttle position measurement is very good relative to the downstream engine information and the additional accuracy, if any since the downstream information is so "noisy", does not warrant the use of the larger filter.

In a like manner the total engine system can be further decoupled into a total of five individual Kalman filters, as illustrated in Figure 3.2. These filters are for throttle and EGR actuators (2 states

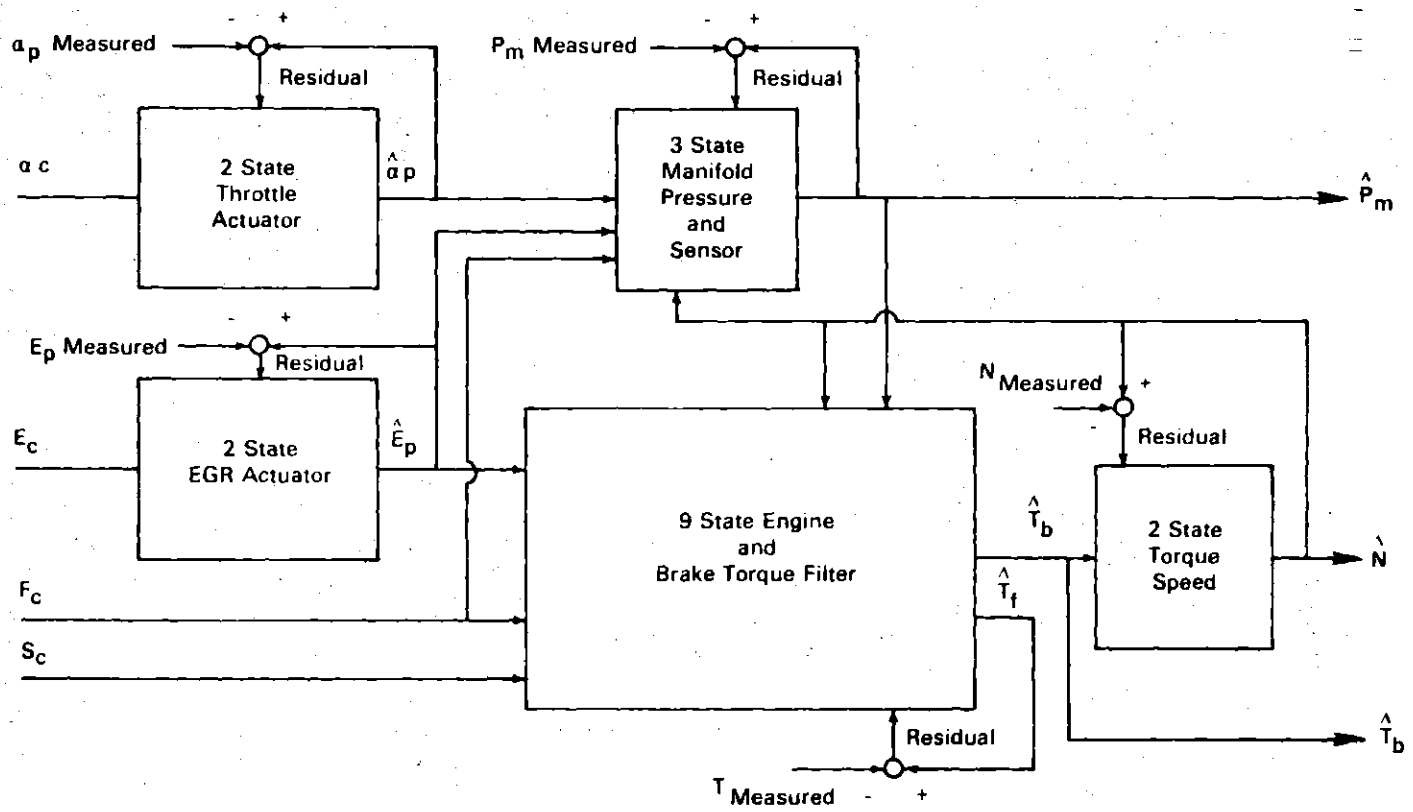

Figure 3.2: Decoupled Filtering Scheme

each), the manifold pressure and sensor dynamics (3 states), the engine brake torque and sensor dynamics (9 states), and the brake torque-engine speed dynamics (2 states).

Summing the results of equation (3.6) for each of these five filters results in a total of 183 multiplications, as contrasted with the 486 required of the full 18 state Kalman filter.

3.3.3 State Reconstructor Summary

The state estimating scheme proposed here uses less than 200 multiplications to estimate all 18 of the engine model states. The algorithm, as summarized in the flow chart of Figure 3.3, consists of five decoupled Kalman filters where the process and measurement noise parameters have been chosen to place the filter poles in the neighborhood of the plant dynamics. The detailed filter designs are included as Appendix D of this report. Figure 3.4 illustrates the closed loop filter poles with the nominally controlled poles shown for comparison.

The most notable computational burden in this filtering scheme is the nine state brake torque and sensor filter. Algorithm simplification attempts will be most fruitful if concentrated on reducing the dimension of this filter - a realistic undertaking since the three state EGR dynamics and the three state torque sensor (see Figure 2.4) might well be reduced.

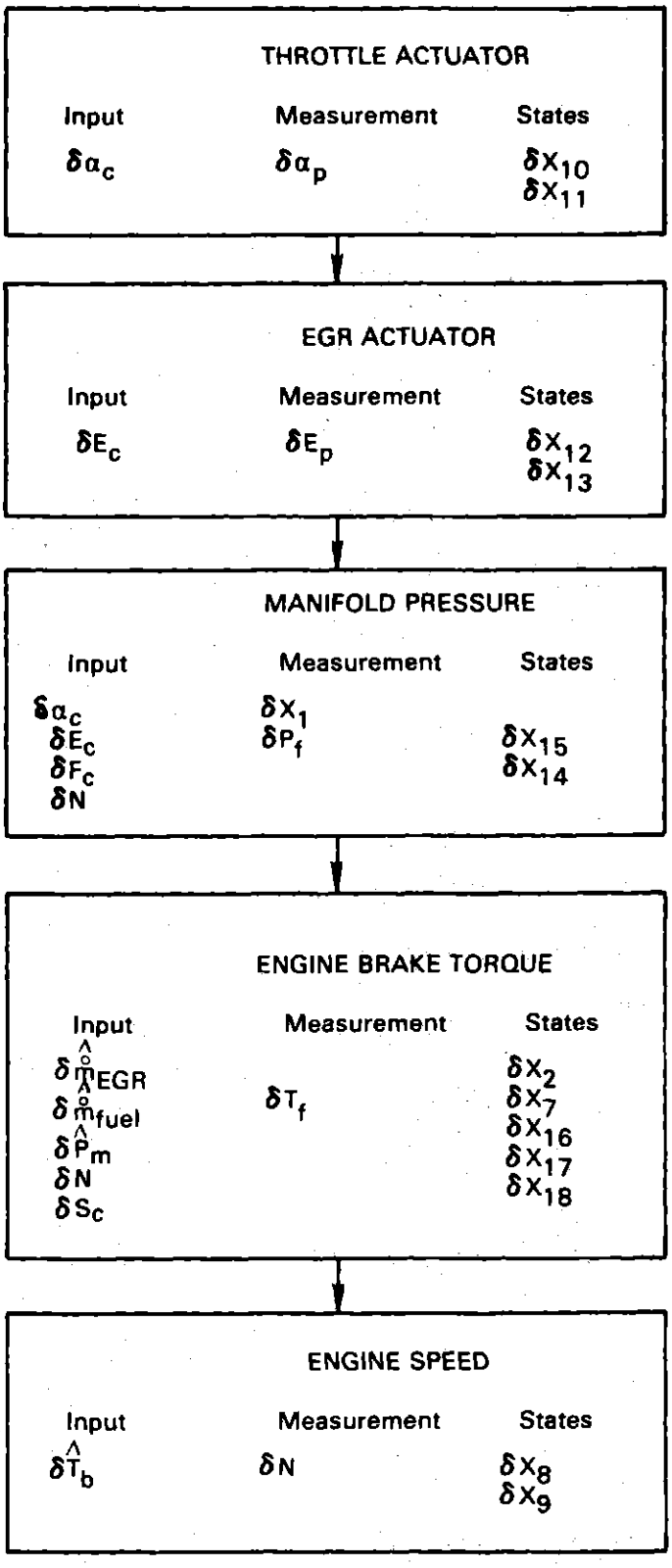

Figure 3.3: State Reconstructor Flow Chart

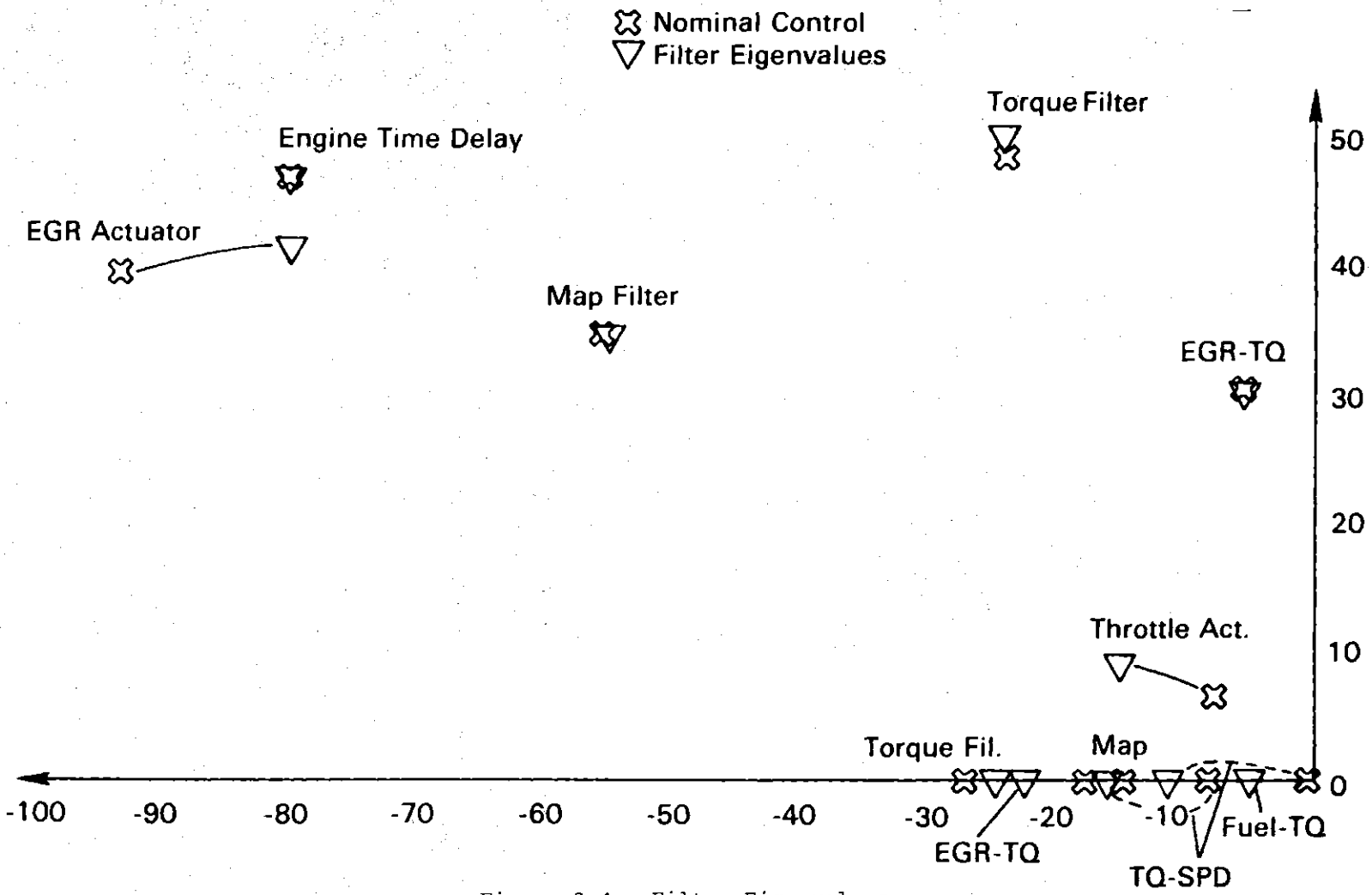

Figure 3.4: Filter Eigenvalues

3.4 Controller Design

The standard steady state discrete linear quadratic control problem can be stated as follows,

$$u = \min_{u} \lim_{L\to\infty} \sum_{k=0}^{L-1} \left[\underline{x}(k)^T \underline{Q}\, \underline{x}(k) + \underline{u}(k)^T \underline{R}\, \underline{u}(k) \right] \tag{3.9}$$

$$\underline{Q} = \underline{Q}^T \geq \underline{0} \qquad \underline{R} = \underline{R}^T > 0$$

subject to the dynamical equation,

$$\underline{x}(k+1) = \underline{A}\, \underline{x}(k) + \underline{B}\, \underline{u}(k) \tag{3.10}$$

where (3.9) represent the minimization of a quadratic cost function subject to the system dynamics in (3.10).

The solution to this optimization problem is the familiar state feedback control law,

$$\underline{u}(k) = -\underline{G}\hat{\underline{x}}(k) \tag{3.11}$$

where $\hat{\underline{x}}(k)$ is the state estimate from the previous section and the feedback gain matrix, G, is given by (see Dorato and Levis [31]),

$$\underline{G} = [\underline{R} + \underline{B}^T \underline{P}\, \underline{B}]^{-1}\, \underline{B}^T \underline{P}\, \underline{A} \tag{3.12}$$

with $\underline{P}$ the unique positive definite matrix solution to the discrete matrix algebraic Riccati equation,

$$\underline{P} = \underline{A}^T \underline{P}\, \underline{A} - \underline{A}^T \underline{P}\, \underline{B}(\underline{R} + \underline{B}^T \underline{P}\, \underline{B})^{-1}\, \underline{B}^T \underline{P}\, \underline{A} + \underline{Q} \tag{3.13}$$

The optimization problem outlined in equation (3.9) must be extended slightly for this application. First the LQ controller is to be designed around the nominally controlled discrete plant model. With the following definitions,

$$\delta\underline{u}(k) = \delta\underline{u}^*(k) + \delta\tilde{\underline{u}}(k)$$

$\delta\underline{u}(k)$ - input to the engine model

$\delta\underline{u}^*(k)$ - LQ control action

$\delta\tilde{\underline{u}}(k)$ - nominal control action

and the discrete plant model (equation (2.23)),

$$\delta\underline{x}(k+1) = \hat{\underline{A}}\delta\underline{x}(k) + \hat{\underline{B}}\delta\underline{u}(k) \tag{3.14a}$$

$$\delta\underline{y}(k) = \underline{C}\delta\underline{x}(k) + \underline{D}\delta\underline{u}(k) \tag{3.14b}$$

and nominal controller (equation (2.25)),

$$\delta\tilde{\underline{u}} = \underline{P}\delta\underline{y} \tag{3.15}$$

the dynamical equations for the LQ design become,

$$\delta\underline{x}(k+1) = (\hat{\underline{A}}+\hat{\underline{B}}\ \underline{P}\ \underline{C})\delta\underline{x}(k) + \hat{\underline{B}}\delta\underline{u}^*(k) \tag{3.16a}$$

$$\delta\underline{y}(k) = (\underline{C}+\underline{D}\ \underline{P}\ \underline{C})\delta\underline{x}(k) + \underline{D}\delta\underline{u}^*(k) \tag{3.16b}$$

noting the following technicality,

$$\underline{P}\ \underline{D} \equiv 0 \tag{3.17}$$

The second extension results from the steady state requirement that the nominal controller do the dc input scheduling (equation (3.1)). This objective is achieved by the introduction of integral control action. Define a differential input, $\delta\underline{v}$, as,

$$\delta\underline{v}(k) = \delta\underline{u}^*(k+1) - \delta\underline{u}^*(k) \tag{3.18}$$

and augment the state vector with $\delta\underline{u}^*$ to obtain,

$$\delta\underline{p}(k) \triangleq \begin{bmatrix} \delta\underline{x}(k) \\ \delta\underline{u}^*(k) \end{bmatrix} \tag{3.19}$$

The dynamical equation, (3.16), now becomes,

$$\delta\underline{p}(k+1) = \begin{bmatrix} \hat{\underline{A}}+\hat{\underline{B}}\,\underline{P}\,\underline{C} & \hat{\underline{B}} \\ \underline{0} & \underline{I} \end{bmatrix} \delta\underline{p}(k) + \begin{bmatrix} \underline{0} \\ \underline{I} \end{bmatrix} \delta\underline{v}(k) \tag{3.20}$$

or, with the following matrix definitions,

$$\tilde{\underline{A}} \triangleq \begin{bmatrix} \underline{A}+\underline{B}\,\underline{P}\,\underline{C} & \underline{B} \\ \underline{0} & \underline{I} \end{bmatrix}$$

$$\tilde{\underline{B}} \triangleq \begin{bmatrix} \underline{0} \\ \underline{I} \end{bmatrix}$$

equation (3.20) becomes,

$$\delta\underline{p}(k+1) = \tilde{\underline{A}}\delta\underline{p}(k) + \tilde{\underline{B}}\delta\underline{v}(k) \tag{3.21}$$

The final step in this integral control problem formulation is to pose the optimization problem as a tracking one, i.e.,

$$\delta v = \min_{\delta v} \left\{ \lim_{L\to\infty} \sum_{k=0}^{L-1} \left[(\delta\underline{p}(k)-\delta\underline{q}(k))^T \tilde{\underline{Q}} (\delta\underline{p}(k)-\delta\underline{q}(k)) + \delta\underline{v}(k)^T \tilde{\underline{R}} \delta\underline{v}(k) \right] \right\} \tag{3.22}$$

where the following definitions have been used,

$$\tilde{\underline{Q}} \triangleq \begin{bmatrix} \underline{Q} & \underline{0} \\ \underline{0} & \underline{R} \end{bmatrix} ; \quad \tilde{\underline{Q}} = \tilde{\underline{Q}}^T \geq 0; \quad \tilde{\underline{R}} = \tilde{\underline{R}}^T > 0$$

$\underline{Q}$ - state weighting matrix

$\underline{R}$ - input weighting matrix

$\tilde{\underline{R}}$ - differential input weighting matrix

and $\underline{q}$ is the state to be tracked.

To satisfy the steady state conditions of equation (3.1), that is no steady state LQ control action, $\underline{q}(k)$ is given by,

$$\underline{q}(k) = \begin{bmatrix} \delta\underline{x}_{ss} \\ \delta\underline{u}^*_{ss} \end{bmatrix} \tag{3.23}$$

where,

$$\delta \underline{u}^*_{ss} = \begin{bmatrix} \delta\alpha_r \\ 0 \\ 0 \\ 0 \end{bmatrix} \tag{3.24}$$

$$\delta \underline{x}_{ss} = (\underline{I} - \hat{\underline{A}} - \hat{\underline{B}}\ \underline{P}\ \underline{C})^{-1}\ \hat{\underline{B}} \delta \underline{u}^*_{ss} \tag{3.25}$$

In Appendix E dynamic programming techniques have been used to verify the solution obtained by Lee et.al. in [32] using a different approach to the optimization of (3.22) subject to the dynamical equation (3.21). Restating that result,

$$\delta \underline{v}(k) = -\underline{G} \delta \underline{p}(k) + \underline{g}(k) \tag{3.26}$$

where G is the discrete LQ gain resulting from the usual optimization problem around the augmented state,

$$\underline{G} = [\tilde{\underline{R}} + \tilde{\underline{B}}^T \underline{P}\ \tilde{\underline{B}}]^{-1}\ \tilde{\underline{B}}^T \underline{P}\ \tilde{\underline{A}} \tag{3.27}$$

with $\underline{P}$ the unique positive definite matrix solution to the augmented discrete matrix algebraic Riccati equation,

$$\underline{P} = \tilde{\underline{A}}^T \underline{P}\ \tilde{\underline{A}} - \tilde{\underline{A}}\ \underline{P}\ \tilde{\underline{B}}(\tilde{\underline{R}} + \tilde{\underline{B}}^T \underline{P}\ \tilde{\underline{B}})^{-1}\ \tilde{\underline{B}}^T \underline{P}\ \tilde{\underline{A}} + \tilde{\underline{Q}} \tag{3.28}$$

and $\underline{g}$ represents the offsetting bias for the integral control tracking problem,

$$\underline{g}(k) = -\underline{G}\underline{q}(k) \tag{3.29}$$

Rewriting (3.26) and separating $\underline{G}$ into the state and control gains with the state reconstructor results from the previous section gives,

$$\left[\underline{G}_x \vdots \underline{G}_u\right] \triangleq \underline{G} \tag{3.30}$$

$$\delta\underline{u}^*(k+1) = (\underline{I}-\underline{G}_u)\delta\underline{u}^*(k) - \underline{G}_x\delta\hat{\underline{x}}(k) - \underline{g}(k) \tag{3.31}$$

$$\underline{g}(k) = -\left[\underline{G}_x \vdots \underline{G}_u\right]\begin{bmatrix}\delta\underline{x}_{ss}\\ \delta\underline{u}^*_{ss}\end{bmatrix} \tag{3.32}$$

From (3.31) and (3.32) with the system dynamics in (3.14) it is clear that a steady state will be reached only when $\delta\underline{u}^*$ satisfies (3.1) and the engine is at the steady state operating condition corresponding to the requested throttle perturbation, $\delta\alpha_r$. This zero steady state step error is typical of this type of control scheme and is directly analogous to the zero error step properties of continuous time washout controllers.

3.5 Shaping Filter Design

The LQ controller is completely specified now in terms of the quadratic weighting matrices $\underline{Q}$, $\underline{R}$, and $\tilde{\underline{R}}$ which uniquely determine the feedback gain matrix, $\underline{G}$. For step changes in the throttle request, however, an undesirable feedthrough condition exists. A step change in this throttle request results in a step change in the offsetting

bias, $\underline{g}$, which is delayed one sample before being presented to the engine as a step input perturbation. In practice this condition can be avoided by the addition of a shaping filter on the offsetting bias, $\underline{g}$. For simplicity uncoupled first order shaping filters were used in this example,

$$\underline{g}^*(k+1) = \underline{\Phi}\,\underline{g}^*(k) + (\underline{I}-\underline{\Phi})\underline{g}(k) \tag{3.33}$$

$$\underline{\Phi} = \text{diag}(\phi_1,\ \phi_2,\ \phi_3,\ \phi_4)$$

$\underline{g}^*$ - filtered offsetting bias signal

Equation (3.31) now becomes,

$$\delta\underline{u}^*(k+1) = (\underline{I}-\underline{G}_u)\delta\underline{u}^*(k) - \underline{G}_x\delta\hat{\underline{x}}(k) - \underline{g}^*(k) \tag{3.34}$$

The complete control structure is presented in Figure 3.5. The perturbed throttle request is first filtered by the input shaping filter before being added to the LQ feedback. That result is then summed with the nominal controls and presented to the digital to analog converter for output to the engine. A block has been included to represent the five decoupled state reconstructors.

3.6 Weighting Matrix Selection

The design problem is now one of choosing the weighting matrices, $\underline{Q}$, $\underline{R}$, and $\tilde{\underline{R}}$, and the shaping filter dynamics, $\underline{\Phi}$, such that the desired

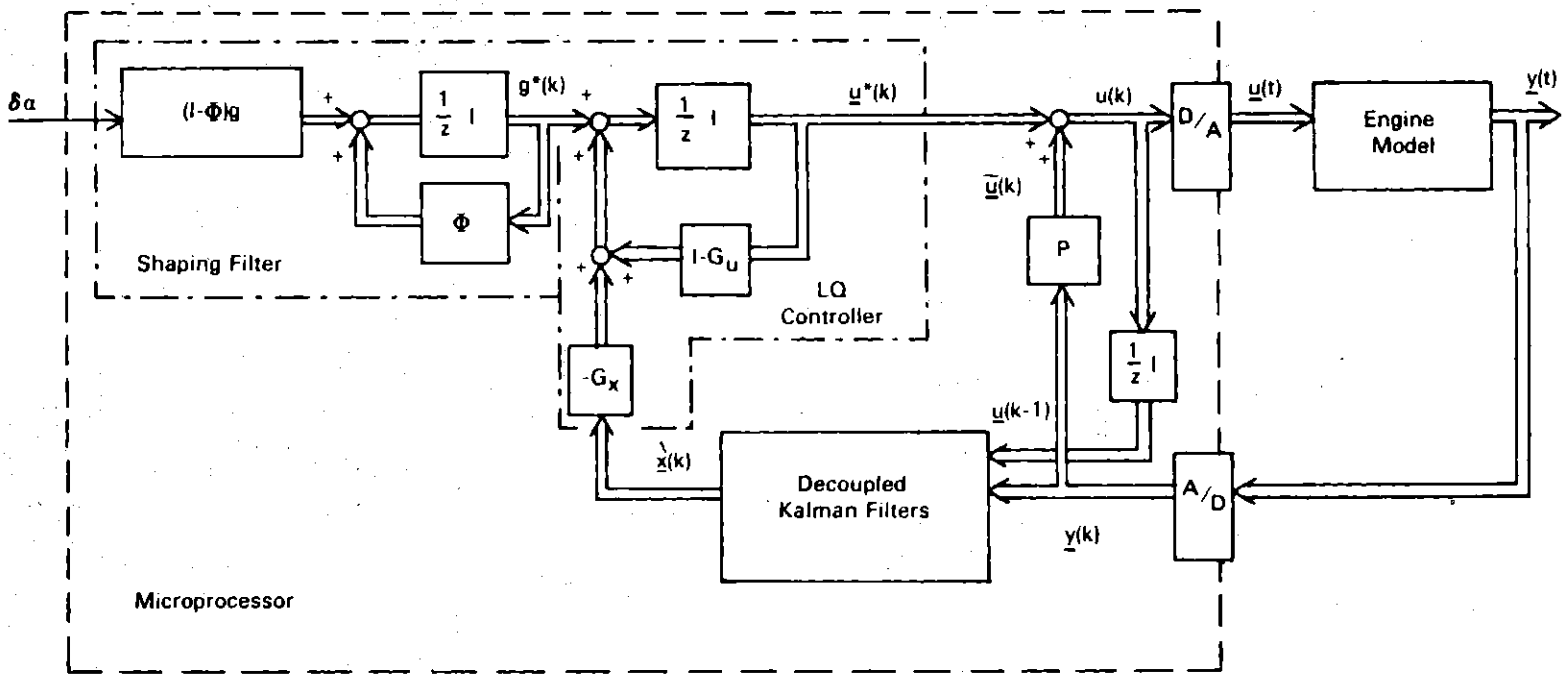

Figure 3.5: Complete Control Strategy

transient behavior is obtained. In practice there is no single correct way of selecting these matrices and a number of techniques are available. If the following identification is made,

$$\delta \underline{z} = \tilde{\underline{C}} \delta \underline{x} \tag{3.35}$$

where $\underline{z}$ represents a vector of pertinent outputs (such as torque, speed, and air/fuel ratio in this example) then a choice of,

$$\underline{Q} = \tilde{\underline{C}}^T \underline{R}_1 \tilde{\underline{C}} \tag{3.36}$$

allows $\underline{R}_1$ to be interpreted as penalizing these pertinent outputs and (3.22) essentially trades off control energy with output response speed. Harvey and Stein in [29] and Stein in [30] present an alternate technique which is based upon approaching a desired closed loop eigenstructure.

The first technique, output weighting, was used in this study to obtain satisfactory transient response to a step throttle change in nonlinear Monte Carlo simulations. The pertinent outputs, $\delta \underline{z}$, were chosen as,

$$\delta \underline{z} = \begin{bmatrix} \delta T_b \\ \delta N \\ \delta P_m \\ \delta \dot{m}_{air} \\ \delta \dot{m}_{fuel} \\ \delta A/F \end{bmatrix} \begin{matrix} \text{brake torque} \\ \text{engine speed} \\ \text{manifold pressure} \\ \text{cylinder air rate} \\ \text{cylinder fuel rate} \\ \text{cylinder air/fuel ratio} \end{matrix} \tag{3.37}$$

with final values for the weighting matrices,

$$\underline{R}_1 = \text{diag}(0.015,\ 0.0075,\ 10.0,\ 1.0,\ 1.0,\ 50.0) \tag{3.38a}$$

$$\underline{R} = \text{diag}(5.0,\ 8000.0,\ 5000.0,\ 1.0) \tag{3.38b}$$

$$\tilde{\underline{R}} = \text{diag}(0.1,\ 0.01,\ 0.002,\ 0.075)\rho \tag{3.38c}$$

and the input shaping filter,

$$\underline{\Phi} = \text{diag}(0.80,\ 0.75,\ 0.0,\ 0.0) \tag{3.39}$$

A plot of the closed loop eigenvalues, the eigenvalues of $(\tilde{\underline{A}}-\tilde{\underline{B}}\ \underline{G})$, as a function of the control matrix scaling factor, ρ, is included as Figure 3.6. The only three plant eigenvalues that move appreciably are the two complex poles associated with the throttle actuator and the torque speed pole associated with the torque converter. The four integrators associated with the integral control all move outward along the negative real axis. A value of ρ=1.0 (see equation 3.38c) was selected for the final LQ design.

3.7 Simulation Results

Nonlinear Monte Carlo simulations were run with the shaping filter, LQ feedback gains, decoupled state reconstructors, and nominal controller all in the control loop. These simulations were extensions of the nominal control simulations conducted in Chapter 2. Colored

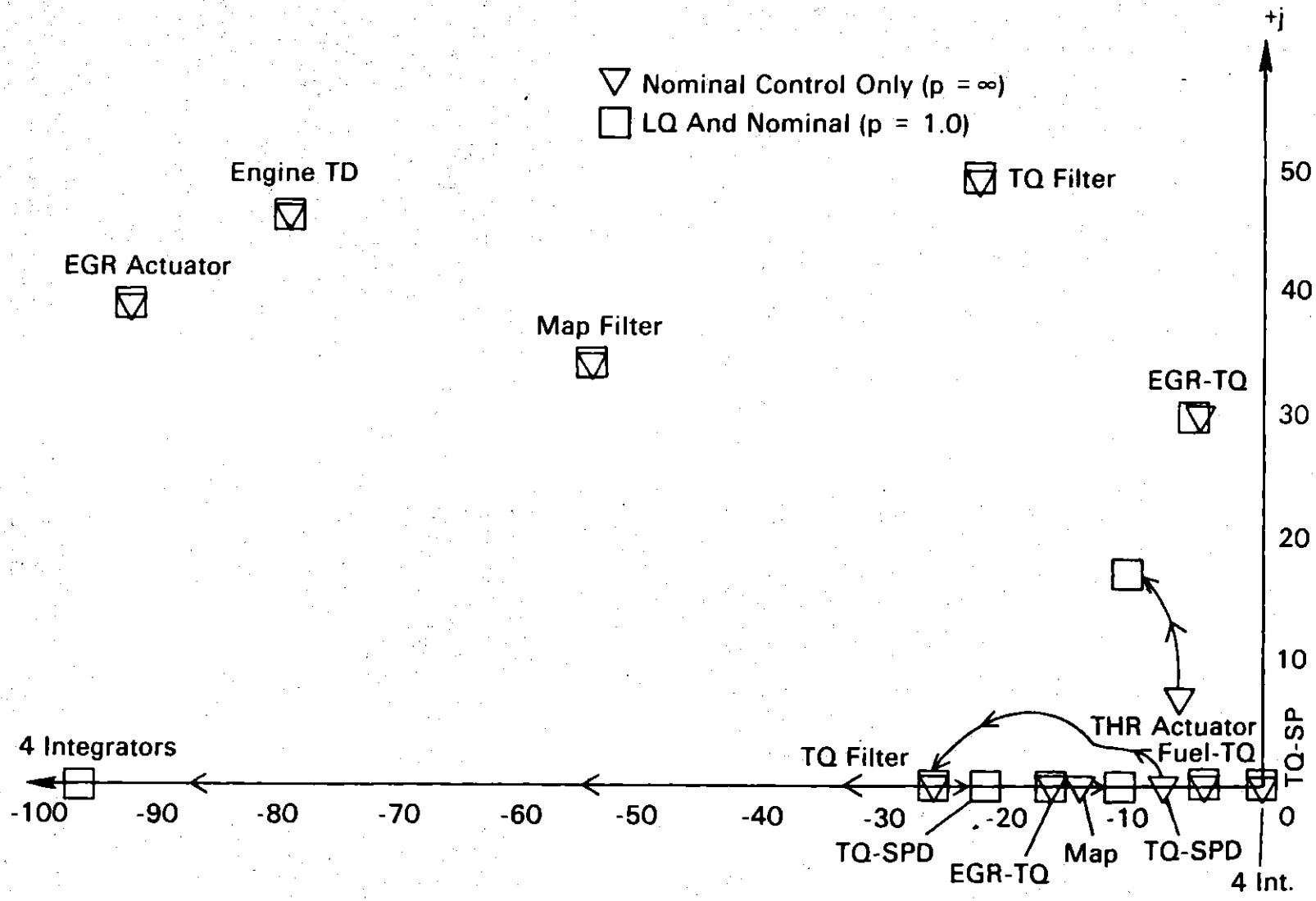

Figure 3.6: Continuous Eigenvalues - LQ Controlled

noise was added to the brake torque and manifold pressure signals to match observed engine measurements. For comparison purposes both the nominal response and the LQ controlled responses are shown in Figure 3.7. All results are for the 17% to 20% step throttle change discussed in Chapter 2, i.e. the 30 to 35 mph acceleration maneuver.

The torque increase is rapid and smooth, predominantly due to the LQ controller's increase in spark advance and coordination of the EGR command and throttle opening with engine speed. The air/fuel ratio deviation is significantly improved by the LQ controller over the nominally controlled response. This is achieved by scheduling a sharp increase in the initial fuel rate while simultaneously scheduling throttle position to maintain dynamic stoichiometry at the cylinders.

For even this relatively small throttle command these LQ results are promising. They essentially indicate that dynamic scheduling of the four inputs can improve the torque response while doing a better job of maintaining stoichiometric operating conditions. Preserving the stoichiometric operating point has the added benefit of improving the accuracy of the linear model since the air-torque and fuel-torque gains are strong function of air/fuel ratio (see Figure 2.3).

3.8 Summary

This chapter first presented the motivation behind the choice of a linear quadratic controller for this engine control problem.

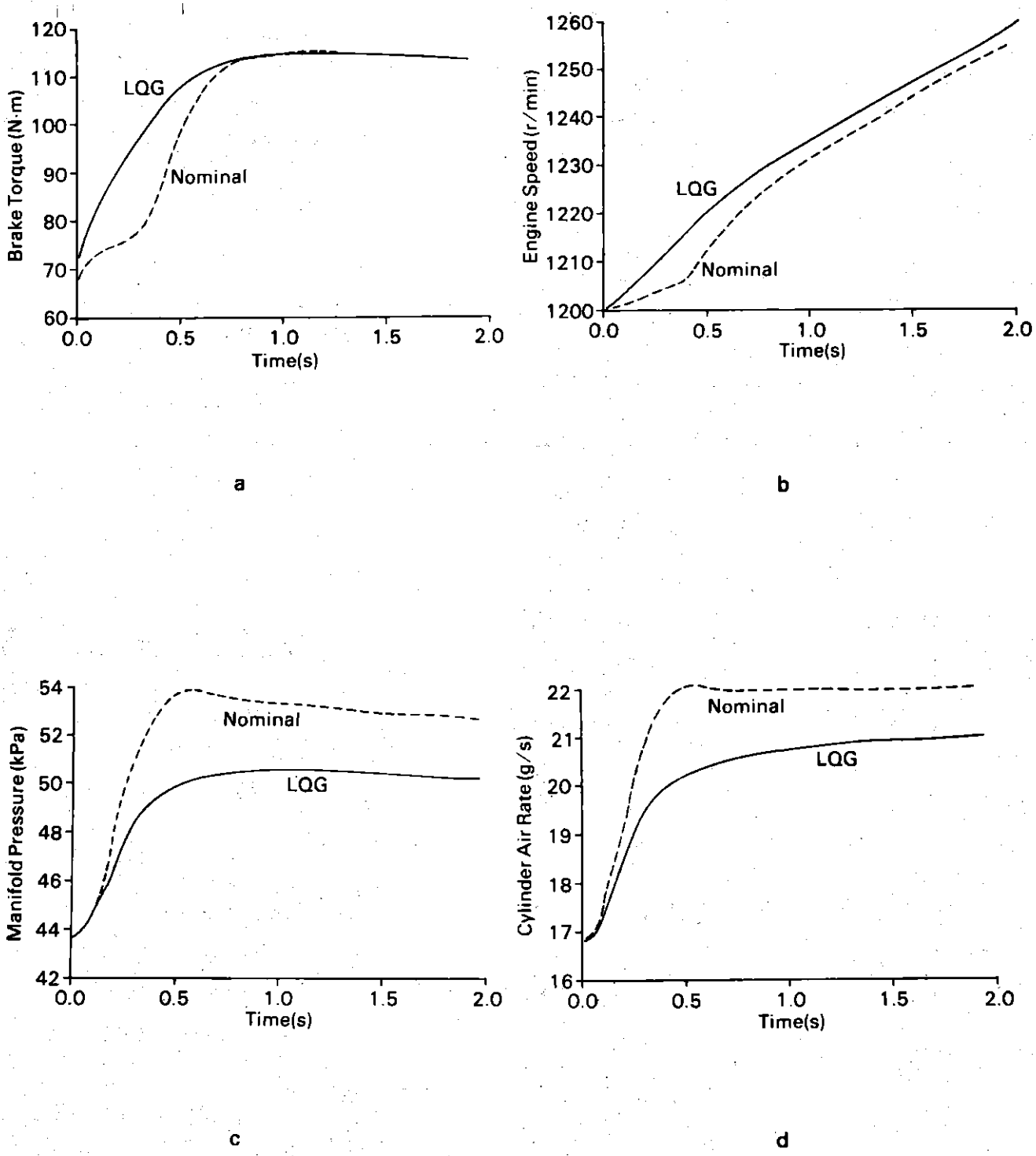

Figure 3.7: LQG Controlled Time Histories

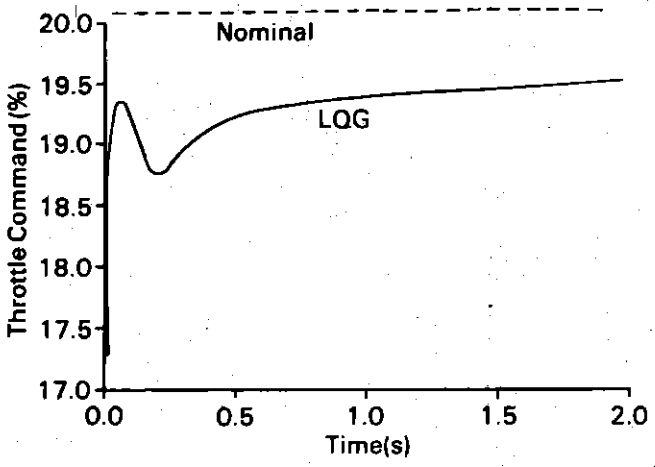
Throttle Command (%)
20.0
19.5
19.0
18.5
18.0
17.5
17.0
Nominal
LQG
0.0
0.5
1.0
1.5
2.0
Time(s)

i

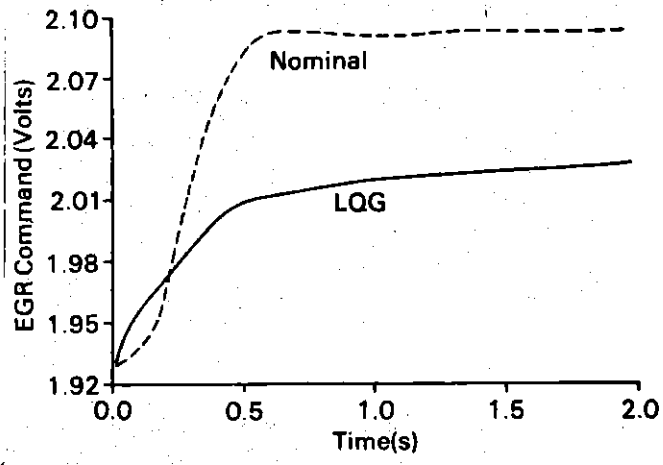
EGR Command (Volts)
2.10
2.07
2.04
2.01
1.98
1.95
1.92
Nominal
LQG
0.0
0.5
1.0
1.5
2.0
Time(s)

j

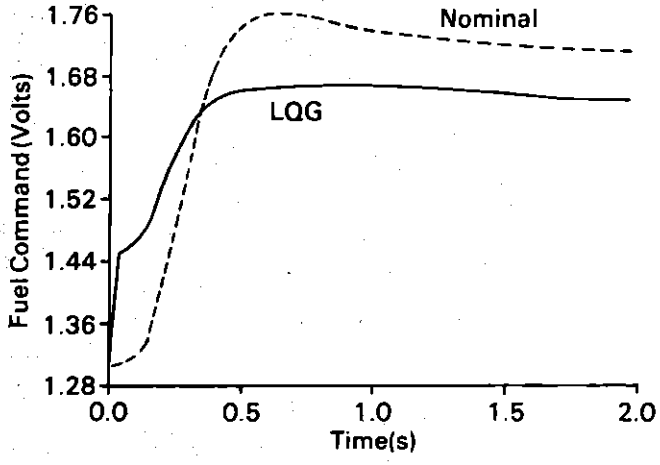
Fuel Command (Volts)
1.76
1.68
1.60
1.52
1.44
1.36
1.28
Nominal
LQG
0.0
0.5
1.0
1.5
2.0
Time(s)

k

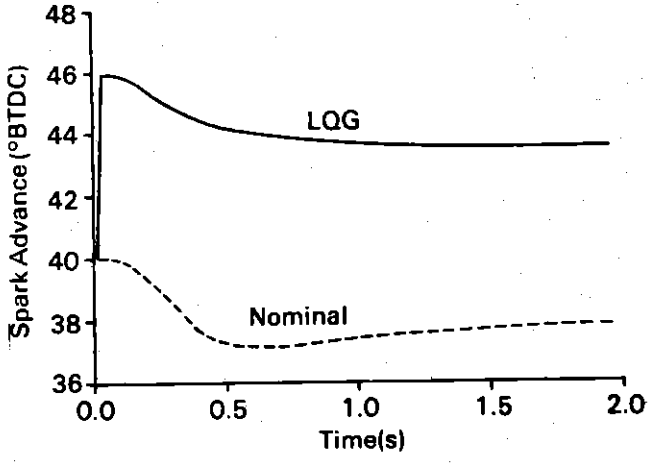
Spark Advance (°BTDC)
48
46
44
42
40
38
36
LQG
Nominal
0.0
0.5
1.0
1.5
2.0
Time(s)

l

The stability, robustness, and implementability properties of LQ controllers were discussed.

The control concept was then formally introduced. What was desired was a dynamical LQ based control system which had the same steady state properties as the nominal controller while improving the brake torque transient response and diminishing the cylinder air/fuel ratio deviations. An integral controller with a state reconstructor and shaping filter was selected.

The state reconstructor consisted of five decoupled Kalman filters in a sub-optimal estimating scheme which reduced the number of multiplications required for implementation from 486 for the optimal "global" filter to 183 for the decoupled sub-optimal scheme. The filter noise intensities were subjectively selected to place the closed loop filter poles in the neighborhood of the plant poles.

The integral LQ control gain was shown in Appendix E to be isomorphic to the standard LQ gain resulting from a properly augmented state description (equation 3.21), a verification of the earlier results by Lee et.al. in [32]. The weighting matrices for the quadratic cost functional were selected using a "real output versus control energy" tradeoff approach with nonlinear numerical simulations providing the means for parameter adjustment.

The command shaping filter was included to limit the frequency content in the input channel control signals to a reasonable level. "Reasonable" here means commensurate with the engine's ability to respond to the offsetting bias required of the integral control scheme. Again, the filter values were chosen in a subjective fashion with the nonlinear numerical simulations providing the final adjusting tool.

Finally, complete nonlinear Monte Carlo simulation results were presented which demonstrated a marked improvement in both the brake torque and cylinder air/fuel ratio transient responses. A time history of the pertinent engine variables in response to a 3% throttle request step perturbation is included as Figure 3.7.

An interesting question now is; How far does the real engine have to be from the assumed model (Figure 2.4), in some sense, before this controller actually drives the system unstable? In other words, what is the robustness of stability for this controller? This robustness question will be formally addressed in the next chapter.

IV. ROBUSTNESS ANALYSIS

"there is no 'thruth in modeling' law in systems theory."

Nils Sandell, 1979

4.1 Introduction and Motivation

Chapter II introduced the development of a linear time invariant model for the engine system which, like most models, was based upon a myriad of simplifying assumptions. Two of the major assumptions were linearity and the imposition of a half engine speed upper frequency limit. In Chapter III a dynamical controller was designed using the linear quadratic control design concept which, in nonlinear simulations, improved the torque and air/fuel ratio response to a mild acceleration maneuver (a 3% step throttle request). The purpose of this chapter is to investigate the expected performance of this controller on a real engine which will differ from the nominal design model.

Only one aspect of this performance will be formally addressed here, that of system stability in the presence of modelling errors, i.e. the robustness of stability. A general consensus seems to be that this is both a prudent and worthwhile approach, as Sandell points out in [23], since stability is an important and fundamental property of useful feedback systems. In addition, it seems to be at least reasonably tractable from an analytic perspective. Stability is also the performance aspect addressed by the gain and phase margin analysis of classical single input single output (SISO) systems.

For comparison purposes this chapter will investigate the robustness of stability properties for three separate engine controllers: the nominal control law which scheduled the engine input, $\delta\underline{u}$, with the measurable outputs, $\delta\underline{y}$, in a memoryless piecewise linear fashion, the theoretical full state feedback LQ controller which dynamically schedules $\delta\underline{u}$ with the engine states, $\delta\underline{x}$, and the realizable linear quadratic gaussian controller which dynamically schedules $\delta\underline{u}$ with $\delta\underline{y}$. This comparison is especially motivated by the fact that the nominal controller studied here mimics the control scheme which is currently found operational on many production automobiles, thus providing a meaningful yardstick against which proposed controllers can be measured.

The characterization of these robustness properties for multiple input feedback systems has been a topic of considerable research recently. Sandell in [23] summarizes the proceedings of an Office of Naval Research seminar on this multivariable robustness issue. In that work he presents a graphic example which clearly demonstrates the fact that, in contrast to single input systems, the multivariable Nyquist criterion in general gives no indication about "nearness to instability" for multi input systems. The concept of return difference matrix invertibility under suitably defined model perturbations is usually introduced to obtain some measure of "nearness to instability" in terms of appropriate matrix norms. The 2-norm or "singular values" are often employed for this

purpose. The formalization of this singular value approach will be outlined and used for the analyses contained in this chapter.

Even this singular value technique is not applicable in a straightforward manner to the engine control problem, however. The use of a discrete controller around a continuous plant presents some hybrid system problems which are still open research questions. For the purposes of this work some simplifying assumptions will be made which permit this discrete controller to be modelled with a moderate degree of accuracy in the continuous time frequency domain, thus providing the basis for a standard singular value robustness analysis.

An overview of the singular value approach with a modicum of definitions will be presented first. This is followed by a detailed analysis of the engine control robustness question for all three control schemes; nominal, LQ, and LQG. The assumptions required for the ad hoc hybrid system analysis are also included. A brief summary, which contains the significant results of this robustness analysis and highlights some of the major difficulties associated with this singular value approach to the robustness question, concludes this chapter.

4.2 Singular Value Approach to Robustness

Figure 4.1a illustrates the feedback system addressed by the singular value robustness theory. The forward path matrix, $\underline{G}(j\omega)$ (or just

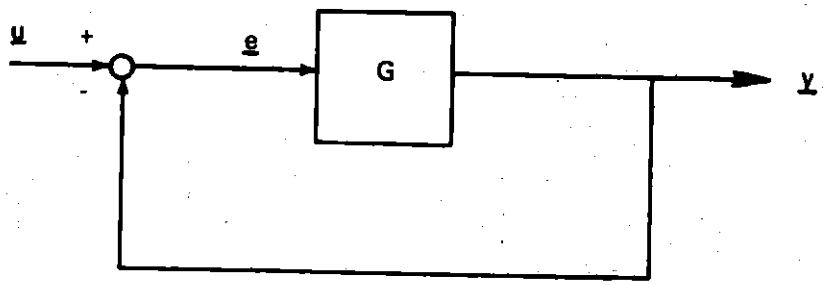

(a)

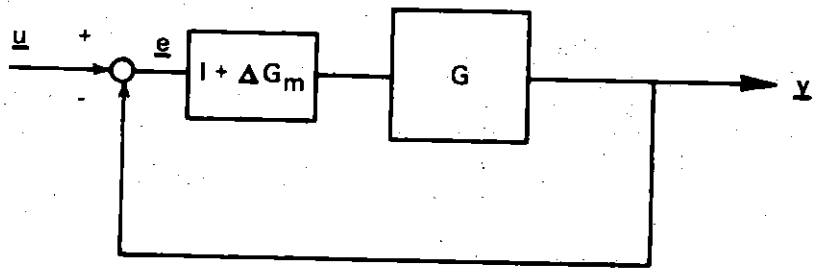

(b)

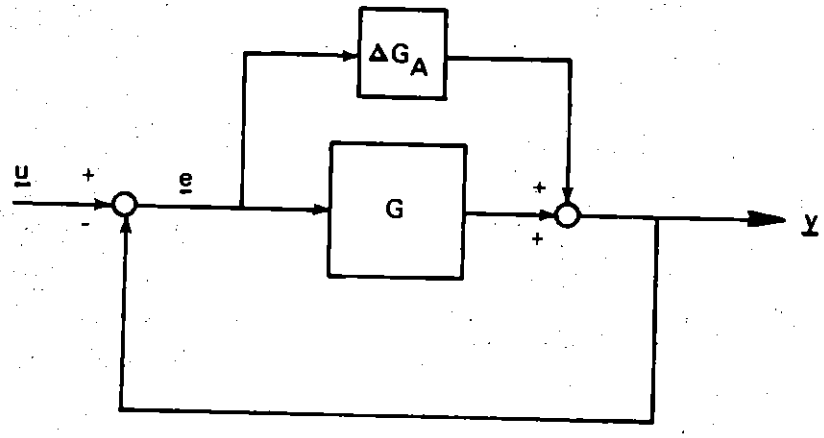

Figure 4.1: Allowable Perturbations

$\underline{G}$, the $j\omega$ will be implied in most of this chapter), represents the Fourier transform of the nominal time invariant linear and causal plant plus any controller used in the loop. The controller is also assumed to be time invariant linear and causal. From basic input-output stability theory (see, for example, theorem 4.3 in Willems [37]) the system in Figure 4.1a is finite gain stable if and only if $(\underline{I}+\underline{G})^{-1}$ exists, is causal, and

$$||(\underline{I}+\underline{G})^{-1}|| < \infty \tag{4.1}$$

This requirement can be restated in terms of the classical Nyquist criterion. This requires the number of encirclements of the origin by the determinant of $(\underline{I}+\underline{G})$ - the return difference matrix - mapped over the infinite radius Nyquist D contour to equal - $\underline{P}$ for stability, where $\underline{P}$ is the number of right half plane poles of the forward path transfer matrix, $\underline{G}$. This is usually written as,

$$N(0, \det(\underline{I}+\underline{G}), D_\infty) = -\underline{P} \tag{4.2}$$

For the SISO case the Nyquist criterion provides an easy graphical means of determining the "nearness to singularity" of the return difference function since (4.2) can be written as,

$$N(-1, G, D_\infty) = -\underline{P} \tag{4.3}$$

affording a simple visual determination of this robustness of stability, as seen in Figure 4.2. Note that when the return difference function becomes singular the number of encirclements changes, violating the Nyquist stability condition.

For the multiple input case (4.2) does not provide this same "measure of robustness" interpretation since the determinant of $(\underline{I}+\underline{G})$ is not a good test for nearness to singularity. The classic example, which was used by Sandell in [20], to illustrate this is the matrix $\underline{A}$, where

$$\underline{A} = \begin{bmatrix} 1 & 100 \\ 0 & 1 \end{bmatrix}$$

The determinant of $\underline{A}$ is 1 whereas its smallest singular value[†] is 0.01 since the additive perturbation $\Delta\underline{A}$,

$$\Delta\underline{A} = \begin{bmatrix} 0 & 0 \\ 0.01 & 0 \end{bmatrix}$$

makes the matrix sum $\underline{A}+\Delta\underline{A}$ singular. Thus the multivariable Nyquist theorem provides only dichotomous information, the system is either

---

[†] the singular values of a matrix, $\sigma(A)$, are defined as,

$$\sigma(\underline{A}) = [\lambda(\underline{A}^H\underline{A})]^{1/2}$$

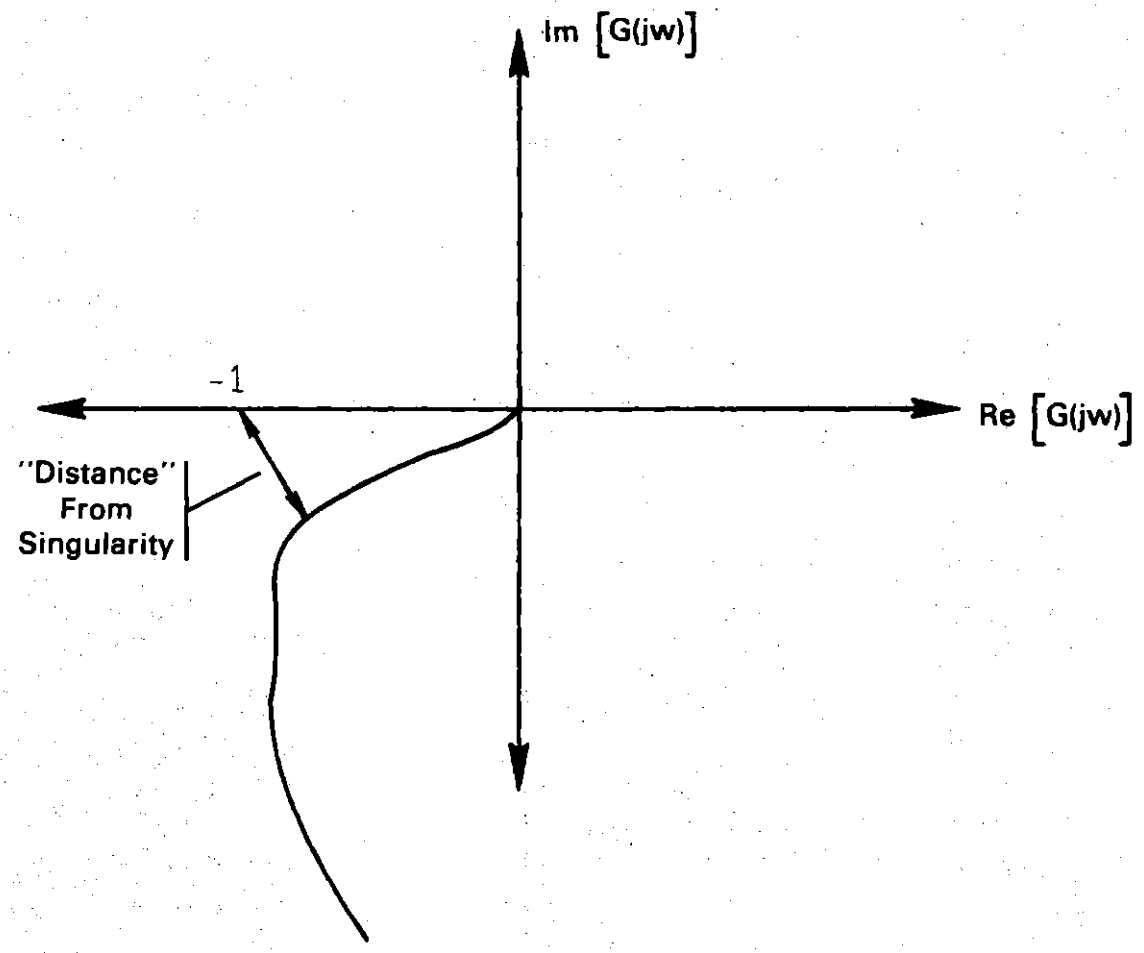

Figure 4.2: Typical SISO Nyquist Diagram

stable or unstable, and another approach for quantifying this nearness to instability must be found.

The approach most often used is the singular value one. Assume that the nominal system, $\underline{G}$, can be subject to multiplicative perturbations as in Figure 4.1b or additive perturbations as in Figure 4.1c, neither simultaneously. Assume further that these perturbations do not change the number of open loop right half plane poles. It can be shown (see theorem 2 of Sandell [20]) that the system remains stable for additive perturbations if,

$$||(\underline{I}+\underline{G})^{-1}\ \Delta\underline{G}_A||_2 < 1 \tag{4.4}$$

and for multiplicative perturbations (see Appendix F if $\underline{G}^{-1}$ does not exist),

$$||(\underline{I}+\underline{G}^{-1})^{-1}\ \Delta\underline{G}_m||_2 < 1 \tag{4.5}$$

Conservative non-directional bounds for equations (4.4) and (4.5) can be obtained using basic matrix theory results. In particular, (4.4) becomes,

$$||\Delta\underline{G}_A||_2 < \frac{1}{||(\underline{I}+\underline{G})^{-1}||_2} \tag{4.6}$$

for stability, while in the multiplicative case stability is retained when

$$||\underline{\Delta G}_m||_2 < \frac{1}{||(\underline{I}+\underline{G}^{-1})^{-1}||_2} \tag{4.7}$$

Up until this time there has been nothing special about the choice of matrix norms, any suitable norm would suffice. Laub in [22] points out the potentially significant computational advantage in the choice of a row or column norm. For most practical systems the spectral norm is usually chosen since it naturally lends itself to the directional analysis included here.

The singular value decomposition of a complex mxn matrix $\underline{A}$ of rank r can be written as,

$$\underline{A} = \underline{U}\ \underline{\Sigma}\ \underline{V}^H \tag{4.8}$$

where $\underline{U}$ and $\underline{V}$ are unitary matrices ($\underline{U}^H\underline{U}=I$, $\underline{V}^H\underline{V}=\underline{I}$, H denotes complex conjugate transpose) and $\underline{\Sigma} = \text{diag}(\sigma_1,\sigma_2,\sigma_3,\ldots,\sigma_m)$ with $\sigma_1>\sigma_2>\ldots>\sigma_r>\sigma_{r+1} = 0 = \sigma_{r+2}=\ldots=\sigma_m$ the diagonal matrix of singular values. The singular value decomposition of the nominally stable return difference function becomes,

$$(\underline{I}+\underline{G}) = \underline{U}\ \underline{\Sigma}\ \underline{V}^H \tag{4.9}$$

where $\sigma_n>0$ since $(\underline{I}+\underline{G})$ is, by our stability assumption, invertible. In fact, this inverse is readily seen to be,

$$(\underline{I}+\underline{G})^{-1} = \underline{V}\ \ \underline{\Sigma}^{-1}\ \underline{U}^H \tag{4.10}$$

Define the 2-norm, or spectral norm, as

$$||\underline{A}||_2 \triangleq [\lambda(\underline{A}^H\underline{A})]^{1/2} = \max_{i=1,n} [\sigma_i] = \bar{\sigma}(\underline{A}) \tag{4.11}$$

where $\bar{\sigma}(\underline{A})$ indicates the maximum singular value of $\underline{A}$.

Using equation (4.4) and (4.10) it is clear that the closed loop system remains stable when subject to additive perturbations if,

$$\bar{\sigma}(\Delta\underline{G}_A) < \underline{\sigma}(\underline{I}+\underline{G}) \tag{4.12}$$

and that the minimum norm additive matrix perturbation $\Delta\underline{G}_A$ which will cause instability is given by,

$$\Delta\underline{G}_A = -\sigma_n \underline{u}_n \underline{v}_n^H \tag{4.13}$$

where the minus sign comes from noting that the sum $(\underline{I}+\underline{G}+\Delta\underline{G}_A)$ is to be singular and the subscript n indicates the singular vectors associated with the smallest singular value.

Similarly, for multiplicative perturbations let,

$$(\underline{I}+\underline{G}^{-1}) = \underline{U}\ \underline{\Sigma}\ \underline{V}^H \tag{4.14}$$

then the closed loop system remains stable when subject to multiplicative perturbations if,

$$\bar{\sigma}(\Delta G_m) < \underline{\sigma}(\underline{I}+\underline{G}^{-1}) \tag{4.15}$$

and the minimum norm multiplicative perturbation which will cause instability is given by,

$$\Delta \underline{G}_m = -\sigma_n \underline{u}_n \underline{v}_n^H \tag{4.16}$$

Equations (4.12) and (4.15) are the major results of the singular value robustness theory. Restated in words they imply that when the real system, the truth model, is written in the form of Figures 4.1b or 4.1c then the closed loop system remains stable for all perturbations with norms smaller than the limits imposed by equation (4.12) or (4.15).

The converse is not necessarily true. Perturbations with large norms might be in a direction which does not drive the return difference matrix singular. This is most clearly seen upon inspection of equations (4.4) or (4.5). The directional information loss is imposed by the conservative bounds adopted in equations (4.6) or (4.7).

A singular value multivariable robustness analysis technique can now be outlined. For the frequency range of interest (in the case of this engine control system this range is from dc to half engine speed) the minimum singular values, $\underline{\sigma}(I+G)$ and $\underline{\sigma}(I+G^{-1})$, are plotted. At the points where these minimum singular values are low (in a subjective sense), indicating that relatively small perturbations could drive the system unstable, the sensitive directions are investigated (equations (4.13) and (4.16)). If these directions seem plausible when compared to the nominal model then a potentially unstable condition exists and

perhaps a controller design change is in order. At the very least the model needs to be verified at that point. If, on the other hand, these directions do not seem plausible when compared to the nominal model then this singular value analysis is not too informative since there may be an entirely different and plausible direction requiring a slightly larger perturbation which makes the return difference matrix singular. This singular value analysis does not quantify that potential.

As an example of this phenomenon consider the matrix $\underline{A}$ such that,†

$$\underline{A} = \begin{bmatrix} 1 & 0 \\ 0 & 10 \end{bmatrix}$$

Assume that the a_{11} entry is, on physical grounds, known with absolute certainty, i.e. $a_{11}=1$. The singular values of $\underline{A}$ are,

$$\sigma_1 = 10$$

$$\sigma_2 = 1$$

The minimum norm $\Delta\underline{A}$ such that $(\underline{A}+\Delta\underline{A})$ is singular is given by (4.13) as,

$$\Delta\underline{A} = -\sigma_2 \underline{u}_2 \underline{v}_2^H = -1 \begin{pmatrix} 1 \\ 0 \end{pmatrix} \quad (1 \quad 0) = \begin{bmatrix} -1 & 0 \\ 0 & 0 \end{bmatrix}$$

---

†This example is due to Norm Lehtomaki.

However, since a_{11} is known with certainty, this perturbation can be ruled out and the next smallest singular perturbation is (by inspection),

$$\Delta\underline{A} = -\sqrt{10}\begin{bmatrix} 0 & 1 \\ 1 & 0 \end{bmatrix}$$

The norm of this second perturbation is, in general, not available from a simple singular value analysis.

There seems to be only two potentially significant results from a singular value analysis as the theory rests today. First, the singular values of $(\underline{I}+\underline{G})$ and $(\underline{I}+\underline{G}^{-1})$ can be very large indicating that the closed loop system is robust to even large perturbations in any direction. Second, the singular value of the return difference matrix can be small and in a plausible modelling error direction (meaning that the real loop transfer gains fall within some envelope described by the nominal model and the expected modelling errors). This would indicate a potentially unstable condition. Small singular values, on the other hand, in a direction which can be deemed, using sound engineering judgement, "implausible" do not yield much useful information. This is because truth model to design model changes in other, more plausible modelling error directions could also be destabilizing with norms only slightly larger than the minimum norm singular value perturbation. A singular value analysis only captures the single worst direction. Research is in progress to quantify alternate perturbations.

These results will now be applied to the engine model and three controllers. Hopefully these "large,""small," and "plausible direction" terms will become more clear with application to this practical example.

4.3 Singular Value Analysis for the Engine Controllers

4.3.1 Hybrid System Assumptions

As was briefly mentioned in the introduction to this chapter the robustness analysis of continuous plants with discrete controllers is still an open research question. One approach commonly taken is to design a continuous time controller, check the robustness properties of this completely continuous system,then discretize the controller for implementation in a microprocessor based system. The drawback to this approach is that the robustness analysis fails to capture the potential for aliasing and imperfect impulse sampling effects on the analog to digital (A/D) conversion on input to the controller and distortion on the digital to analog (D/A) conversion on output from the controller. Further, the discretization procedure usually used matches step response, not frequency response.

An alternate approach is to discretize the plant, design a discrete controller, and analyze the robustness of this completely discrete system. In addition to ignoring the A/D and D/A effects this technique

only provides robustness results (ΔG_A and ΔG_m) in terms of discrete model perturbations, whereas the original plant model is, by assumption, continuous.

A compromise solution will be adopted here. The original continuous time plant has already been discretized and a discrete controller designed in Chapters II and III. The sampling interval, T, has been chosen as 0.020 seconds, a 50 Hz sampling rate. This, together with the A/D and D/A converters constitutes the system pictured in Figure 4.3a. What is required for the singular value robustness analysis is the unity feedback system shown in Figure 4.3b. The forward path gain, $\underline{G}(j\omega)$, can be determined as follows.

The continuous engine model, $\underline{F}(j\omega)$, maps $e(j\omega)$ into $y(j\omega)$,

$$\underline{y}(j\omega) = \underline{F}(j\omega)\underline{e}(j\omega) \tag{4.17}$$

For analysis purposes assume that the A/D converter is an impulse sampler. This yields the discrete Fourier transform (see, for example, Oppenheim and Schaeffer [42] or Kuo [45]),

$$\hat{\underline{y}}(e^{j\omega T}) = \frac{1}{T} \sum_{n=-\infty}^{+\infty} \underline{y}(j\omega + j\,\frac{2\pi n}{T}) \tag{4.18}$$

The transformed discrete time numerical algorithm maps these measurements into the discrete control values,

$$\hat{\underline{u}}(e^{j\omega T}) = \underline{C}(e^{j\omega T})\hat{\underline{y}}(e^{j\omega T}) \tag{4.19}$$

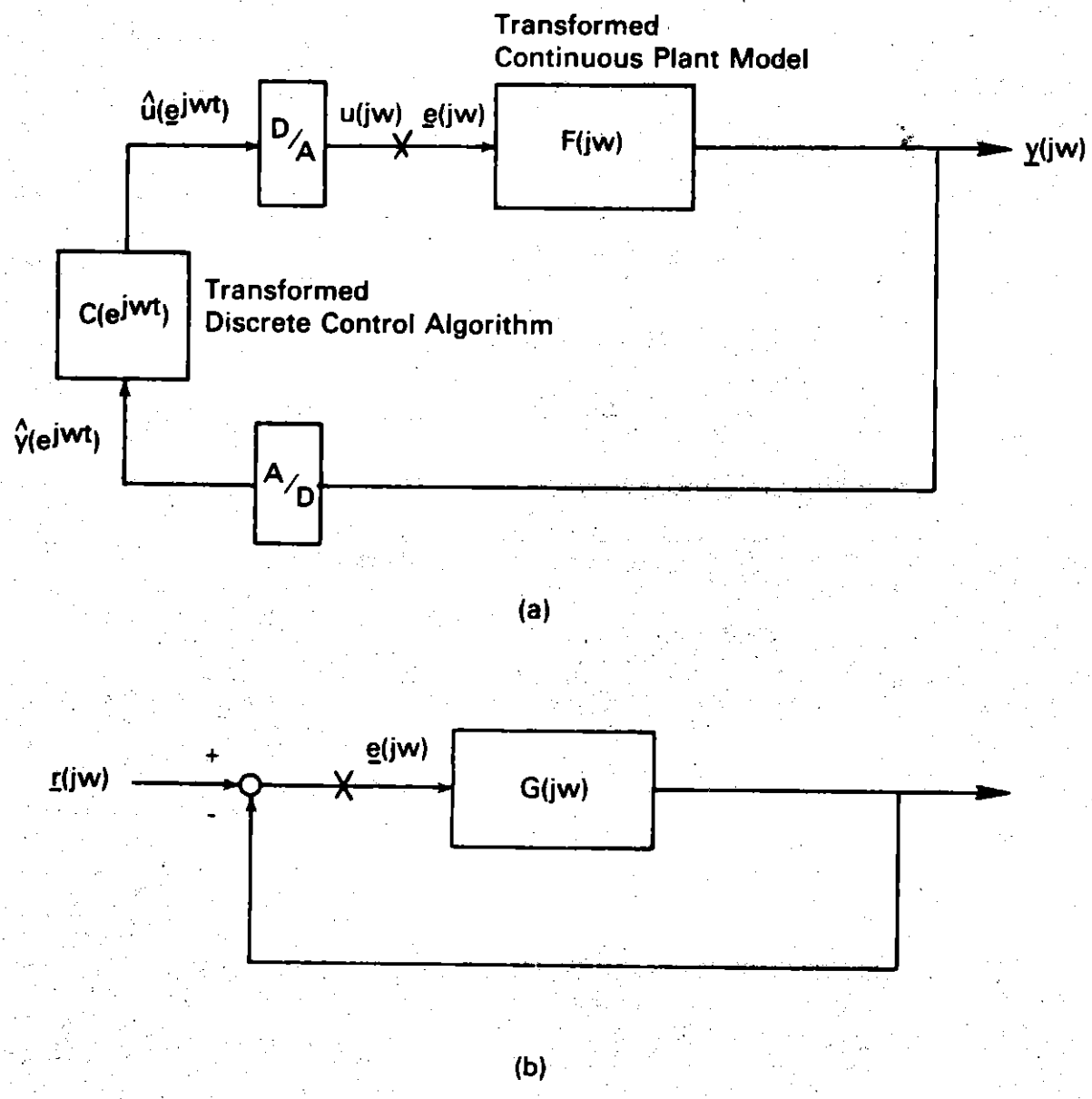

Figure 4.3: Hybrid System Description

The digital to analog converter is modelled as a perfect zero order hold device,

$$\underline{u}(j\omega) = \frac{1-e^{-j\omega T}}{j\omega} \; \underline{u}(e^{j\omega T}) \tag{4.20}$$

Combining equations (4.17)-(4.20) with a minus sign added for the negative feedback configuration required in Figure 4.3 yields

$$\underline{u}(j\omega) = - \frac{1-e^{-j\omega T}}{j\omega T} \; \underline{C}(e^{j\omega T}) \sum_{n=-\infty}^{+\infty} \left[F\left(j\omega + j\,\frac{2\pi n}{T}\right) \underline{e}\left(j\omega + j\,\frac{2\pi n}{T}\right) \right] \tag{4.21}$$

Two additional assumptions will be made for computational considerations. First, assume that the measurements, $F(j\omega)\underline{e}(j\omega)$, are bandlimited to avoid aliasing at the Nyquist frequency of 25 Hz. This is a good assumption since the brake torque and manifold pressure (the only high frequency signals) sensors were chosen to avoid this aliasing. These two sensor filters are at -33 and -16 db respectively at 25 Hz. In fact, experimental tests confirm that the major frequency components of the measurement signals are in the dc to 10 Hz region.

The second assumption concerns the zero order hold calculation. As Figure 4.4 demonstrates even with no aliasing the output signal, $\underline{u}(j\omega)$, contains power in the higher frequency ranges. Practically, however, the zero order hold function attenuates even the 40 Hz

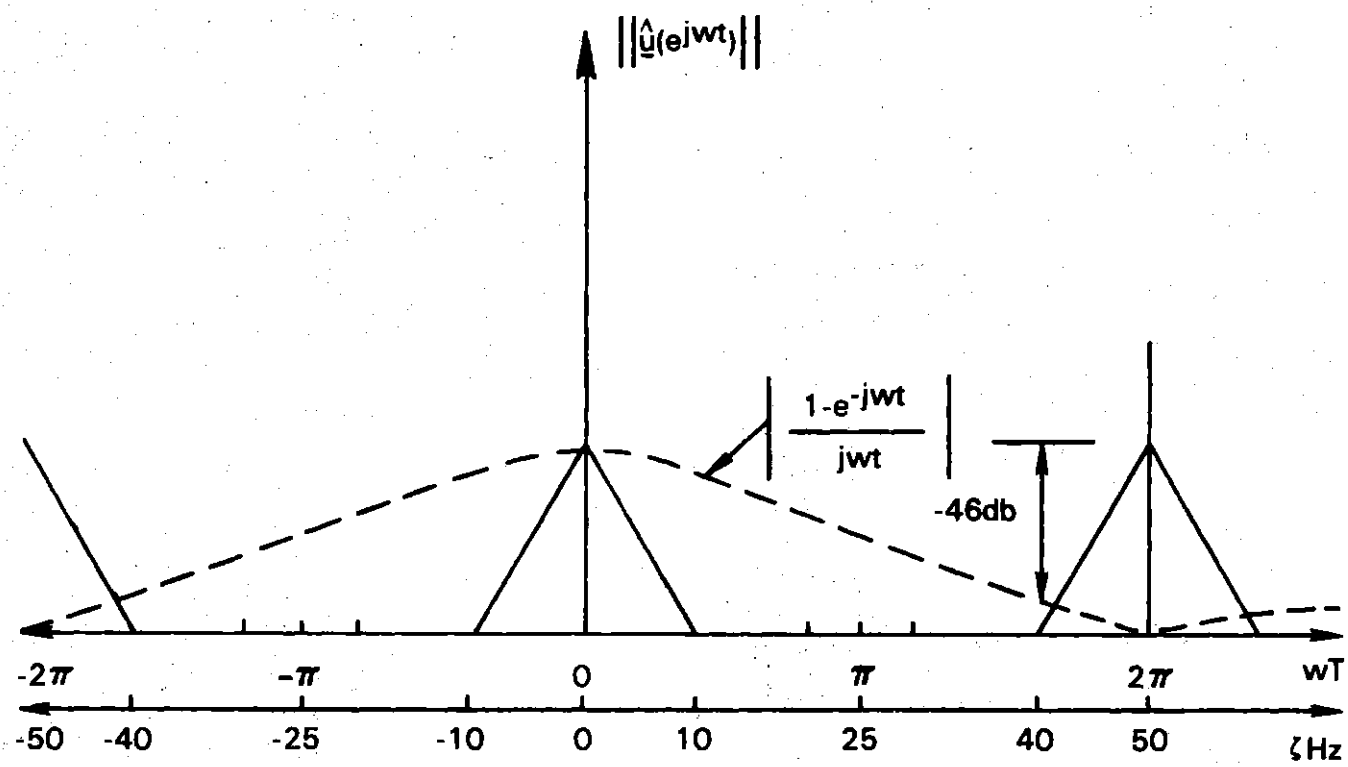

Figure 4.4: Zero Order Hold Distortion

component by -46 db and only the fundamental lobe needs to be considered when calculating the transfer function in (4.21).

These two assumptions lead to the final equation for the forward path gain required for the singular value analysis,

$$G(j\omega) = - \frac{1-e^{-j\omega T}}{j\omega T} \underline{C}(e^{j\omega T})\underline{F}(j\omega) \qquad (4.22)$$

Equation (4.22) will, in general, be accurate whenever the sampling rate is high enough to avoid aliasing on input and neglect high frequency components in the zero order hold calculation. It captures the essence of a continuous plant, discrete controller, and low frequency distortion upon D/A conversion. A number of rather restrictive idealizations (such as impulse sampling) and assumptions have been made, however, and the interpretation of the results obtained with this approach should be conditioned upon these simplifications.

4.3.2 Loop Transfer Functions

The development of equation 4.22 now permits the singular value analysis for the three control systems, nominal, LQ, and LQG, to proceed. The calculation of the forward path gain, $G(j\omega)$, requires the formulation of a plant transfer function, $F(j\omega)$, and discrete controller transfer function, $C(e^{j\omega T})$, for each of the three control schemes.

Figure 4.5 presents the block diagram for the nominal controller. The plant transfer function can be identified from equation (2.3) as,

$$\underline{F}(j\omega) = \underline{C}(j\omega\underline{I}-\underline{A})^{-1}\underline{B} + \underline{D} \tag{4.23}$$

and the memoryless nominal controller, $\underline{P}$, results in a forward path gain from (4.22) of,

$$\underline{G}_{NOM}(j\omega) = - \frac{1-e^{-j\omega T}}{j\omega T} \underline{P}\ \underline{F}(j\omega) \tag{4.24}$$

Figure 4.6 presents the block diagram for the theoretical full state feedback case presented in Chapter III from which the following forward path gain can be derived,

$$\underline{G}_{LQ}(j\omega) = - \frac{1-e^{-j\omega T}}{j\omega T} \left[(z\underline{I}-\underline{I}+\underline{G}_u)^{-1}\underline{G}_x + \underline{P}\ \underline{C}\right]\Big|_{z=e^{j\omega T}} \cdot \left[(j\omega\underline{I}-\underline{A})^{-1}\underline{B}\right] \tag{4.25}$$

Finally, from Figure 4.7 for the realizable LQG design the following difference equations can be written,

$$\hat{\underline{x}}(k) = \overline{\underline{A}}\ \hat{\underline{x}}(k-1) + \overline{\underline{B}}\ \underline{u}(k-1) + \underline{H}\ \underline{y}(k) \tag{4.26}$$

$$\underline{u}^*(k) = (\underline{I}-\underline{G}_u)\underline{u}^*(k-1) - \underline{G}_x\ \hat{\underline{x}}(k-1) \tag{4.27}$$

$$\underline{u}(k) = (\underline{I}-\underline{G}_u)\underline{u}^*(k-1) - \underline{G}_x\ \hat{\underline{x}}(k-1) + \underline{P}\ \underline{y}(k) \tag{4.28}$$

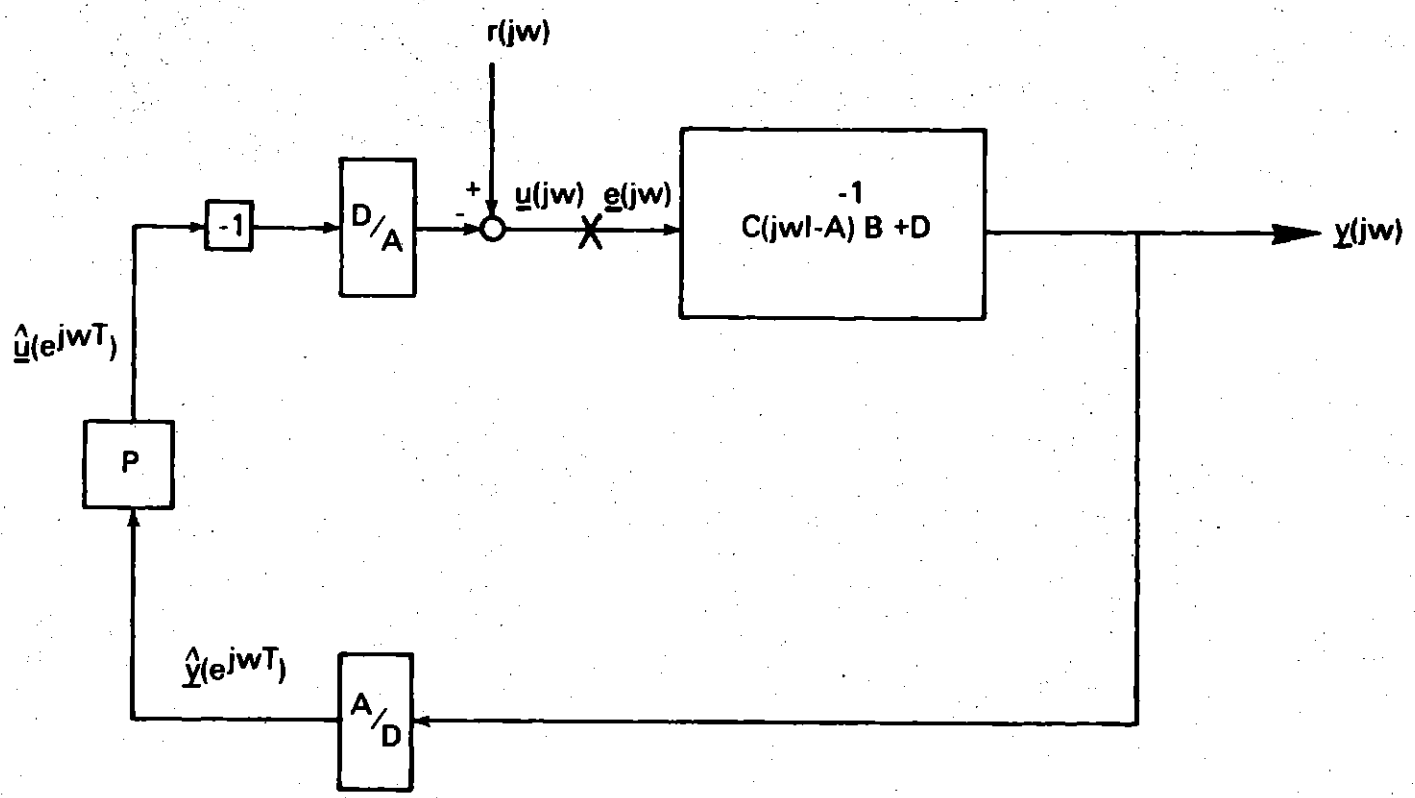

Figure 4.5: A Block Diagram for the Nominal Controller

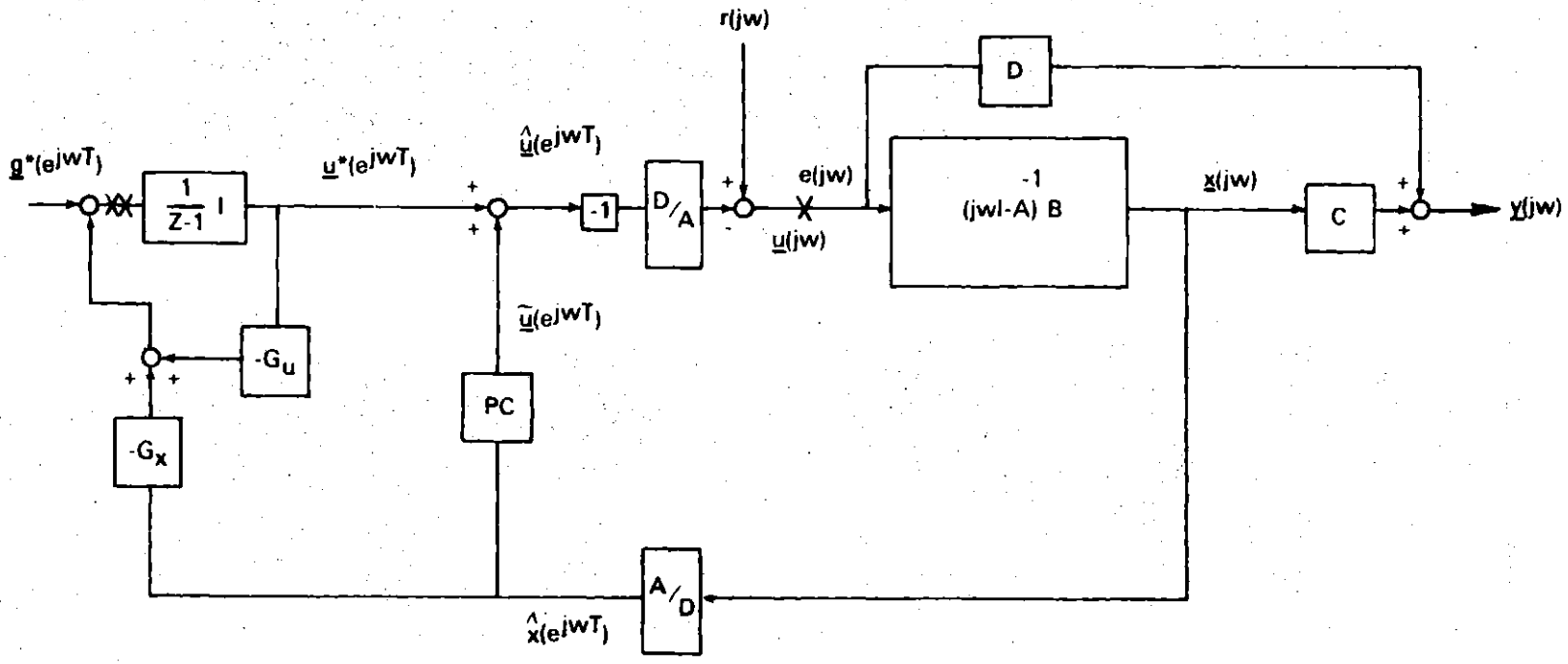

Figure 4.6: LQ Block Diagram

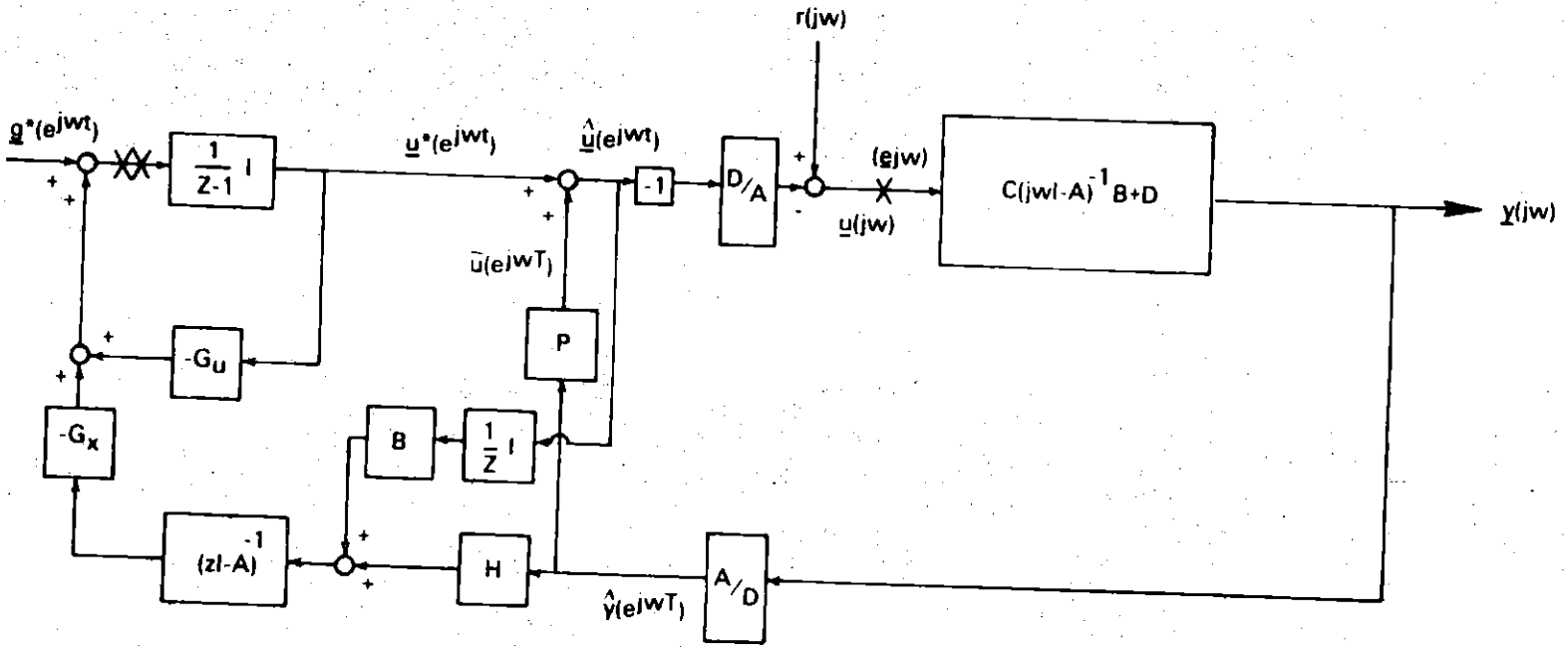

Figure 4.7: LQG Block Diagram

where $\bar{A}$, $\bar{B}$, and $\bar{H}$ are from the five decoupled Kalman filter designs and $\underline{u}^*$ represents the LQ control action. Concatenating (4.26)-(4.28) into a single 26 state discrete system results in,

$$\underline{z}(k) \triangleq \begin{bmatrix} \hat{\underline{x}}(k) \\ \underline{u}^*(k) \\ \underline{u}(k) \end{bmatrix}$$

$$\underline{z}(k) = \tilde{\underline{A}}\,\underline{z}(k-1) + \tilde{\underline{B}}\,\underline{y}(k) \tag{4.29a}$$

$$u(k) = \tilde{\underline{C}}\,\underline{z}(k-1) + \underline{P}\,\underline{y}(k) \tag{4.29b}$$

$$\tilde{\underline{A}} = \begin{bmatrix} \bar{\underline{A}} & 0 & \bar{\underline{B}} \\ -\underline{G}_x & (\underline{I}-\underline{G}_u) & 0 \\ -\underline{G}_x & (\underline{I}-\underline{G}_u) & 0 \end{bmatrix} \quad \tilde{\underline{B}} = \begin{bmatrix} \underline{H} \\ 0 \\ \underline{P} \end{bmatrix} \quad \tilde{\underline{C}} = \left[\begin{array}{c:c:c} -\underline{G}_x & (\underline{I}-\underline{G}_u) & 0 \end{array}\right]$$

which can be transformed and combined with the plant transfer function in (4.23) to yield,

$$\underline{G}_{LQG}(j\omega) = -\frac{1-e^{-j\omega T}}{j\omega T}\left[\tilde{\underline{C}}(z\underline{I}-\tilde{\underline{A}})^{-1}\,\tilde{\underline{B}} + \underline{P}\right]\Bigg|_{z=e^{j\omega T}} \cdot \underline{F}(j\omega) \tag{4.30}$$

4.3.3 Results and Analysis

The forward path gains in equations (4.24), (4.25), and (4.30) can be combined with the results of the previous section, equations (4.12)

and (4.15), to obtain the so called singular value diagrams ($\underline{\sigma}(\underline{I}+\underline{G})$ and $\underline{\sigma}(\underline{I}+\underline{G}^{-1})$) for the three control schemes. Figure 4.8 illustrates this diagram for the case of multiplicative perturbations. The ordinate represents, in db, the maximum allowable multiplicative perturbation in any direction while maintaining stability for the nominal, LQ, and LQG controllers. The abscissa is the analog frequency variable in Hz.

There are three significant aspects to this singular value plot. First, at low frequencies a relatively small multiplicative perturbation (-18 db) in the right direction will lead to instability. Second, at all frequencies the LQG control scheme is at least as good as the nominal controller. And finally, above about 2 Hz the LQG control scheme is significantly more robust, in this singular value sense, than the theoretical full state feedback LQ case.

The small multiplicative perturbation required for instability at low frequencies presents a potential problem. If this perturbation is in a direction in which the original plant model, $\underline{F}(j\omega)$, is susceptible to errors then all three controllers will, in all likelihood, be destabilizing. This is an intuitively unsettling result since nominal controllers similar to the one presented here have functioned satisfactorily on production automobiles for years. Further analysis is now presented which indicates that this direction is indeed not a plausible one for modelling errors of this magnitude to occur in.

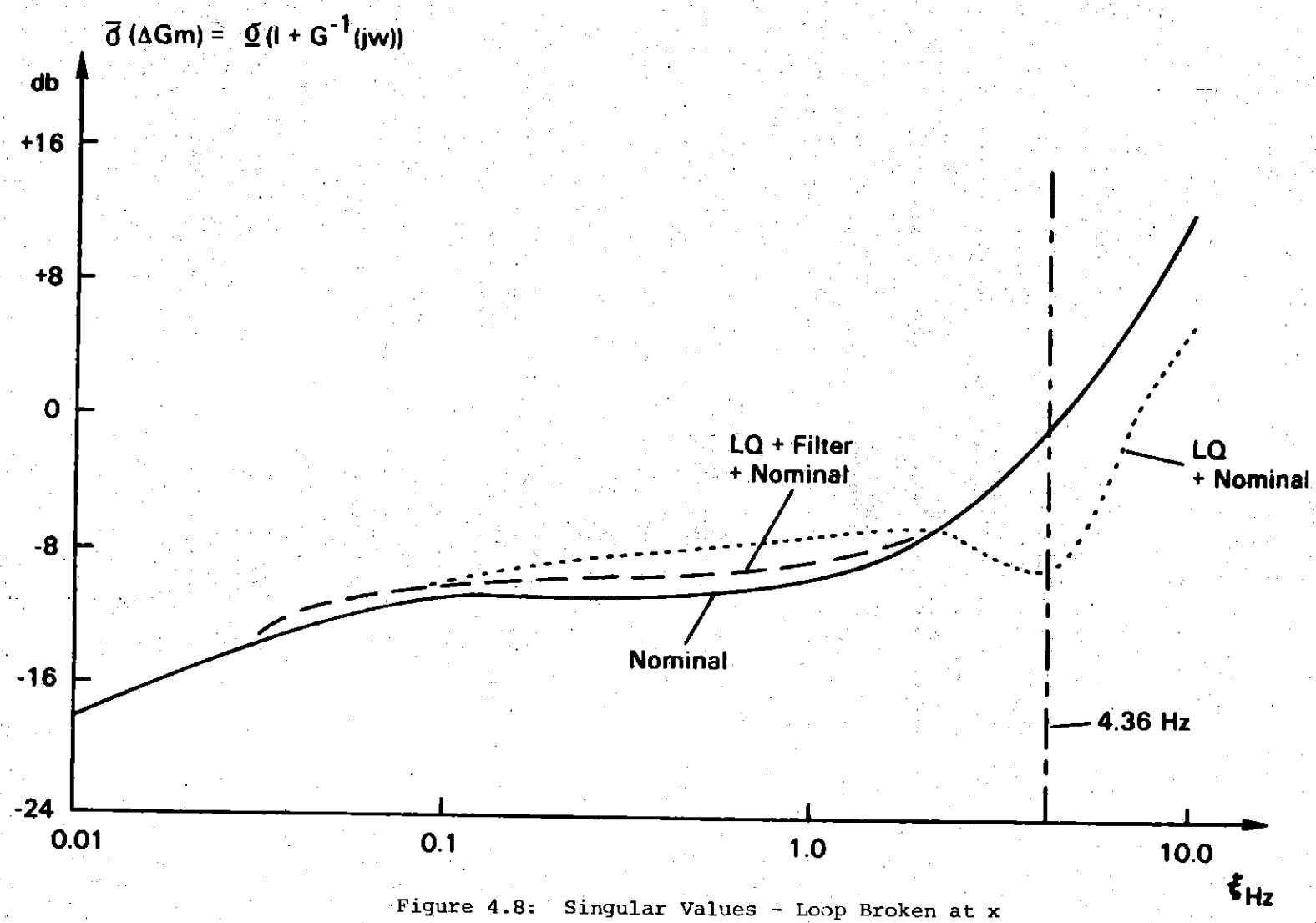

Figure 4.8: Singular Values - Loop Broken at x

The sensitive multiplicative direction was calculated using equation (4.16) at these low frequencies (10^{-5} Hz, essentially dc). For the nominal control scheme this resulted in a minimum norm destabilizing multiplicative perturbation of (see Figure 4.1b),

$$\left(\underline{I}+\Delta G_m\right)_{NOM} = \begin{bmatrix} 1.0 & 0 & 0 & 0 \\ 0 & 1.0 & 0.003 & -0.043 \\ 0 & 0.0 & 0.992 & 0.109 \\ 0 & 0.0 & 0.0 & 1.001 \end{bmatrix} \tag{4.31}$$

and, for the LQG controller,

$$\left(I+\Delta G_m\right)_{LQG} = \begin{bmatrix} 1.003 & 0.0 & 0.0 & -0.017 \\ 0.006 & 1.001 & 0.0 & -0.031 \\ 0.021 & 0.003 & 0.998 & -0.105 \\ 0.0 & 0.0 & 0.0 & 0.999 \end{bmatrix} \tag{4.32}$$

The LQ direction is essentially the same as the LQG case.

The nonlinear closed loop numerical simulations presented in Chapter III were rerun with these multiplicative perturbations included in the loop. As Figure 4.9 indicates the singular value analysis correctly predicts a dramatically deteriorated, if not unstable, response. This is to be expected since the coupling terms from spark advance to fuel and EGR commands in (4.31) and (4.32), though small in norm, have a significant effect on these control variables. Reference can be made

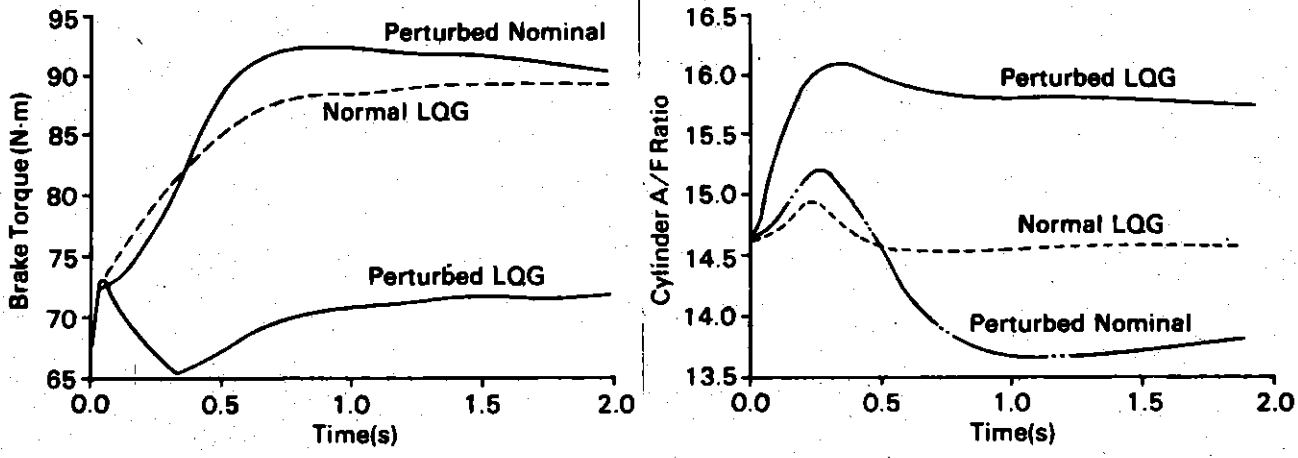

a
Torque

b
A/F

Multiplicative Perturbation = $(I + \Delta G_M)$ =

$$\begin{bmatrix} 1.00 & 0.0 & 0.0 & -0.017 \\ 0.0 & 1.00 & 0.0 & -0.031 \\ 0.021 & 0.0 & 1.00 & -0.1045 \\ 0.0 & 0.0 & 0.0 & 1.00 \end{bmatrix}$$

Figure 4.9: Perturbed System Simulation Results

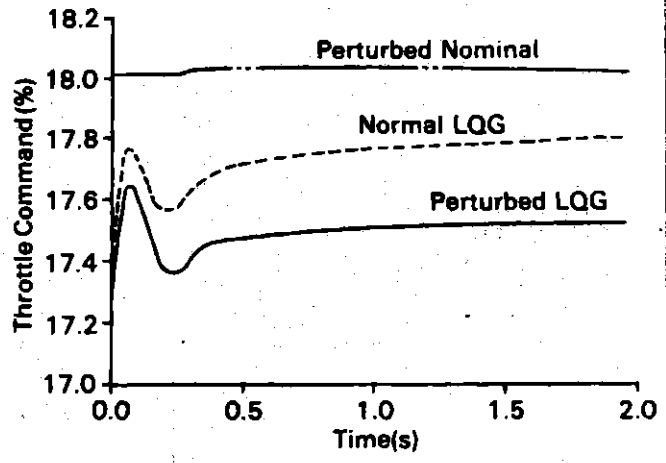

c
Throttle

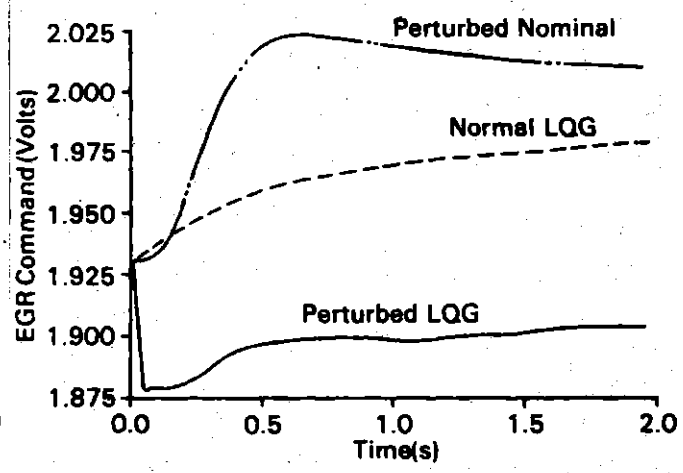

d
EGR

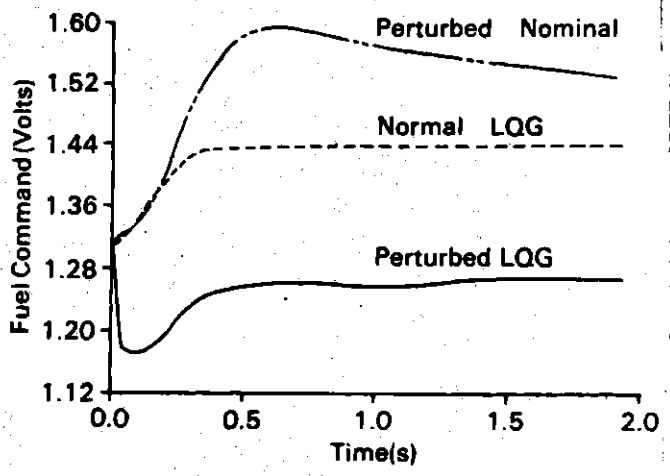

e
Fuel

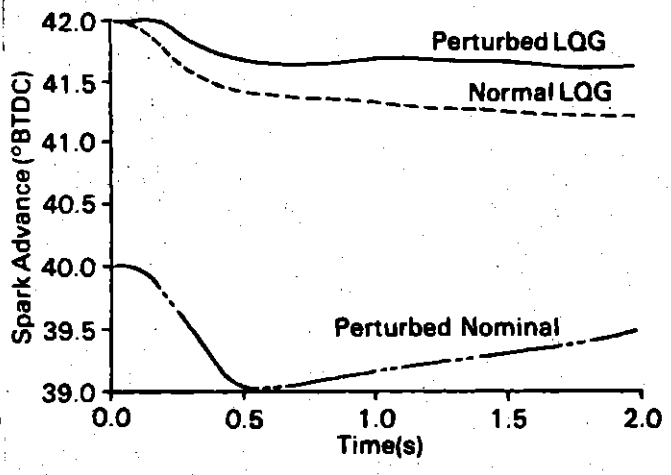

f
Spark

to the dotted lines in this figure for comparison with the normal (unperturbed) EGR, fuel, and spark command variations to a 1% throttle step.

This directional implausibility argument can be quantified by attributing the required forward path gain change, where possible, to the continuous plant model and not the controller. This is a reasonable approach since the control algorithm is microprocessor based and no uncertainty enters there whereas the engine model is always an approximation to reality and there can be much uncertainty in the model development.

Figure 4.10 illustrates the unity feedback scheme under investigation. The controller is represented as a transfer matrix, H, which maps the engine outputs, $\delta\underline{y}$, into the control variables, $\delta\underline{u}$,

$$-\delta\underline{u} = -\begin{bmatrix} \delta\alpha_c \\ \delta E_c \\ \delta F_c \\ \delta S \end{bmatrix} = \underline{H}\delta\underline{y} = \underline{H}\begin{bmatrix} \delta T_b \\ \delta N \\ \delta P_m \\ \delta\alpha_p \\ \delta E_p \\ \delta T_f \\ \delta P_f \end{bmatrix} \tag{4.33}$$

The real engine, or truth model $\hat{\underline{F}}$, is modelled as the transfer matrix, $\underline{F}$, which maps the multiplicatively perturbed control variables, $\delta\underline{u}$, into the engine outputs,

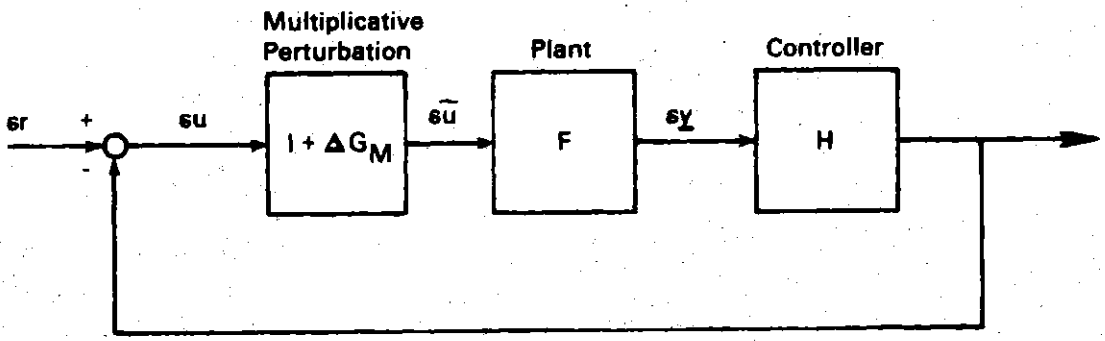

Figure 4.10: Perturbed Unity Feedback System

$$\delta \underline{y} = \underline{F}\delta \underline{u} = \underline{F}(\underline{I}+\Delta \underline{G}_M)\,\delta \underline{u} \tag{4.34}$$

where $\underline{F}$ is given by equation (4.23), the linear model developed in Chapter II, for both the nominal and LQG case.

The minimum norm multiplicatively perturbed destabilizing forward path gain is, from (4.33) and (4.34),

$$\underline{G} = \underline{H}\,\underline{F}(\underline{I}+\Delta \underline{G}_M) \tag{4.35}$$

As previously mentioned the controller, $\underline{H}$, is assumed to have no uncertainty and is fixed at its nominal values. The set of all real engine models, $\hat{\underline{F}}$, which result in this unstable forward path gain is then readily seen to be,

$$\hat{\underline{F}} = \underline{F}(\underline{I}+\Delta \underline{G}_M) + \underline{M} \tag{4.36}$$

where $\underline{M}$ is an arbitrary matrix which lies entirely in the nullspace of $\underline{H}$, i.e.

$$\underline{H}\,\underline{M} \equiv 0 \tag{4.37}$$

The question of directional implausibility has now been translated into the "reasonableness" of all $\hat{\underline{F}}$ given by (4.36).

For the nominal control scheme this matrix $\underline{M}$ can be found by taking all possible combinations of the basis vectors for the nullspace of the controller, $\underline{H}$. In this case, from Figure 4.5,

$$\underline{H} = \underline{P}$$

$$N(\underline{P}) = \begin{bmatrix} 1 & 0 & 0 & 0 & 0 \\ 0 & 0 & 0 & 0 & 0 \\ 0 & 1 & 0 & 0 & 0 \\ 0 & 0 & 1 & 0 & 0 \\ 0 & 0 & 0 & 1 & 0 \\ 0 & 0 & 0 & 0 & 1 \\ 0 & 0 & 0 & 0 & 0 \end{bmatrix} \tag{4.38}$$

As can be readily seen from equations (4.38) and (4.36) the second (engine speed) and seventh (filtered manifold pressure) rows of $\hat{\underline{F}}$ remain, for the nominal control scheme, invariant with $\underline{M}$. These two rows are, therefore, given by,

$$\begin{bmatrix} \hat{f}_2 \\ \hline \hat{f}_7 \end{bmatrix} = \begin{bmatrix} f_2 \\ \hline f_7 \end{bmatrix} (\underline{I}+\Delta\underline{G}_M)_{\text{NOMINAL}} \tag{4.39}$$

and, at dc,

$$\begin{bmatrix} \hat{f}_2 \\ \hline \hat{f}_7 \end{bmatrix} = \begin{bmatrix} 23.6 & -288.6 & 783.5 & 10.5 \\ 2.18 & 16.18 & -19.34 & -0.2717 \end{bmatrix} (\underline{I}+\Delta\underline{G}_M)_{\text{NOMINAL}}$$

$\hat{f}_i$ - i'th row of $\hat{\underline{F}}$

For the LQG controller pictured in Figure 4.7 the controller nullspace is characterized by the vectors,

$$\underline{N}(\underline{H}) = \begin{bmatrix} 1 & 0 & 0 \\ 0 & 0 & 0.00886 \\ 0 & 1 & 0 \\ 0 & 0 & 0.0005 \\ 0 & 0 & 0.0002 \\ 0 & 0 & 1.0000 \\ 0 & 0 & 0.0004 \end{bmatrix} \tag{4.40}$$

which indicates that a change of 1 RPM in the second (engine speed) column of equation (4.36) would require a simultaneous change of 113 Nm in the sixth (filtered torque) column. Nominally a change of 1 RPM requires only a 0.061 Nm change in brake torque. Physically the car cannot pull 113 Nm of torque for a 1 RPM change in engine speed under these operating conditions. Ruling this improbable occurence out also results in the class of all LQG controlled second and seventh rows of $\hat{\underline{F}}$ being invariant with $\underline{M}$ and equation (4.39) holds for both the nominal and LQG controllers.

For this dc gain analysis the important parameter turns out to be the last entry in the first row of (4.39), the forward path steady state gain from spark advance to engine speed. For the assumed model, $\underline{F}$, this gain is 10.5 Nm/degree. The nominally controlled multiplicative perturbation would require a real gain of 108 Nm/degree while the LQG controlled system would require a similar gain of 62.8 Nm/degree. In either case the required variation is extreme (almost an order of magnitude), especially since the dc gain from spark advance to engine

speed is easily determined and not much error is expected in that value.

Summarizing this directional argument, the required multiplicative variation was first calculated using (4.16). The loop gain was found from Figure 4.10 and the class of all engine "truth models" which would result in this gain was characterized by equation (4.36), assuming that the controller, $\underline{H}$, had no uncertainty.

Finally, order of magnitude errors in the dc gain from spark advance to engine speed were demonstrated as requirements for the truth model, $\hat{\underline{F}}$, to result in this unstable loop gain. This direction is classified as "implausible" since these order of magnitude changes are deemed unlikely and the -18 db low frequency singular values are not catastrophic. Recall from the previous discussion, however, that there is a possibility of the existence of a "plausible" direction with a slightly larger singular value. This singular value analysis can only find the one worst direction.

Referring again to Figure 4.8; approximately 0.1 Hz and above the required destabilizing perturbation must have a norm around -10 db, significantly higher than the required dc values. In all cases the LQG controller is at least as robust as the nominal controller. In the high frequencies, 2 to 10 Hz, the singular values take a sharp turn upward requiring minimum norm perturbations as high as +10 db before incipient instability. This is especially desirable behavior since the imposition of a half engine speed model cutoff frequency in

Chapter II makes the plant model least accurate in these high frequencies.

In the 4 to 10 Hz region the LQ controller with theoretical full state feedback is less robust, in this singular value sense, than the implementable LQG system with state estimation. This result is also not surprising since state reconstructors with appropriate gains can add more rolloff at high frequencies. This is the case in the engine example as is readily verified by plotting the forward path frequency response matrix (the plant-controller- A/D - D/A combination), $G(j\omega)$, for both cases. Although the numerical results are too cumbersome for inclusion here suffice it to say that, in general, the LQG Bode plots roll off in the 1-2 Hz region while the LQ responses are flat out to the 8-10 Hz region. The LQ system, therefore, has enough gain at these high frequencies to be susceptible, in this robustness sense, to a smaller norm destabilizing perturbation.

4.3.4 LQ Robustness Margins

The well known linear quadratic robustness guarantees exist in the LQ and LQG control loops at the points marked xx in Figures 4.6 and 4.7. Although this point is not too interesting on physical grounds, since natural uncertainties enter the system at the points marked x in these figures, it is worthwhile to adopt a pedantic perspective for a moment and verify the LQ guarantees at these points. Of course the

inclusion of a hybrid system with A/D and D/A converters nullifies the hard singular value guarantees (multiplicative -6 db, additive 0 db) for the LQ case and there are no LQG guarantees; still it is interesting to investigate these effects on the analysis.

Figure 4.11 presents the singular value diagrams, both additive and multiplicative, for the LQ and LQG controllers. Except for the 4.36 Hz region, where the LQ system falls just below the 0 and -6 db points, the guaranteed specifications are easily met. In all cases the LQG robustness is comparable to the full state feedback LQ case. Again in the 4.36 Hz region the filter based LQG system is more robust than the LQ controller.

4.4 Summary

This chapter has addressed the question of system robustness from a "nearness to instability" perspective. Three separate control schemes were discussed, the conventional nominal control, the theoretic full state feedback LQ case, and the realizable LQG case, all of which were presented in Chapter III. A singular value approach was used in examining this robustness question since it best captures the simultaneous variation issue inherent in multivariable stability theory.

This approach was briefly introduced and the singular values described as a measure of the nearness to singularity of the return difference matrix. Small singular values indicate an almost unstable

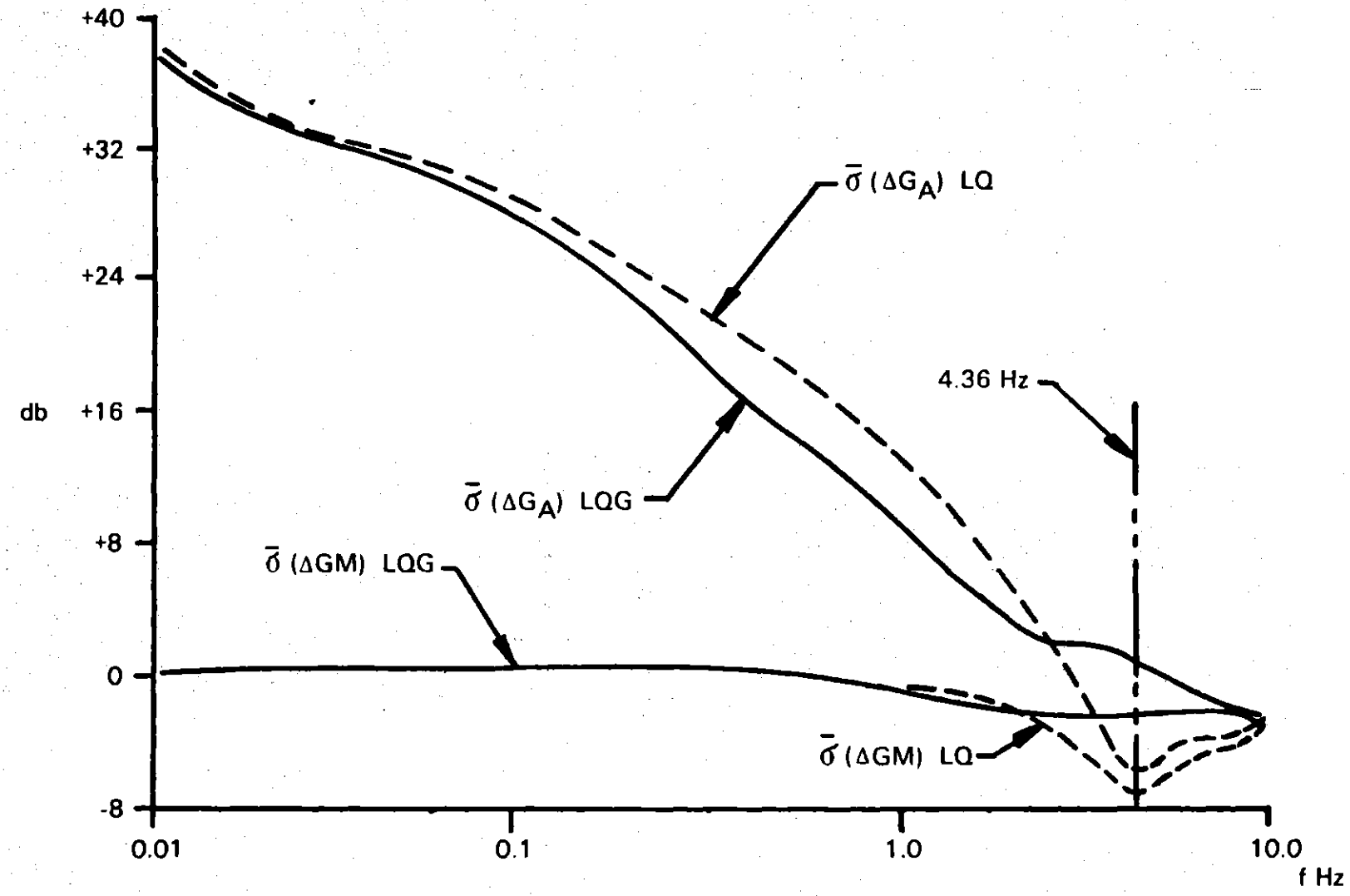

Figure 4.11: Singular Values - Loop Broken at xx

condition. Large singular values resulted from a control design which was robustly stable in every direction. This singular value approach was then applied to the engine example at hand with the results presented in Figure 4.8.

The small singular values at very low frequencies were attributed to an unlikely modelling error direction since order of magnitude gain changes would be required in the spark advance - engine speed path. There may be another more plausible direction with a slightly larger singular value, however, which is not apparent from this "one worst direction" analysis. At all frequencies the LQG controller was at least as robust as the nominal controller. Above 2 Hz the LQG case was better than the full state feedback LQ controller.

This analysis does not indicate that the LQG controller will work satisfactorily on a production automobile, but the fact that the LQG results were everywhere comparable to the nominal controller and that a plausibly sensitive direction was not revealed combines with the large singular values in the 2-10 Hz range to lend credence to the belief that this linear quadratic approach with state reconstructors can be successfully implemented.

Finally, this example graphically illustrates a major drawback of the singular value robustness theory as it exists today, i.e. its inability to see beyond the single worst perturbation direction.

Further research is required to help quantify this robustness measure when, as in this example, the worst direction can be ruled out or limited in some appropriate sense.

Chapter V will summarize the complete modelling, controller design, and robustness results for this work.

V. FINDINGS, CONCLUSIONS, RECOMMENDATIONS

" 'creative engineering' - the art of making approximation and still obtaining something that works."

Michael Athans, 1971

5.1 Introduction

The previous three chapters have addressed in detail the modelling, controller design, and robustness issues of this multivariable engine control problem. This chapter will attempt to present a brief summary of the major results or findings of this research, a synopsis of the conclusions to be drawn, and recommendations for further study.

5.2 Summary of Results - Findings

5.2.1 Engine Model

Chapter II presented a linear model for the engine - vehicle system which was intended to represent a multi-cylinder gasoline powered internal combustion engine with an automatic transmission (for torque converter slippage) about a single operating point. The engine was a 5.7L V-8 equipped with a stock cast iron divided intake manifold, electronic ignition, throttle body fuel injection, dc motor throttle control, and exhaust gas recirculation. The operating point was chosen as 48 kph (30 mph) road load. The model, as described, was intended to be accurate in the dc to half engine speed frequency range, was linear, and - to a great extent - was based upon the physical principles of

kinematics and thermodynamics.

This modelling problem was subdivided into six general areas, manifold pressure, mass transport, brake torque, engine speed, actuators, and sensors. Of these areas the most difficult to describe were the mass transport dynamics associated with the fuel and EGR flows. Physical models were presented or referenced for the pressure, air transport, torque, speed, actuator and sensor dynamics. The air-fuel-torque relationship was highly nonlinear (see Figure 2.3), necessitating the extensive use of nonlinear simulations throughout this research. Figure 2.4 presented the final Laplace transformed block diagram for this complete 18 state linearized engine model. The state equations, constant values, and dynamic system matrices were included as Appendices A, B, and C, respectively.

The discretization procedure used to obtain the discrete model required of this LQ control scheme was presented. The concept of a nominal controller which was intended to mimic the control scheme prevalent on todays production automobiles was introduced and developed. All 18 modes in this nominally controlled system were found to be completely controllable and observable, and the tight coupling between inputs and outputs was demonstrated. Finally, nonlinear Monte Carlo simulation results were presented for the nominally controlled model as Figure 2.7. This figure exhibited the type of small signal step response one might expect from an engine - vehicle system operating

around this nominal load point. A 0.4 second hesitation is seen in the torque response to even a 3% throttle command step while the air/fuel ratio leans out to 17:1. This indicates that even when the nominal control scheme schedules steady state values accurately there is still room for transient response improvement.

5.2.2 Controller Design

Chapter III first presented the motivation behind the use of this linear quadratic control approach, i.e. the inherent robustness of LQ designs (although there are no LQG robustness guarantees), the relative ease of implementation, and, from the first chapter, its natural ability to successfully address coupled system designs. The work done by Cassidy, Athans, and Lee in [3], indicating a significant improvement in the engine transient response with an LQ controller, also served to motivate this research.

A decoupled Kalman filtering scheme was used to estimate the 18 engine states from five readily obtainable engine outputs, filtered brake torque, filtered manifold pressure, throttle position, EGR position, and engine speed. The slightly sub-optimal decoupling approach resulted in less than 200 total multiplications for the complete state reconstructor implementation while an optimal 18 state Kalman filter would have required 486 multiplications. The Kalman filter noise parameters were subjectively chosen to place the filter poles in

the vicinity of the nominally controlled system's eigenvalues. The complete filter designs are included as Appendix D.

A standard LQ problem was posed and solved for an integral "washout" controller which dynamically coordinated the four engine inputs with the 18 estimated states while allowing the nominal controller to hierarchically schedule the steady state input values. A dynamic programming solution to this problem, which confirms the earlier results obtained by Lee et.al., in [32], was included as Appendix E. The quadratic weight design parameters were selected using an "output weighting versus control energy" approach with the nonlinear Monte Carlo simulations (including the state reconstructors) serving as the basis for the final weight selection. The selected numerical values for these matrices are included in Chapter III.

A command shaping filter was incorporated to regulate the frequency content of the input signals to levels commensurate with the engine's ability to physically respond. Figure 3.5 illustrated the final microprocessor based control concept complete with state reconstructors, feedback gains, nominal controls, and the shaping filter.

Figure 3.7 presented the complete nonlinear simulation results comparing the final LQG design with the baseline nominal control approach. The torque and air/fuel ratio deviation responses were dramatically improved. The hesitation seen in the nominally controlled torque response is completely eliminated by the LQG system while the

maximum LQG air/fuel deviation to the same 3% throttle step is limited to less than 1 ratio, about 15.4:1. These results are primarily obtained by immediately increasing the fuel rate (much as a conventional accelerator pump might do), coordinating the throttle movement, decreasing the rate of EGR increases, and increasing the spark advance, all of which seem like "reasonable" things to do if a smooth air/fuel and torque response is desired.

5.2.3 Robustness Analysis

Chapter IV addressed the question of the robustness of stability for the final LQG controller design. The use of the singular value multivariable robustness theory for this analysis was justified in that it seems to be the most widely accepted theory available which can readily handle such tightly coupled systems. The notion of "nearness to singularity" of the return difference matrix and the concept of direction to this closest singular point was introduced as prefatory material for the analysis presented in this chapter.

The hybrid system problem inherent in the use of microprocessor controllers for continuous systems was sidestepped by making some simplifying assumptions regarding the A/D and D/A conversion processes. Basic to these assumptions, and the concurrent accuracy of these results, is the premise that the sampling rate was sufficiently high to avoid signal aliasing by a wide margin.

The loop transfer function, or forward path gain, was calculated for the three separate control schemes, nominal, LQ, and LQG, and a computer program was used to find and plot the singular values for all three cases. Figure 4.8 presents the results of this program. The significant aspects of this plot are first that the LQG scheme has large singular values, indicating a robust design, at the high frequencies (4 to 10 Hz) where the most modelling errors are expected. Second, at all frequencies the LQG controller is comparable to or better than the baseline nominal control scheme in this singular value sense. Third that at high frequencies the LQG controller is more robust than the theoretical full state feedback case (see Appendix G), and fourth that at low frequencies all three systems are only marginally stable when viewed from this singular value perspective.

As was developed at great length in Chapter IV these small singular values at low frequencies can be misleading. Although it is true that these extremely small perturbations can drive the closed loop system unstable (as exhibited in Figure 4.9) they are in an "implausible" modelling error direction requiring spark advance to engine speed dc gain modelling errors of six times or greater.

These low frequency results help to highlight the two major drawbacks of this singular value analysis. The first is that this non-directional approach tends to be overly conservative. When an

implausible direction is flagged out as the smallest perturbation to singularity and can be ruled out very little information is really obtained. A slightly larger perturbation in a different and plausible direction might also drive the system unstable. The second is that, for examples with a plant and controller (see Figure 4.10), singular perturbations are in terms of the complete forward path gain (the plant-controller product) instead of just the plant model where most deviations are expected to occur. It is often difficult to translate these forward path gain perturbations into the class of model perturbations which would result in this same forward path gain (destabilizing) while still interpreting the result.

5.3 Conclusions

This thesis represents the culmination of a research project designed to determine the feasibility of an LQG control scheme for automotive engine control and to ready such a scheme for a test cell application. This report is the second major work to reach the same conclusion (see Casidy, Athans, and Lee [3]); Linear quadratic control with dynamic input coordination can improve driveability and diminish the air/fuel ratio deviations over conventional memoryless control schemes about a single operating point.

Unlike the previous work, however, this research goes farther in that full state feedback is not assumed (state reconstructors were designed), a discrete controller was tested, a physical model was used, and a robustness analysis conducted. The outcome of this study is still the same, even with these additions, and is that significant gains can be achieved in the systems transient performance with the use of this LQG controller.

An even stronger statement can be made with regards to the probable success of this controller since complete nonlinear Monte Carlo simulations were included (Figure 3.7) to form the basis for these conclusions. In addition, in the high frequency range (4 to 10 Hz), where the greatest modelling errors are expected, the large singular values presented in Chapter IV and reviewed in the previous section are indicative of a robustly stable control design. The small singular values at low frequencies, however, render the robustness analysis at those frequencies inconclusive and a general robustness statement cannot be made.

The use of decoupled state reconstructors and the integral control scheme resulted in a control algorithm requiring approximately 250 multiplications, readily implementable in a suitably configured micro-computer system. In addition, the use of a smaller (and consequently less accurate) system dimension could reduce this number even further at the expense of modelling accuracy. The washout integral scheme

permits the bulk of the numerical calculations to be performed after the engine inputs (the D/A converters) have been set. Only the five nominal control multiplications need to be performed between the sampling of the A/D and the setting of the D/A converters. The state reconstruction and feedback gain calculations can be performed between sampling instants, even further aiding the implementability of the proposed control scheme.

In short the final result of this research is a promising LQG controller about a single operating point which is ready for test cell implementation.

5.4 Recommendations

As with all controller designs the ultimate test is in the implementation. In this case a reasonable test for this LQG scheme about a single operating point is to implement the controller (essentially Figure 3.5) in a computer controlled test cell environment and compare the real LQG controlled engine responses in this operating region with baseline nominal controllers. Prior to this implementation a confirmation of the dc gains at the operating point would seem appropriate since the robustness analysis indicates a potential for instability at low frequencies, as seen in Figure 4.8. The actuator and sensor model parameters included here are for a specific test site and must be

chosen to best describe the actual hardware used in the implementation. The quadratic weighting matrix selection included is for a ballpark torque - air/fuel ratio response and may, of course, be tailored to the specific engine - vehicle design objectives. The results obtained so far are encouraging and actual test data, if even at this single operating point, would be useful confirmation of these simulation studies. It is to obtain this confirmation that a test cell implementation program is recommended at this time.

Further recommendations for the development of more linear models, controllers, and controller scheduling would seem more suitable when this single operating point control scheme has been successfully demonstrated in the test cell.

There are, of course, some spinoff recommendations relating to the general singular value multivariable robustness theory and its use for analyzing linear systems. The two major drawbacks to this theory were highlighted in this report. They are,

- the non-directional limits inherent in this analysis tend to result in overly conservative robustness results since implausible error directions cannot be quantified
- for this plant-controller combination perturbation limits are in terms of the forward path gain instead of only plant modelling errors.

Much research has yet to be done in this multivariable robustness field in general, and specifically the singular value applications to this field, before it can be said to be a well developed analysis/ design tool. Although it can be useful even now it will be even more so when these two major drawbacks are better understood.

Finally, as pretroleum products become more expensive and emission constraints more stringent every control design tool and engineering resource available to the automotive industry will be focused on this dynamic input coordination problem. When literally millions of units are built each year the potential savings are too great for even a single theory to remain unresearched. Even if the LQG concept proposed here never finds its way into production automobiles, though all of the first indications are favorable, this research and testing still should offer valuable insight into this complex and difficult problem.

APPENDIX A

MODEL EQUATIONS

A. MODEL EQUATIONS

This appendix develops the actual state equations, in continuous time, used to develop the engine model referenced throughout this thesis, i.e. the $\underline{A}$, $\underline{B}$, $\underline{C}$, and $\underline{D}$ matrices. Figure 2.4 forms the starting place for this appendix.

Define the following two vectors,

$$\delta\underline{u} = \begin{bmatrix} \delta\alpha_c \\ \delta E_c \\ \delta F_c \\ \delta S_c \end{bmatrix} \begin{array}{l} \text{perturbed throttle command (\%)} \\ \text{perturbed EGR valve command (volts)} \\ \text{perturbed fuel command (volts)} \\ \text{perturbed spark advance (degrees)} \end{array}$$

$$\delta\underline{x} = \begin{array}{ll} \delta x_1 & \text{manifold pressure} \\ \left.\begin{array}{l}\delta x_2 \\ \delta x_3 \\ \delta x_4\end{array}\right\} & \text{EGR} \\ \delta x_5 & \text{fuel rate} \\ \left.\begin{array}{l}\delta x_6 \\ \delta x_7\end{array}\right\} & \text{Pade time delay approximation} \\ \left.\begin{array}{l}\delta x_8 \\ \delta x_9\end{array}\right\} & \text{Engine speed} \\ \left.\begin{array}{l}\delta x_{10} \\ \delta x_{11}\end{array}\right\} & \text{throttle actuator} \\ \left.\begin{array}{l}\delta x_{12} \\ \delta x_{13}\end{array}\right\} & \text{EGR actuator} \\ \left.\begin{array}{l}\delta x_{14} \\ \delta x_{15}\end{array}\right\} & \text{manifold pressure filter} \\ \left.\begin{array}{l}\delta x_{16} \\ \delta x_{17} \\ \delta x_{18}\end{array}\right\} & \text{torque filter} \end{array}$$

Let the delay differential system depicted in Figure 2.4 be approximated by a finite dimensional differential system where the following second order Padé approximant is used to represent the unilateral Laplace transformed time delay, τ,

$$e^{-\tau s} \simeq \frac{12-6\tau s + \tau^2 s^2}{12+6\tau s + \tau^2 s^2} \tag{A.1}$$

Using Figure 2.4 and beginning with the manifold pressure dynamics,

$$\delta P_m = \frac{\alpha_1}{s+\alpha_1}\left(k_8\delta N + k_7\left[\delta\dot{m}_{\substack{air\\in}} + \delta\dot{m}_{\substack{EGR\\in}} + k_9\delta\dot{m}_{\substack{fuel\\in}}\right]\right) \tag{A.2}$$

From a linearized (2.4), (2.5), and (2.6) of this text,

$$\delta\dot{m}_{\substack{air\\in}} = k_1\delta\alpha_p + k_2\delta P_m \tag{A.3}$$

$$\delta\dot{m}_{\substack{EGR\\in}} = k_5\delta E_p + k_6\delta P_m \tag{A.4}$$

$$\delta\dot{m}_{\substack{fuel\\in}} = k_3\delta F_c + k_4\delta N \tag{A.5}$$

Finally, substituting the above definitions into equation (A.2) and reverting to the time domain,

$$\dot{\delta x}_1 = [-\alpha_1 + \alpha_1 k_7 k_2 + \alpha_1 k_7 k_6]\delta x_1 + [\alpha_1 k_8 + \alpha_1 k_7 k_9 k_4]\delta x_8 + \alpha_1 k_7 k_1 \delta x_{11} + \alpha_1 k_7 k_5 \delta x_{13} + \alpha_1 k_7 k_9 k_3 \delta F_c \tag{A.6}$$

The third order EGR-torque dynamics can be written as,

$$\delta E = \left(\frac{\alpha_5 \alpha_7^2}{(s^2+2\alpha_8\alpha_7 s+\alpha_7^2)(s+\alpha_5)}\right)\left(k_5 \delta E_p + k_6 \delta P_m\right) \tag{A.7}$$

$$\delta E \triangleq \delta x_4$$

and a state space realization becomes,

$$\begin{bmatrix} \dot{\delta x}_2 \\ \dot{\delta x}_3 \\ \dot{\delta x}_4 \end{bmatrix} = \begin{bmatrix} -2\alpha_8\alpha_7 & -\alpha_7^2 & 0 \\ 1 & 0 & 0 \\ 0 & \alpha_5 & -\alpha_5 \end{bmatrix} \begin{bmatrix} \delta x_2 \\ \delta x_3 \\ \delta x_4 \end{bmatrix} + \begin{bmatrix} \alpha_7^2 k_6 \\ 0 \\ 0 \end{bmatrix} \delta x_1 + \begin{bmatrix} \alpha_7^2 k_5 \\ 0 \\ 0 \end{bmatrix} \delta x_{13} \tag{A.8}$$

Similarly, for the fuel-torque dynamics,

$$\dot{\delta m}_{\substack{\text{fuel} \\ \text{cyl}}} = \left(\frac{\alpha_6}{s+\alpha_6}\right) \dot{\delta m}_{\substack{\text{fuel} \\ \text{in}}} \tag{A.9}$$

$$\dot{\delta x}_5 = -\alpha_6 \delta x_5 + \alpha_6 k_4 \delta x_8 + \alpha_6 k_3 \delta F_c \tag{A.10}$$

For the Pade approximant to the engine time delay let the indicated torque, δT_i, be given as,

$$\delta T_i \triangleq k_{12}\delta k_4 + k_{13}\delta x_5 + k_{11}k_{18}\delta P_m + k_{11}k_{17}\delta N$$
$$+ k_{14}\delta P_m - k_{11}\delta x_4 - k_{11}\delta x_5$$

$$\delta T_i = (k_{12}-k_{11})\delta x_4 + (k_{13}-k_{11})\delta x_5 + (k_{14}+k_{11}k_{18})\delta P_m + k_{11}k_{17}\delta N \tag{A.11}$$

Then following the procedure outlined in reference [34],

$$\delta T_d \triangleq \frac{12-6Ts + T^2s^2}{12+6T_s + T^2s^2}\,\delta T_i \tag{A.12}$$

$$\begin{bmatrix}\delta\dot{x}_6\\ \delta\dot{x}_7\end{bmatrix} = \begin{bmatrix}0 & 1\\ -12/T^2 & -6/T\end{bmatrix}\begin{bmatrix}\delta x_6\\ \delta x_7\end{bmatrix} + \begin{bmatrix}-12/T\\ 72/T^2\end{bmatrix}\delta T_i \tag{A.13}$$

$$\delta T_d = \delta x_6 + \delta T_i \tag{A.14}$$

$$\delta T_d = \delta x_6 + (k_{12}-k_{11})\delta x_4 + (k_{13}-k_{11})\delta x_5$$
$$+ (k_{14}+k_{11}k_{18})\delta P_m + k_{11}k_{17}\delta N \tag{A.15}$$

From Figure 2.4 the brake torque is seen to be,

$$\delta T_b = \delta T_d + k_{16}\delta N + k_{15}\delta S_c \tag{A.16}$$

$$\delta T_b = \delta x_6 + (k_{12}-k_{11})\delta x_4 + (k_{13}-k_{11})\delta x_5 + (k_{14}+k_{11}k_{18})\delta x_1 + (k_{11}k_{17}+k_{16})\delta x_8 + k_{15}\delta S_c \tag{A.17}$$

With this brake torque expression the torque-speed dynamics become,

$$\delta N = \left(\frac{k_{10}\,\dfrac{\alpha_3\alpha_4}{\alpha_2}\,(s+\alpha_2)}{s^2 + (\alpha_3+\alpha_4)s+\alpha_3\alpha_4} \right)\delta T_b \tag{A.18}$$

$$\begin{bmatrix} \delta\dot{x}_8 \\ \delta\dot{x}_9 \end{bmatrix} = \begin{bmatrix} 0 & 1 \\ -\alpha_3\alpha_4 & -(\alpha_3+\alpha_4) \end{bmatrix} \begin{bmatrix} \delta x_8 \\ \delta x_9 \end{bmatrix} + \begin{bmatrix} k_{10}\,\dfrac{\alpha_3\alpha_4}{\alpha_2} \\ \\ k_{10}\alpha_3\alpha_4 - k_{10}\,\dfrac{\alpha_3\alpha_4}{\alpha_2}\,(\alpha_3+\alpha_4) \end{bmatrix} \delta T_b \tag{A.19}$$

and with the following definitions,

$$\delta N \triangleq \delta x_8 \qquad \sigma \triangleq \frac{k_{10}\alpha_3\alpha_4}{\alpha_2} \qquad \gamma = k_{10}\alpha_3\alpha_4 - \frac{k_{10}\alpha_3\alpha_4}{\alpha_2}\left(\alpha_3+\alpha_4\right)$$

(A.17) in (A.19) yields the final result,

$$\begin{aligned}\delta\dot{x}_8 = {} & \sigma(k_{14}+k_{11}k_{18})\delta x_1 + \sigma(k_{13}-k_{11})\delta x_5 + \sigma(k_{12}-k_{11})\delta x_4 \\ & + \sigma\delta x_6 + \sigma(k_{11}k_{17}+k_{16})\delta x_8 + \delta x_9 + \sigma k_{15}\delta S_c\end{aligned} \tag{A.20}$$

$$\begin{aligned}\delta\dot{x}_9 = {} & \gamma(k_{14}+k_{11}k_{18})\delta x_1 + \gamma(k_{13}-k_{11})\delta x_5 + \gamma(k_{12}-k_{11})\delta x_4 \\ & + \gamma\delta x_6 + [\gamma(k_{11}k_{17}+k_{16})-\alpha_3\alpha_4]\delta x_8 \\ & - (\alpha_3+\alpha_4)\delta x_9 + \gamma k_{15}\delta S_c\end{aligned} \tag{A.21}$$

The throttle actuator is modelled as a second order system,

$$\delta\alpha_p = \left(\frac{\alpha_9^2}{s^2 + 2\alpha_9\alpha_{10}s + \alpha_9^2}\right)\delta\alpha_c$$

$$\begin{bmatrix}\delta\dot{x}_{10} \\ \delta\dot{x}_{11}\end{bmatrix} = \begin{bmatrix}-2\alpha_9\alpha_{10} & -\alpha_9^2 \\ 1 & 0\end{bmatrix}\begin{bmatrix}\delta x_{10} \\ \delta x_{11}\end{bmatrix} + \begin{bmatrix}\alpha_9^2 \\ 0\end{bmatrix}\delta\alpha_c \tag{A.22}$$

$$\delta x_{11} \triangleq \delta\alpha_p$$

The EGR actuator is also modelled as a second order system,

$$\delta E_p = \left(\frac{\alpha_{11}^2}{s^2 + 2\alpha_{11}\alpha_{12}s + \alpha_{11}^2} \right) \delta E_c$$

$$\begin{bmatrix} \dot{\delta x}_{12} \\ \dot{\delta x}_{13} \end{bmatrix} = \begin{bmatrix} -2\alpha_{12}\alpha_{11} & -\alpha_{11}^2 \\ 1 & 0 \end{bmatrix} \begin{bmatrix} \delta x_{12} \\ \delta x_{13} \end{bmatrix} + \begin{bmatrix} \alpha_{11}^2 \\ 0 \end{bmatrix} \delta E_c \qquad \text{(A.23)}$$

$$\delta x_{13} \triangleq \delta E_p$$

For most digital control applications the noisy torque and pressure signals must be filtered to avoid aliasing. Two standard filters readily available in the test cell where the data was collected were found acceptable for this purpose. For manifold pressure,

$$\delta P_f = \left(\frac{\alpha_{13}^2}{(s+\alpha_{13})^2} \right) \delta P_m$$

$$\begin{bmatrix} \dot{\delta x}_{14} \\ \dot{\delta x}_{15} \end{bmatrix} = \begin{bmatrix} -\alpha_{13} & \alpha_{13} \\ 0 & \alpha_{13} \end{bmatrix} \begin{bmatrix} \delta x_{14} \\ \delta x_{15} \end{bmatrix} + \begin{bmatrix} 0 \\ \alpha_{13} \end{bmatrix} \delta x_1 \qquad \text{(A.24)}$$

$$\delta P_f = \delta x_{14}$$

and, for brake torque,

$$\delta T_f = \left(\frac{\alpha_{15}^2 \alpha_{14}}{(s+\alpha_{14})(s^2+2\alpha_{15}\alpha_{16}s+\alpha_{15}^2)} \right) \delta T_b$$

$$\begin{bmatrix} \dot{\delta x}_{16} \\ \dot{\delta x}_{17} \\ \dot{\delta x}_{18} \end{bmatrix} = \begin{bmatrix} -\alpha_{14} & \alpha_{14} & 0 \\ 0 & 0 & 1 \\ 0 & -\alpha_{15}^2 & -2\alpha_{15}\alpha_{16} \end{bmatrix} \begin{bmatrix} \delta x_{16} \\ \delta x_{17} \\ \delta x_{18} \end{bmatrix} + \begin{bmatrix} 0 \\ 0 \\ \alpha_{15}^2 \end{bmatrix} \delta T_b \qquad \text{(A.25)}$$

$$\delta T_f = \delta x_{16}$$

The parameter values are included in Appendix B of this report. Equations (A.6), (A.8), (A.10), (A.13), (A.19), (A.22)-(A.25) can be concatenated to form the 18 state continuous time system described in equation (2.3).

APPENDIX B

CONSTANTS

APPENDIX B: CONSTANTS

This appendix presents the numerical values for the nominal conditions and the constants used throughout this text.

NOMINAL CONDITIONS

5.7 L V-8
Divided cast iron intake manifold
Equipped with Throttle Body Fuel Injection (TBFI)
and Exhaust Gas Recirculation (EGR)

Nominal operating point, χ,

Brake Torque	T_b	67	N_m
Engine Speed	N	1200	RPM
Manifold Pressure	P_m	43.7	kP_a
Air Rate	$\dot{m}_{air}$	16.79	g/s
Fuel Rate	$\dot{m}_{fuel}$	1.15	g/s
EGR Rate	$\dot{m}_{EGR}$	1.8	(based on torque)
Air/Fuel Ratio	AF	14.6:1	
Throttle Position	α_p	17%	
EGR Command	E_c	1.93 Volts	
Fuel Command	F_c	1.35 Volts	
Spark Advance	S	40° BTDC	
Exhaust Temperature	T_{exh}	400°c	

Exhaust Pressure	P_{exh}	102.3 kP_a
Manifold Temperature	T_{man}	35°c
Ambient Temperature	T_o	22.8°c
Ambient Pressure	P_o	101.3 kP_a
Engine Efficiency	η	0.70

CONSTANT PARAMETER VALUES

The model parameters presented here are empirical except where indicated. The empirical results were used in the simulations.

k_1	throttle angle to air rate gain	1.72 g/s/%
k_2	manifold pressure to air rate gain	0.0 g/s/kPa
k_3	fuel command to fuel rate gain	0.72 g/s/Volt
	calculated from reference [15]	0.85
k_4	engine speed to fuel rate gain	942×10^{-6} g/s/RPM
	calculated from reference [15]	958×10^{-6}
k_5	EGR pintle to EGR flow gain	5.38 g/s/Volt
k_6	manifold pressure to EGR flow gain	0.0 g/s/Volt
k_7	mass flow to pressure gain	1.62 kPa/g/s
	calculated from reference [15]	1.75
k_8	engine speed to pressure gain	-0.0271 kPa/RPM
	calculated from reference [15]	-0.0255

k_9	"ideal gas" fraction of fuel rate	0.80
k_{10}	torque-speed gain	$16.3^{RPM/N_m}$
k_{11}	air-torque gain	$-2.05\ ^{N_m/g/s}$
k_{12}	EGR-torque gain	$-9.11\ N_m/g/s$
k_{13}	fuel-torque gain	$110.8\ ^{N_m/g/s}$
k_{14}	manifold pressure-torque gain	$2.07\ ^{N_m/kP_a}$
k_{15}	spark advance-torque gain	$1.10\ ^{N_m/deg}$
k_{16}	speed-torque gain	$-0.093\ ^{N_m/RPM}$
k_{17}	speed-cylinder air rate gain (from equation (2.11))	$0.0165\ ^{g/s}/_{RPM}$
k_{18}	manifold pressure to cylinder air rate gain (from equation (2.11))	$0.577\ ^{g/s}/_{kPa}$
η^*	wide open throttle volumetric efficiency	0.81
η	volumetric efficiency	0.70
τ	engine sample time delay (from equation (2.21))	0.0375 sec
α_1	manifold pressure pole (from equation (2.10))	$15.2\ ^{rad/sec}$ 18.0
α_2	torque-speed zero	$1.26\ ^{rad/sec}$
α_3	torque-speed pole 1	$0.0318\ ^{rad/sec}$
α_4	torque-speed pole 2	$10.7\ ^{rad/sec}$
α_5	EGR-torque pole	$19.5\ ^{rad/sec}$

α_6	fuel-torque pole	4.56 $^{rad}/_{sec}$
α_7	EGR resonant frequency	30.7 $^{rad}/_{sec}$
α_8	EGR damping ratio	0.169
α_9	throttle actuator resonant frequency	10.0 $^{rad}/_{sec}$
α_{10}	throttle actuator damping ratio	0.707
α_{11}	EGR actuator resonant frequency	89.2 $^{rad}/_{sec}$
α_{12}	EGR actuator damping ratio	0.89
α_{13}	vacuum filter poles	67 $^{rad}/_{sec}$
α_{14}	torque filter pole	26.7 $^{rad}/_{sec}$
α_{15}	torque filter resonant frequency	54.4 $^{rad}/_{sec}$
α_{16}	torque filter damping ratio	0.438
k	ratio of specific heats	1.36
r	compression ratio	8:1
D	engine displacement	5.74×10^{-3} m^3
V_m	manifold volume	2.8×10^{-3} m^3
C_1	engine speed-EGR command	0.0005 $^{Volts}/_{RPM}$
C_2	manifold pressure-EGR command	0.015 $^{Volts}/_{kPa}$
C_3	engine speed-spark advance	0.010 $^{deg}/_{RPM}$
C_4	manifold pressure-spark advance	-0.300 $^{deg}/_{kPa}$
C_7	manifold pressure-fuel command	0.04478 $^{Volts}/_{kPa}$
C'	$\left.\frac{\partial P_e}{\partial P_m}\right\|_{\chi}$	0.07

APPENDIX C

Matrices

Matrices

In this appendix the actual numerical values for the pertinent matrices referenced in Chapters II and III are presented.

From Equation (2.3) we have,

$$\begin{aligned} \delta\dot{\underline{x}} &= \underline{A}\delta\underline{x} + \underline{B}\delta\underline{u} \\ \delta\underline{y} &= \underline{C}\delta\underline{x} + \underline{D}\delta\underline{u} \end{aligned} \tag{C.1}$$

where the matrices $\underline{A}$, $\underline{B}$, $\underline{C}$, and $\underline{D}$ were developed in Appendix A.

The state and control vectors were defined in Appendix A. The output vector is given as,

$$\delta\underline{y} = \begin{bmatrix} \delta T_b \\ \delta N \\ \delta P_m \\ \delta \alpha_p \\ \delta E_p \\ \delta T_f \\ \delta P_f \end{bmatrix}$$

δT_b — brake torque (Nm)
δN — engine speed (RPM)
δP_m — manifold pressure, intake (kPa)
$\delta \alpha_p$ — throttle position (%)
δE_p — EGR pintle position (volts)
δT_f — filtered brake torque (Nm)
δP_f — filtered manifold pressure (kPa)

The nominal controller was defined in Chapter II as,

$$\delta\underline{\tilde{u}} = \underline{P}\delta\underline{y} \tag{C.2}$$

The linear quadratic control developed in Chapter III is given as,

$$\delta\underline{v} = -\begin{bmatrix} \underline{G}_x & \underline{G}_u \end{bmatrix} \begin{bmatrix} \delta\underline{\hat{x}} \\ \delta\underline{u}^* \end{bmatrix} \tag{C.3}$$

$$\delta\underline{v}(k) = \delta\underline{u}^*(k+1) - \delta\underline{u}^*(k)$$

The DC gains for the open loop system are,

$$\underline{F}_{ol} = \underline{C}(-\underline{A})^{-1}\underline{B} + \underline{D} \tag{C.4}$$

and for the nominally controlled system,

$$\underline{F}_{nom} = (\underline{C} + \underline{D}\underline{P}\underline{C})(-\underline{A} - \underline{B}\underline{P}\underline{C})^{-1}\underline{B} + \underline{D} \tag{C.5}$$

The eigenvalues presented here are given by the solutions to,

$$\text{Open Loop} \qquad \det(\lambda\underline{I} - \underline{A}) = 0 \tag{C.6}$$

$$\text{Nominal Control} \qquad \det(\lambda\underline{I} - \underline{A} - \underline{B}\underline{P}\underline{C}) = 0 \tag{C.7}$$

$$\text{LQ Control} \qquad \frac{1}{\Delta}\ell n\{\det(\lambda\underline{I} - \underline{A}_{cl}) = 0\} \tag{C.8}$$

where,

$$\underline{A}_{cl} \triangleq \begin{bmatrix} \hat{\underline{A}}+\hat{\underline{B}}\underline{P}\underline{C} & \hat{\underline{B}} \\ -\underline{G}_x & \underline{I}-\underline{G}_u \end{bmatrix}$$

and $\hat{A}$, $\hat{B}$ are the discrete matrices given in Chapter II as,

$$\hat{\underline{A}} \triangleq e^{\underline{A}\Delta} \qquad\qquad \hat{\underline{B}} \triangleq \int_0^{\Delta} e^{\underline{A}(\Delta - \tau)}\underline{B}d\tau$$

$$\Delta = 0.020$$

and the natural log is used in (C.8) to reflect the discrete eigenvalues into their continuous counterparts (this natural log transformation is not unique so the unaliased continuous form is used).

Finally, the controllability and observability matrices were defined in Chapter II as,

$$\underline{\Psi} = \text{Controllability Matrix} = \underline{YB} \tag{C.9}$$

$$\underline{\Gamma} = \text{Observability Matrix} = \underline{CX} \tag{C.10}$$

where Y and X are the matrices of the suitably normalized left and right eigenvectors of the nominally controlled system matrix ($\underline{A} + \underline{BPC}$).

Numerical values for these matrices are included in this section.

	1	2	3	4	5	6	7	8	9	10	11	12	13	14	15	16	17	18
1	-15.20	0.0	0.0	0.0	0.0	0.0	0.0	-.3934	0.0	0.0	42.35	0.0	132.5	0.0	0.0	0.0	0.0	0.0
2	0.0	-10.38	-942.5	0.0	0.0	0.0	0.0	0.0	0.0	0.0	0.0	0.0	5071.0	0.0	0.0	0.0	0.0	0.0
3	0.0	1.0	0.0	0.0	0.0	0.0	0.0	0.0	0.0	0.0	0.0	0.0	0.0	0.0	0.0	0.0	0.0	0.0
4	0.0	0.0	19.48	-19.48	0.0	0.0	0.0	0.0	0.0	0.0	0.0	0.0	0.0	0.0	0.0	0.0	0.0	0.0
5	0.0	0.0	0.0	0.0	-4.56	0.0	0.0	0.0043	0.0	0.0	0.0	0.0	0.0	0.0	0.0	0.0	0.0	0.0
6	-284.0	0.0	0.0	2258.	-36110.	0.0	1.0	10.84	0.0	0.0	0.0	0.0	0.0	0.0	0.0	0.0	0.0	0.0
7	45440.0	0.0	0.0	-3.6d5	5.8d6	-8533.	-160.	-1734.	0.0	0.0	0.0	0.0	0.0	0.0	0.0	0.0	0.0	0.0
8	3.927	0.0	0.0	-31.23	499.3	4.425	0.0	-.5613	1.0	0.0	0.0	0.0	0.0	0.0	0.0	0.0	0.0	0.0
9	-37.13	0.0	0.0	295.3	-4722.	-41.84	0.0	4.967	-10.71	0.0	0.0	0.0	0.0	0.0	0.0	0.0	0.0	0.0
10	0.0	0.0	0.0	0.0	0.0	0.0	0.0	0.0	0.0	-14.14	-100.	0.0	0.0	0.0	0.0	0.0	0.0	0.0
11	0.0	0.0	0.0	0.0	0.0	0.0	0.0	0.0	0.0	1.0	0.0	0.0	0.0	0.0	0.0	0.0	0.0	0.0
12	0.0	0.0	0.0	0.0	0.0	0.0	0.0	0.0	0.0	0.0	0.0	-158.8	-7957.	0.0	0.0	0.0	0.0	0.0
13	0.0	0.0	0.0	0.0	0.0	0.0	0.0	0.0	0.0	0.0	0.0	1.0	0.0	0.0	0.0	0.0	0.0	0.0
14	0.0	0.0	0.0	0.0	0.0	0.0	0.0	0.0	0.0	0.0	0.0	0.0	0.0	-67.0	67.0	0.0	0.0	0.0
15	67.0	0.0	0.0	0.0	0.0	0.0	0.0	0.0	0.0	0.0	0.0	0.0	0.0	0.0	-67.0	0.0	0.0	0.0
16	0.0	0.0	0.0	0.0	0.0	0.0	0.0	0.0	0.0	0.0	0.0	0.0	0.0	0.0	0.0	-26.73	26.73	0.0
17	0.0	0.0	0.0	0.0	0.0	0.0	0.0	0.0	0.0	0.0	0.0	0.0	0.0	0.0	0.0	0.0	0.0	1.0
18	2628.0	0.0	0.0	-2.1d4	3.34d5	2962.	0.0	-375.7	0.0	0.0	0.0	0.0	0.0	0.0	0.0	0.0	-2962.	-47.66

The Continuous Time A Matrix

ROW 1	0.0	0.0	14.18	0.0
ROW 2	0.0	0.0	0.0	0.0
ROW 3	0.0	0.0	0.0	0.0
ROW 4	0.0	0.0	0.0	0.0
ROW 5	0.0	0.0	3.283	0.0
ROW 6	0.0	0.0	0.0	0.0
ROW 7	0.0	0.0	0.0	0.0
ROW 8	0.0	0.0	0.0	4.867
ROW 9	0.0	0.0	0.0	-46.02
ROW 10	100.0	0.0	0.0	0.0
ROW 11	0.0	0.0	0.0	0.0
ROW 12	0.0	7957.0	0.0	0.0
ROW 13	0.0	0.0	0.0	0.0
ROW 14	0.0	0.0	0.0	0.0
ROW 15	0.0	0.0	0.0	0.0
ROW 16	0.0	0.0	0.0	0.0
ROW 17	0.0	0.0	0.0	0.0
ROW 18	0.0	0.0	0.0	3258.0

The Continuous Time B Matrix

	1	2	3	4	5	6	7	8	9	10	11	12	13	14	15	16	17	18
1	0.8874	0.0	0.0	-7.058	112.9	1.0	0.0	-.1269	0.0	0.0	0.0	0.0	0.0	0.0	0.0	0.0	0.0	0.0
2	0.0	0.0	0.0	0.0	0.0	0.0	0.0	1.0	0.0	0.0	0.0	0.0	0.0	0.0	0.0	0.0	0.0	0.0
3	1.0	0.0	0.0	0.0	0.0	0.0	0.0	0.0	0.0	0.0	0.0	0.0	0.0	0.0	0.0	0.0	0.0	0.0
4	0.0	0.0	0.0	0.0	0.0	0.0	0.0	0.0	0.0	0.0	1.0	0.0	0.0	0.0	0.0	0.0	0.0	0.0
5	0.0	0.0	0.0	0.0	0.0	0.0	0.0	0.0	0.0	0.0	0.0	0.0	1.0	0.0	0.0	0.0	0.0	0.0
6	0.0	0.0	0.0	0.0	0.0	0.0	0.0	0.0	0.0	0.0	0.0	0.0	0.0	0.0	0.0	1.0	0.0	0.0
7	0.0	0.0	0.0	0.0	0.0	0.0	0.0	0.0	0.0	0.0	0.0	0.0	0.0	1.0	0.0	0.0	0.0	0.0

The Continuous Time C Matrix

ROW 1	0.0	0.0	0.0	0.0	1.0
ROW 2	0.0	0.0	0.0	0.0	0.0
ROW 3	0.0	0.0	0.0	0.0	0.0
ROW 4	0.0	0.0	0.0	0.0	0.0
ROW 5	0.0	0.0	0.0	0.0	0.0
ROW 6	0.0	0.0	0.0	0.0	0.0
ROW 7	0.0	0.0	0.0	0.0	0.0

The Continuous Time D Matrix

$$\underline{P} = \begin{bmatrix} 0 & 0 & 0 & 0 & 0 & 0 & 0 \\ 0 & 0.0005 & 0 & 0 & 0 & 0 & 0.015 \\ 0 & 0 & 0 & 0 & 0 & 0 & 0.04478 \\ 0 & 0.010 & 0 & 0 & 0 & 0 & -0.300 \end{bmatrix}$$

Nominal Control Feedback Matrix

$$\underline{F}_{ol} = \begin{bmatrix} 1.446 & -17.68 & 47.98 & 0.6431 \\ 23.60 & -288.60 & 783.5 & 10.500 \\ 2.176 & 16.18 & -19.3 & -.2717 \\ 1.000 & 0 & 0 & 0 \\ 0 & 1.000 & 0 & 0 \\ 1.446 & -17.68 & 47.98 & 0.6431 \\ 2.176 & 16.18 & -19.3 & -.2717 \end{bmatrix}$$

Open Loop DC Gain Matrix

$$\underline{F}_{nom} = \begin{bmatrix} 4.062 & 0.0750 & 28.39 & 0.3659 \\ 66.33 & 1.2240 & 463.60 & 5.9750 \\ 1.642 & 10.500 & -10.93 & -.1554 \\ 1.000 & 0 & 0 & 0 \\ 0 & 1.000 & 0 & 0 \\ 4.062 & 0.0750 & 28.39 & 0.3659 \\ 1.642 & 10.500 & -10.93 & -.1554 \end{bmatrix}$$

Closed Loop DC Gain Matrix

ROW 1	2.346d-01	-5.591d-03	1.564d-01	-1.430d-01	-9.754d+00	-9.011d-04	-5.409d-06	-1.160d-02
	-1.833d-05	1.614d-01	2.939d+00	-1.880d-04	-2.060d-02	-3.464d-02	-1.441d-02	0.0
	0.0	0.0	1.294d+00	-1.455d-02	-5.867d-01	-1.138d-03		
ROW 2	4.494d-03	-2.244d-05	-7.112d-03	-6.937d-04	5.835d-02	-2.106d-06	-1.057d-08	-1.718d-04
	-1.551d-05	2.376d-04	1.128d-02	1.586d-04	2.064d-02	1.004d-03	5.143d-04	0.0
	0.0	0.0	3.277d-04	1.031d+00	5.384d-03	-2.616d-06		
ROW 3	-1.385d-03	2.696d-04	2.588d-03	6.906d-03	4.111d-01	-7.847d-07	-1.550d-08	1.922d-04
	1.634d-05	-5.204d-04	-1.365d-02	1.056d-04	1.901d-02	1.942d-03	8.748d-04	0.0
	0.0	0.0	-9.186d-04	1.345d-02	1.028d+00	-1.022d-07		
ROW 4	1.067d-02	-1.132d-03	-3.026d-02	-3.359d-02	-4.621d-01	4.245d-04	2.673d-06	2.901d-02
	2.559d-03	-1.986d-03	-1.282d-02	-2.161d-04	-4.916d-02	-2.208d-03	-6.731d-04	0.0
	0.0	0.0	-4.293d-03	-1.551d-02	-2.970d-02	9.361d-01		

The Feedback Gain Matrix $\underline{G} = [\underline{G}_x \quad \underline{G}_u]$

$$\underline{q} = \begin{bmatrix} 1.64 \\ 0.0 \\ 0.311 \\ 0.311 \\ 0.115 \\ 0.0 \\ 3213.9 \\ 66.33 \\ -17.98 \\ 0.0 \\ 1.0 \\ 0.0 \\ 0.0578 \\ 1.64 \\ 1.64 \\ 4.06 \\ 4.06 \\ 0.0 \\ 1.0 \\ 0.0 \\ 0.0 \\ 0.0 \end{bmatrix}$$

Desired Augmented State for 1% α_r

$$\underline{g} = [\, \underline{G}_x \;\; \underline{G}_u \,]\underline{q} = \begin{bmatrix} 2.63 \\ 0.0158 \\ 0.0517 \\ 1.81 \end{bmatrix}$$

Required Steady State Input Bias for 1% α_r

EIGENVALUES

No.	Description	Open Loop	Nominal	LQ
1	Torque-Speed	-0.053	-0.092	-0.097
2	Fuel-Torque	-4.30	-4.84	-4.05
3	EGR-Torque	-5.18+j30.3	-5.22+j30.2	-5.86+j30.2
4	EGR-Torque	-5.18-j30.3	-5.22-j30.2	-5.86-j30.2
5	Throttle Actuator	-7.07+j7.07	-7.07+j7.07	-11.6+j16.9
6	Throttle Actuator	-7.07-j7.07	-7.07-j7.07	-11.6-j16.9
7	Torque-Speed	-12.47	-8.03	-22.9
8	Manifold Pressure	-14.29	-15.4	-11.6
9	EGR-Torque	-19.48	-17.3	-16.6
10	Torque Filter	-23.8+j48.9	-23.8+j48.9	-23.8+j48.9
11	Torque Filter	-23.8-j48.9	-23.8-j48.9	-23.8-j48.9
12	Torque Filter	-26.7	-26.7	-26.7
13	Manifold Pressure Filter	-67.0	-55.6+j34.2	-55.5+j34.3
14	Manifold Pressure Filter	-67.0	-55.6-j34.2	-55.5-j34.3
15	Engine Time Delay (Pade)	-79.9+j45.6	-79.9+j45.9	-79.9+j45.9
16	Engine Time Delay (Pade)	-79.9-j45.6	-79.9-j45.9	-79.9-j45.9
17	EGR Actuator	-79.4+j40.7	-93.0+j38.5	-93.0+j38.4
18	EGR Actuator	-79.4-j40.7	-93.0-j38.5	-93.0-j38.4
19	Integrator			-137.1
20	Integrator			-197.5
21	Integrator			-679.6
22	Integrator			-736.6

Eng. TD	ROW 1	4.946d-03	1.338d+01	3.349d+00	1.222d-03
	ROW 2	4.946d-03	1.338d+01	3.349d+00	1.222d-03
EGR Act.	ROW 3	3.678d-02	9.714d+01	8.783d-01	1.897d-03
	ROW 4	3.678d-02	9.714d+01	8.783d-01	1.897d-03
MAP Fil.	ROW 5	1.006d-01	7.886d+01	1.367d+00	2.435d-03
	ROW 6	1.006d-01	7.886d+01	1.367d+00	2.435d-03
TQ Fil.	ROW 7	8.795d-03	4.400d+00	3.326d+00	2.164d-01
	ROW 8	8.795d-03	4.400d+00	3.326d+00	2.164d-01
EGR-TQ	ROW 9	1.043d-01	4.845d+01	3.000d-01	4.707d-03
	ROW 10	1.043d-01	4.845d+01	3.000d-01	4.707d-03
TQ Fil.	ROW 11	2.857d-01	1.621d+01	3.517d+00	7.498d-02
EGR-TQ	ROW 12	4.515d+00	1.489d+01	4.425d-01	5.665d-02
MAP	ROW 13	4.460d+00	1.580d+00	1.422d+00	5.767d-02
Thr. Act.	ROW 14	9.950d+00	0.0	0.0	0.0
	ROW 15	9.950d+00	0.0	0.0	0.0
TQ-Spd	ROW 16	5.664d+00	1.329d+01	3.953d+00	2.441d-02
Fuel-TQ	ROW 17	1.815d+00	3.571d+00	3.562d+00	1.896d-03
TQ-Spd.	ROW 18	5.017d-01	4.602d-02	3.429d+00	4.314d-02

The Controllability Matrix Magnitude

	Eng. TD EGR-TQ Fuel-TQ	Eng.TD EGR-TQ TQ-Speed	EGR Act. TQ Filter	EGR Act. EGR-TQ	Map Filter MAP	Map Filter Thr. Act.	TQ Filter Thr. Act.	TQ Filter TQ-Spd.
ROW 1	9.845d-03	9.845d-03	1.166d-02	1.166d-02	1.159d-02	1.159d-02	1.309d-17	1.309d-17
	3.368d-03	3.368d-03	0.0	6.685d-03	6.330d-03	4.479d-03	4.479d-03	4.062d-03
	3.619d-03	7.674d-03						
ROW 2	5.187d-04	5.187d-04	6.290d-04	6.290d-04	8.201d-04	8.201d-04	8.982d-19	8.982d-19
	4.821d-04	4.821d-04	0.0	4.036d-03	5.552d-03	2.290d-03	2.290d-03	6.543d-03
	2.022d-03	6.200d-02						
ROW 3	5.519d-06	5.519d-06	3.221d-04	3.221d-04	7.461d-04	7.461d-04	2.786d-19	2.786d-19
	4.818d-06	4.818d-06	0.0	1.373d-04	2.887d-04	1.664d-03	1.664d-03	6.970d-04
	9.090d-05	1.625d-03						
ROW 4	0.0	0.0	0.0	0.0	0.0	0.0	0.0	0.0
	0.0	0.0	0.0	0.0	0.0	3.787d-04	3.787d-04	0.0
	0.0	0.0						
ROW 5	1.717d-06	1.717d-06	1.845d-04	1.845d-04	3.154d-04	3.154d-04	2.394d-19	2.394d-19
	2.908d-07	2.908d-07	0.0	8.399d-06	1.389d-05	3.425d-05	3.425d-05	1.231d-05
	6.295d-07	6.566d-06						
ROW 6	1.794d-03	1.794d-03	2.162d-03	2.162d-03	4.823d-03	4.823d-03	1.002d-02	1.002d-02
	3.350d-03	3.350d-03	1.000d+00	2.354d-02	1.781d-02	6.439d-03	6.439d-03	6.639d-03
	4.739d-03	7.712d-03						
ROW 7	1.097d-05	1.097d-05	1.028d-03	1.028d-03	3.508d-03	d.508d-03	1.358d-18	1.358d-18
	4.571d-06	4.571d-06	0.0	2.514d-04	4.853d-04	2.051d-03	2.051d-03	9.092d-04
	1.055d-04	1.630d-03						

The Observability Matrix Magnitude

APPENDIX D

Decoupled Kalman Filter Designs

Decoupled Kalman Filter Designs

This appendix presents the specific decoupled Kalman Filter designs.

1. Throttle Actuator Filter

The continuous time Laplace Transformed throttle actuator model is,

$$\delta\alpha_p(s) = \left(\frac{(\alpha_9)^2}{s^2 + 2\alpha_9\alpha_{10}s + (\alpha_9)^2} \right) \delta\alpha_c(s)$$

where all constant values used here are given in Appendix B of this report.

The state variable realization used in the continuous time model was,

$$\begin{bmatrix} \delta\dot{x}_{10} \\ \delta\dot{x}_{11} \end{bmatrix} = \begin{bmatrix} -2\alpha_9\alpha_{10} & -(\alpha_9)^2 \\ 1 & 0 \end{bmatrix} \begin{bmatrix} \delta x_{10} \\ \delta x_{11} \end{bmatrix} + \begin{bmatrix} (\alpha_9)^2 \\ 0 \end{bmatrix} \delta\alpha_c \tag{D.1}$$

$$\delta\alpha_p = \begin{bmatrix} 0 & 1 \end{bmatrix} \begin{bmatrix} \delta x_{10} \\ \delta x_{11} \end{bmatrix}$$

which, with the obvious matrix definitions becomes,

$$\begin{aligned} \delta\dot{\underline{x}} &= \underline{A}\delta\underline{x} + \underline{B}\delta\underline{u} \\ \delta\underline{y} &= \underline{C}\delta\underline{x} \end{aligned} \tag{D.2}$$

Following the standard discretization procedure used in Chapter II to obtain discrete models equation (D.2) becomes (with noise added),

$$\begin{aligned} \delta\underline{x}(k+1) &= \hat{\underline{A}}\delta\underline{x}(k) + \hat{\underline{B}}\delta\underline{u}(k) + \underline{\xi}(k) \\ \delta\underline{y}(k) &= \underline{C}\delta\underline{x}(k) + \underline{\theta}(k) \end{aligned} \tag{D.3}$$

$$\hat{\underline{A}} = e^{\underline{A}\Delta} \qquad \hat{\underline{B}} = \int_0^{\Delta} e^{\underline{A}(\Delta-\tau)}\underline{B}d\tau$$

$$E\{\underline{\xi}(k)\underline{\xi}(1)^T\} = \underline{\Xi}\delta(k-1) \qquad E\{\underline{\xi}(k)\} = \underline{0}$$

$$E\{\underline{\theta}(k)\underline{\theta}(1)^T\} = \underline{\Theta}\delta(k-1) \qquad E\{\underline{\theta}(k)\} = \underline{0}$$

$$\delta(n) = \begin{cases} 0 & n \neq 0 \\ 1 & n = 0 \end{cases}$$

The Kalman filter for (D.3) to estimate $\delta\underline{x}(k)$ using measurements up to $\delta\underline{y}(k)$ becomes,

$$\delta\hat{\underline{x}}(k+1) = (\hat{\underline{A}} - \underline{H}\underline{C}\hat{\underline{A}})\delta\hat{\underline{x}}(k) + (\hat{\underline{B}} - \underline{H}\underline{C}\hat{\underline{B}})\delta\underline{u}(k) + \underline{H}\delta\underline{y}(k+1) \qquad (D.4)$$

$$\delta\hat{\underline{x}}(0) = E\{\delta\underline{x}(0)\}$$

where the filter gain, H, is given by,

$$\underline{H} = \underline{\Sigma}\underline{C}^T[\underline{C}\underline{\Sigma}\underline{C}^T + \underline{\Theta}]^{-1} \qquad (D.5)$$

$$\underline{\Sigma} = \hat{\underline{A}}\underline{\Sigma}\hat{\underline{A}}^T - \hat{\underline{A}}\underline{\Sigma}\underline{C}^T[\underline{C}\underline{\Sigma}\underline{C}^T + \underline{\Theta}]^{-1}\underline{C}\underline{\Sigma}\hat{\underline{A}} + \underline{\Xi} \qquad (D.6)$$

$$\underline{\Sigma} \geq 0$$

For the filter designs presented here Ξ and Θ were chosen to locate the poles of the filter in the neighborhood of the controller poles for the physical device. Simulation studies for the entire closed loop system were conducted and these values of Ξ and Θ adjusted to achieve satisfactory response characteristics without undue noise amplification. The following values were chosen for the throttle actuator,

$$\underline{\Xi} = \begin{bmatrix} 5.0 & 0.0 \\ 0.0 & 0.1 \end{bmatrix} \qquad \underline{\Theta} = 0.75$$

resulting in,

$$\underline{H} = \begin{bmatrix} -0.3629 \\ 0.2876 \end{bmatrix}$$

	Eigenvalues	
	Controller	Filter
Discrete	0.7497 ± j0.2611	0.7214 ± j0.1283
Equivalent Continuous	-11.6 ± j16.9	-15.6 ± j8.80

2. EGR Actuator Filter

The continuous time EGR actuator model is,

$$\delta E_p(s) = \left(\frac{\alpha_{11}^2}{s^2 + 2\alpha_{12}\alpha_{11}s + \alpha_{11}^2} \right) \delta E_c(s)$$

In the state variable realization of this text this transfer function becomes,

$$\begin{bmatrix} \delta\dot{x}_{12} \\ \delta\dot{x}_{13} \end{bmatrix} = \begin{bmatrix} -2\alpha_{12}\alpha_{11} & -\alpha_{11}^2 \\ 1 & 0 \end{bmatrix} \begin{bmatrix} \delta x_{12} \\ \delta x_{13} \end{bmatrix} + \begin{bmatrix} \alpha_{11}^2 \\ 0 \end{bmatrix} \delta E_c$$

$$\delta E_p = \begin{bmatrix} 0 & 1 \end{bmatrix} \begin{bmatrix} \delta x_{12} \\ \delta x_{13} \end{bmatrix}$$

In a manner entirely analogous to that used for the throttle actuator the equations become,

$$\begin{aligned} \delta\underline{\dot{x}} &= \underline{A}\delta\underline{x} + \underline{B}\delta\underline{u} \\ \delta\underline{y} &= \underline{C}\delta\underline{x} \end{aligned} \tag{D.7}$$

and, in discrete form,

$$\begin{aligned} \delta\underline{x}(k+1) &= \hat{\underline{A}}\delta\underline{x}(k) + \hat{\underline{B}}\delta\underline{u}(k) + \underline{\xi}(k) \\ \delta\underline{y}(k) &= \underline{C}\delta\underline{x}(k) + \underline{\theta}(k) \end{aligned} \tag{D.8}$$

Again choosing $\underline{\Xi}$ and $\underline{\Theta}$ for pole placement and noise rejection the final results are,

$$\underline{\Xi} = \begin{bmatrix} 0.1 & 0.0 \\ 0.0 & 0.04 \end{bmatrix} \qquad \underline{\Theta} = 2.0$$

$$\underline{H} = \begin{bmatrix} -0.2509 \\ 0.02319 \end{bmatrix}$$

Eigenvalues

	Controller	Filter
Discrete	0.1121 ± j0.1083	0.1359 ± j0.1495
Equivalent Continuous	-93.0 ± j38.4	-80.0 ± j41.7

3. Manifold Pressure Filter

The block diagram from Figure 2.4 gives,

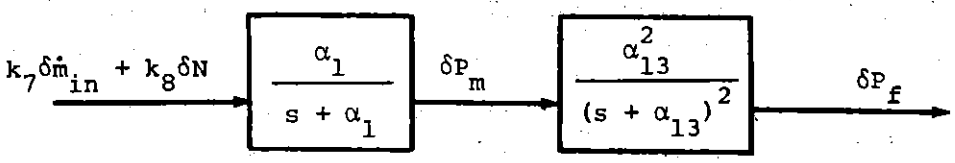

$$\delta\dot{m}_{in} = k_1\delta\alpha_p + k_5\delta E_p + k_3k_9\delta F_c + k_4k_9\delta N + (k_2 + k_6)\delta P_m$$

In state variable form this becomes,

$$\begin{bmatrix} \delta\dot{x}_1 \\ \delta\dot{x}_{15} \\ \delta\dot{x}_{14} \end{bmatrix} = \begin{bmatrix} -\alpha_1 + \alpha_1k_7k_2 + \alpha_1k_7k_6 & 0 & 0 \\ \alpha_{13} & -\alpha_{13} & 0 \\ 0 & \alpha_{13} & -\alpha_{13} \end{bmatrix} \begin{bmatrix} \delta x_1 \\ \delta x_{15} \\ \delta x_{14} \end{bmatrix} \qquad (D.9)$$

$$+ \begin{bmatrix} \alpha_1k_7k_1 & \alpha_1k_7k_5 & \alpha_1k_7k_9k_3 & \alpha_1k_8+\alpha_1k_7k_9k_4 \\ 0 & 0 & 0 & 0 \\ 0 & 0 & 0 & 0 \end{bmatrix} \begin{bmatrix} \delta\alpha_p \\ \delta E_p \\ \delta F_c \\ \delta N \end{bmatrix}$$

and the output equation,

$$\delta P_f = \begin{bmatrix} 0 & 0 & 1 \end{bmatrix} \begin{bmatrix} \delta x_1 \\ \delta x_{15} \\ \delta x_{14} \end{bmatrix} \tag{D.10}$$

Using an identical procedure the discrete Kalman filter noise parameters become,

$$\underline{\Xi} = \begin{bmatrix} 25.0 & 0.0 & 0.0 \\ 0.0 & 10.0 & 0.0 \\ 0.0 & 0.0 & 2.5 \end{bmatrix} \qquad \underline{\Theta} = 100.0$$

$$\underline{H} = \begin{bmatrix} 0.1662 \\ 0.1887 \\ 0.2009 \end{bmatrix}$$

	Eigenvalues	
	Controller	Filter
Discrete	0.2184	0.2552 ± j0.2088
	0.3788	
	0.4886	0.7937
Equivalent Continuous	-76.1	-55.5 ± j34.3
	-48.5	
	-35.8	-11.6

4. Engine Filter

A block diagram for the engine filter can be formed by taking the EGR dynamics, fuel dynamics, Padé approximant to the engine time delay, and the torque filter blocks in Figure 2.4. The inputs are engine speed, manifold pressure, inlet EGR mass flow rate, inlet fuel mass flow rate, and spark advance. The output, or measurement, is the filtered brake torque signal. When combined with Appendix A of this report this results in the following continuous time state equation,

$$\begin{bmatrix} \delta\dot{x}_2 \\ \delta\dot{x}_3 \\ \delta\dot{x}_4 \\ \delta\dot{x}_5 \\ \delta\dot{x}_6 \\ \delta\dot{x}_7 \\ \delta\dot{x}_{16} \\ \delta\dot{x}_{17} \\ \delta\dot{x}_{18} \end{bmatrix} = \begin{bmatrix} -2\alpha_8\alpha_7 & -\alpha_7^2 & 0 & 0 & 0 & 0 & 0 & 0 & 0 \\ 1 & 0 & 0 & 0 & 0 & 0 & 0 & 0 & 0 \\ 0 & \alpha_5 & -\alpha_5 & 0 & 0 & 0 & 0 & 0 & 0 \\ 0 & 0 & 0 & -\alpha_6 & 0 & 0 & 0 & 0 & 0 \\ 0 & 0 & \sigma_1 & \sigma_2 & 0 & 1 & 0 & 0 & 0 \\ 0 & 0 & \sigma_3 & \sigma_4 & \frac{-12}{T^2} & \frac{-6}{T} & 0 & 0 & 0 \\ 0 & 0 & 0 & 0 & 0 & 0 & -\alpha_{14} & \alpha_{14} & 0 \\ 0 & 0 & 0 & 0 & 0 & 0 & 0 & 0 & 1 \\ 0 & 0 & 0 & 0 & 0 & 0 & 0 & -\alpha_{15}^2 & \sigma_5 \end{bmatrix} \begin{bmatrix} \delta x_2 \\ \delta x_3 \\ \delta x_4 \\ \delta x_5 \\ \delta x_6 \\ \delta x_7 \\ \delta x_{16} \\ \delta x_{17} \\ \delta x_{18} \end{bmatrix}$$

$$+ \begin{bmatrix} \alpha_7^2 & 0 & 0 & 0 & 0 \\ 0 & 0 & 0 & 0 & 0 \\ 0 & 0 & 0 & 0 & 0 \\ 0 & \alpha_6 & 0 & 0 & 0 \\ 0 & 0 & \beta_1 & \beta_2 & 0 \\ 0 & 0 & \beta_3 & \beta_4 & 0 \\ 0 & 0 & 0 & 0 & 0 \\ 0 & 0 & 0 & 0 & 0 \\ 0 & 0 & \beta_5 & \beta_6 & k_{15}\alpha_{15}^2 \end{bmatrix} \begin{bmatrix} \delta m_{EGR\ in} \\ \delta m_{fuel\ in} \\ \delta P_m \\ \delta N \\ \delta S \end{bmatrix}$$

where,

$$\sigma_1 = -\frac{12}{T}(k_{12} - k_{11}) \qquad \beta_1 = -\frac{12}{T}(k_{14} + k_{11}k_{18})$$

$$\sigma_2 = -\frac{12}{T}(k_{13} - k_{11}) \qquad \beta_2 = -\frac{12}{T}(k_{11}k_{17})$$

$$\sigma_3 = \frac{72}{T^2}(k_{12} - k_{11}) \qquad \beta_3 = \frac{72}{T^2}(k_{14} + k_{11}k_{18})$$

$$\sigma_4 = \frac{72}{T^2}(k_{13} - k_{11}) \qquad \beta_4 = \frac{72}{T^2}(k_{11}k_{17})$$

$$\sigma_5 = -2\alpha_{15}\alpha_{16} \qquad \beta_5 = \alpha_{15}^2(k_{14} + k_{11}k_{18})$$

$$\beta_6 = \alpha_{15}^2(k_{16} + k_{11}k_{17})$$

and the output equation becomes,

$$\delta T_f = [\ 0\ \ 0\ \ 0\ \ 0\ \ 0\ \ 0\ \ 1\ \ 0\ \ 0\ ]\ \delta\underline{x} \qquad \text{(D.12)}$$

This system can be discretized and the Kalman filter designed as with the previous three filters. The parameters chosen were,

$$\underline{\Xi} = \text{diag}(0.1,\ 0.5,\ 2.0,\ 0.0001,\ 25.0,\ 15.0,\ 0.1,\ 1.0,\ 5.0)$$

$$\underline{\Theta} = 5000.0$$

yielding a filter gain matrix of,

$$\underline{H} = \begin{bmatrix} -0.007735 \\ 0.0004358 \\ -0.0004571 \\ 0.000007706 \\ 0.007476 \\ 1.158 \\ 0.01958 \\ 0.01989 \\ -0.3264 \end{bmatrix}$$

and the eigenvalues,

	Eigenvalues	
Discrete	Controller	Filter
Fuel-Torque	0.9222	0.9117
EGR - Torque	0.7322 ± j0.5051	0.7404 ± j0.5124
EGR - Torque	0.7180	0.6321
Torque Filter	0.3466 ± j0.5151	0.3461 ± j0.5158
Torque Filter	0.5859	0.6171
Engine Time Delay (Padé approximant)	0.1230 ± j0.1608	0.1217 ± j0.1611
Equivalent Continuous		
Fuel-Torque	-4.05	-4.62
EGR - Torque	-5.86 ± j30.2	-5.25 ± j30.3
EGR - Torque	-16.6	-23.0
Torque Filter	-23.8 ± j48.9	-23.8 ± j50.0
Torque Filter	-26.7	-24.1
Engine Time Delay (Padé approximant)	-79.9 ± j45.9	-80.0 ± j46.2

5. Torque-Speed Filter

The torque-speed transfer function is (from Figure 2.4),

$$\delta N(s) = \left\{ \frac{\frac{k_{10}\alpha_3\alpha_4}{\alpha_2}(s + \alpha_2)}{(s + \alpha_3)(s + \alpha_4)} \right\} \delta T_b(s)$$

resulting in the state variable description,

$$\begin{bmatrix} \dot{\delta x}_8 \\ \dot{\delta x}_9 \end{bmatrix} = \begin{bmatrix} 0 & 1 \\ -\alpha_3\alpha_4 & -(\alpha_3+\alpha_4) \end{bmatrix} \begin{bmatrix} \delta x_8 \\ \delta x_9 \end{bmatrix} + \begin{bmatrix} k_{10}\alpha_3\alpha_4/\alpha_2 \\ (k_{10}\alpha_3\alpha_4/\alpha_2)(\alpha_2-\alpha_3-\alpha_4) \end{bmatrix} \delta T_b$$

$$\delta N = \begin{bmatrix} 1 & 0 \end{bmatrix} \begin{bmatrix} \delta x_8 \\ \delta x_9 \end{bmatrix}$$

The following discrete noise parameters,

$$\underline{\Xi} = \begin{bmatrix} 1.0 & 0.0 \\ 0.0 & 10.0 \end{bmatrix} \qquad \underline{\Theta} = 10.0$$

result in the filter gain matrix

$$\underline{H} = \begin{bmatrix} 0.2740 \\ 0.06958 \end{bmatrix}$$

and the eigenvalues,

	Eigenvalues	
	Controller	Filter
Discrete	0.9981	0.7905
	0.6331	0.7413
Equivalent Continuous	-0.0972	-11.75
	-22.9	-14.97

APPENDIX E

A DYNAMIC PROGRAMMING SOLUTION TO THE DISCRETE TIME LINEAR QUADRATIC TRACKING PROBLEM

A DYNAMIC PROGRAMMING SOLUTION TO THE DISCRETE TIME LINEAR QUADRATIC TRACKING PROBLEM

This appendix presents a discrete time dynamic programming solution to the discrete time linear quadratic tracking problem presented in Chapter III. The infinite time horizon problem is solved to derive an optimal control policy for the LQ controller and this result is compared with previous work [32].

From Chapter III we wish to find an optimal control policy, v, such that

$$v = \min_{v} \left\{ \lim_{N\to\infty} \sum_{k=0}^{N-1} \left[(\underline{p}(k)-\underline{q}(k))^T \underline{Q} (\underline{p}(k)-\underline{q}(k)) + v(k)^T \underline{R} v(k) \right] \right\} \qquad (E.1)$$

subject to the state equation,

$$\underline{p}(k+1) = \underline{A}\,\underline{p}(k) + \underline{B}\,\underline{v}(k) \qquad \begin{matrix} \underline{p}(k) \in R^n \\ \underline{v}(k) \in R^m \end{matrix} \qquad (E.2)$$

where the tildas (~) have been dropped from equation (3.20) to arrive at (E.2) for clarity in this appendix. The assumptions are,

$$\underline{Q} = \underline{Q}^T \geq \alpha\, \underline{I} \qquad \alpha \geq 0$$

$$\underline{R} = \underline{R}^T \geq \beta\, \underline{I} \qquad \beta > 0$$

$$[\underline{A}, \underline{B}] \qquad \text{completely controllable}$$

In equation (E.1) q(k) represents the state to be tracked and, for the purpose of this steady state analysis, is assumed to be a

constant. This corresponds to letting the engine reach steady state in response to a step throttle perturbation and thus deriving the optimal steady state control. In practice $\underline{q}$ will be a linear function of the driver's throttle request.

We will solve this problem in four basic steps. First we will solve (E.1) for a fixed but arbitrary N. Second we note the similarity of our results to the standard LQ problem and make use of previous work to argue the existence of a steady state solution. Third we find this steady state solution and note its intuitive nature. Finally we verify this result using previous work [32].

Solution for fixed but Arbitrary N

From the principle of optimality (Bellman [36]) we have that the optimal cost to go, $V(\underline{p}(k),k)$, defined as,

$$V(\underline{p}(k),k) = \min_{\substack{v(k) \\ \vdots \\ v(N-1)}} \sum_{i=k}^{N-1} \left[(\underline{p}(i)-\underline{q})^T \underline{Q} (\underline{p}(i)-\underline{q}) + \underline{v}(i)^T \underline{R}\, \underline{v}(i) \right] \qquad \text{(E.3)}$$

$$k=0,1,2,\ldots, N-1$$

$$\underline{p}(k) \in R^n$$

satisfies the following recursive equation,

$$V(\underline{p}(k),k) = \min_{\underline{v}(k)} \left\{ \left[(\underline{p}(k)-\underline{q})^T \underline{Q} (\underline{p}(k)-\underline{q}) + \underline{v}(k)^T \underline{R}\, \underline{v}(k) \right] + V(\underline{A}\, \underline{p}(k) + \underline{B}\, \underline{v}(k),\ k+1) \right\} \tag{E.4}$$

with the boundary condition corresponding to no terminal penalty,

$$V(\underline{p}(N),N) = 0 \tag{E.5}$$

As in all dynamic programming algorithms the success hinges upon one's ability to correctly postulate the form of the value function, V. Some mathematical induction combined with a little luck leads to the following.

$$V(p(k),k) = \underline{p}(k)^T\, \underline{P}_k\, \underline{p}(k) + 2\underline{S}_k^T\, \underline{p}(k) + w_k \tag{E.6}$$

It is now straightforward to use (E.6) in (E.4) and the first derivative condition yields,

$$\underline{v}(k) = -(\underline{R}+\underline{B}^T\underline{P}_{k+1}\underline{B})^{-1}\, \underline{B}^T\underline{P}_{k+1}\, \underline{A}\, \underline{p}(k) - (\underline{R}+\underline{B}^T\underline{P}_{k+1}\underline{B})^{-1}\, \underline{B}^T\underline{S}_{k+1} \tag{E.7}$$

while the positive definitness of the second derivative assures us that this is indeed the minimum.

Equation (E.6) with (E.7) in (E.4) now yields the recursive equations for $\underline{P}_k$, $\underline{S}_k$, and w_k. Making the indicated substitutions and combining similar terms (leaving out the tedious intermediary steps),

$$\underline{P}_k = \underline{Q} + \underline{A}^T\underline{P}_{k+1}\underline{A} - \underline{A}^T\underline{P}_{k+1}\underline{B}(\underline{R}+\underline{B}^T\underline{P}_{k+1}\underline{B})^{-1}\, \underline{B}^T\underline{P}_{k+1}\underline{A} \tag{E.8}$$

$$\underline{P}_N = 0$$

$$\underline{S}_k = -\underline{Q}\underline{q} - \underline{A}^T\underline{P}_{k+1}\underline{B}(\underline{R}+\underline{B}^T\underline{P}_{k+1}\underline{B})^{-1}\ \underline{B}^T\underline{S}_{k+1} + \underline{A}^T\underline{S}_{k+1} \qquad (E.9)$$

$$\underline{S}_N = 0$$

$$w_k = \underline{q}^T\underline{Q}\underline{q} - \underline{S}_{k+1}^T\underline{B}(\underline{R}+\underline{B}^T\underline{P}_{k+1}\underline{B})^{-1}\ \underline{B}^T\underline{S}_{k+1} + w_{k+1} \qquad (E.10)$$

$$w_N = 0$$

Similarities to the Standard LQ Problem

The first term in E.7 is the standard linear quadratic feedback gain term, with the discrete algebraic Riccati equation, (E.8), also being a standard result. It is well known. (Theorem 3 of Dorato and Levis [31] or Theorem 6.29 of Kwakernaak and Sivan [39]) that, as N approaches infinity, the controllability assumption in (E.2) guarantees a unique steady state positive definite solution to (E.8). Denoting this solution as $\bar{\underline{P}}$,

$$\underline{Q} - \underline{A}^T\bar{\underline{P}}\,\underline{A} - \underline{A}^T\bar{\underline{P}}\,\underline{B}(\underline{R}+\underline{B}^T\bar{\underline{P}}\,\underline{B})^{-1}\ \underline{B}^T\bar{\underline{P}}\,\underline{A} - \bar{\underline{P}} = 0 \qquad (E.11)$$

Now denoting the steady state solution to (E.9) as $\bar{\underline{S}}$ and using the solution to (E.11) above,

$$\bar{\underline{S}} = -\left[\underline{I} + \underline{A}^T\bar{\underline{P}}\,\underline{B}(\underline{R}+\underline{B}^T\bar{\underline{P}}\,\underline{B})^{-1}\ \underline{B}^T - \underline{A}^T\right]^{-1}\underline{Q}\,\underline{q}$$

or

$$\bar{\underline{S}} = -\left[\underline{I} - (\underline{A}-\underline{B}\,\underline{G})^T\right]^{-1}\underline{Q}\,\underline{q} \qquad (E.12)$$

where the feedback gain matrix, G, is defined as,

$$\underline{G} \triangleq (\underline{R}+\underline{B}^T\underline{\bar{P}}\,\underline{B})^{-1}\,\underline{B}^T\underline{\bar{P}}\,\underline{A}$$

and the inverse in (E.12) is guaranteed to exist since the closed loop matrix, $\underline{A}-\underline{B}\,\underline{G}$, is exponentially stable.

At steady state one would expect, on physical grounds, that $v_{ss}=0$ (since $\underline{v}$ represents a differential control, i.e. $\underline{v}(k)\triangleq\underline{u}^*(k+1)-\underline{u}^*(k)$). Further, at steady state the system should track $\underline{q}$, that is $\underline{p}_{ss}(k)=\underline{q}$. Using these results with (E.7), we wish to show,

$$\underline{V}_{ss}(k) = 0 = -(\underline{R}+\underline{B}^T\underline{\bar{P}}\,\underline{B})^{-1}\,\underline{B}^T\underline{P}\,\underline{A}\,\underline{p}_{ss} - (\underline{R}+\underline{B}^T\underline{\bar{P}}\,\underline{B})^{-1}\,\underline{B}^T\underline{S} \qquad \text{(E.13)}$$

Noting that the steady state dynamical equation gives,

$$\underline{p}_{ss} = \underline{A}\,\underline{p}_{ss} + \underline{B}\,\underline{v}_{ss}$$

$$\underline{v}_{ss} = 0 \quad \text{by hypothesis}$$

$$\underline{p}_{ss} = \underline{q} \quad \text{by hypothesis}$$

$$\underline{q} = \underline{A}\,\underline{q} \qquad \text{(E.14)}$$

Substituting (E.12) in (E.13) and letting $\underline{p}_{ss}=\underline{q}$,

$$(\underline{R}+\underline{B}^T\underline{\bar{P}}\,\underline{B})^{-1}\,\underline{B}^T\underline{\bar{P}}\,\underline{A}\,\underline{q} = (\underline{R}+\underline{B}^T\underline{\bar{P}}\,\underline{B})^{-1}\,\underline{B}^T[\underline{I}-\underline{A}^T+\underline{G}^T\underline{B}^T]^{-1}\,\underline{Q}\,\underline{q} \qquad \text{(E.15)}$$

without loss in generality eliminate the first inverse and B^T from both sides of (E.15),

$$\bar{P}\,A\,q = [I - A^T + G^T B^T]^{-1}\,Q\,q$$

eliminating the remaining inverse yields,

$$\bar{P}\,A\,q - A^T\bar{P}\,A\,q + G^T B^T\bar{P}\,A\,q = Q\,q \tag{E.16}$$

using (E.14) in (E.16),

$$[Q + A^T\bar{P}\,A - A^T\bar{P}\,B(R + B^T\bar{P}\,B)^{-1}\,B^T\bar{P}\,A - \bar{P}]q = 0 \tag{E.17}$$

Since (E.17) must be true for all q satisfying (E.14) we can write,

$$Q + A^T\bar{P}\,A - A^T\bar{P}\,B(R + B^T\bar{P}\,B)^{-1}\,B^T\bar{P}\,A - \bar{P} = 0$$

which is identical to the algebraic Riccati equation (E.11). Therefore the intuitive steady state behavior is verified - the system tracks q with no steady state differential input. Since (E.13) is thus verified we can state that the optimal control becomes,

$$v(k) = -G\,p(k) + G\,q \tag{E.18}$$

where

$$G = (R + B^T\bar{P}\,B)^{-1}\,B^T\bar{P}\,A \tag{E.19}$$

and $\bar{P}$ is the unique positive definite solution to the algebraic Riccati equation,

$$\underline{Q} + \underline{A}^T\bar{\underline{P}}\,\underline{A} - \underline{A}^T\bar{\underline{P}}\,\underline{B}(\underline{R}+\underline{B}^T\bar{\underline{P}}\,\underline{B})^{-1}\,\underline{B}^T\bar{\underline{P}}\,\underline{A} - \bar{\underline{P}} = 0 \tag{E.20}$$

Verification

Equation (E.18) can be rewritten as,

$$v(k) = -\underline{G}(\underline{p}(k)-\underline{q}) \tag{E.21}$$

Following the procedure outlined by Lee et.al. in [32] we define a differential state,

$$\underline{\zeta}(k) = \underline{p}(k) - \underline{q} \tag{E.22}$$

then, from (E.2) and (E.14),

$$\underline{\zeta}(k+1) = \underline{A}\,\underline{\zeta}(k) + \underline{B}\,\underline{v}(k) \tag{E.23}$$

and (E.1) becomes,

$$v = \min_{v}\left\{\lim_{N\to\infty}\sum_{k=0}^{N-1}\left[\underline{\zeta}(k)^T\underline{Q}\,\underline{\zeta}(k) + \underline{v}(k)^T\underline{R}\,\underline{v}(k)\right]\right\} \tag{E.24}$$

which is recognized as a standard LQ problem, the solution to which is (E.21) where $\underline{G}$ is given by (E.19) and (E.20). This result is, of course, identical to the dynamic programming result summarized in (E.18)-(E.20).

APPENDIX F

ROBUSTNESS ANALYSIS FOR NON-INVERTIBLE FORWARD PATH TRANSFER FUNCTIONS

ROBUSTNESS ANALYSIS FOR NON-INVERTIBLE FORWARD PATH TRANSFER FUNCTIONS

In this appendix the singular value results stated in Chapter IV for the invertible loop transfer function are developed for the non-invertible case.

For the multiplicatively perturbed system shown in Figure 4.1 the loop transfer function can be written as,

$$[I+G(I+\Delta G)]\underline{e} = \underline{u} \tag{F.1}$$

multiplying the inner product and adding and subtracting ΔG gives

$$[(I+G)+(I+G)\Delta G - \Delta G]\underline{e} = \underline{u} \tag{F.2}$$

factoring,

$$(I+G)[I + \Delta G -(I+G)^{-1}\Delta G]\underline{e} = \underline{u} \tag{F.3}$$

where the inverse is guaranteed to exist since the nominal plant is stable. Rewriting (F.3),

$$(I+G)[I +[I-(I+G)^{-1}]\Delta G]\underline{e} = \underline{u} \tag{F.4}$$

A singular value decomposition results, in,

$$[I-(I+G)^{-1}] = U\Sigma V^H \tag{F.5}$$

$$[I-(I+G)^{-1}]^{-1} = V\Sigma^{-1}U^H \tag{F.6}$$

The minimum norm singular perturbation, ΔG, now becomes,

$$\Delta G = -\sigma_n^{-1} \underline{v}_n \underline{u}_n^H \tag{F.7}$$

which is easily verified since

$$\left[(I+G)\left\{I+[I-(I+G)^{-1}][-\sigma_n^{-1} V_n U_n^H\right\}\right]$$

is non-invertible.

APPENDIX G

ROBUSTNESS: CAN LQG BEAT LQ?

ROBUSTNESS: CAN LQG BEAT LQ?[†]

Abstract

This appendix describes a simple example where a wide range of optimal filter gains lead to improved robustness over the full state feedback control law.

I. Introduction

The robustness guarantees of linear quadratic optimal controllers are well known, that is a 6db reduction margin, a theoretically infinite gain margin, and 60° phase margin in each channel [27]. The full state feedback requirement for implementation is frequently not met, however, and state reconstructors (observers) must be used. As Doyle illustrates in [25] the inclusion of these observers rescinds the LQ robustness guarantees, each design must be individually checked to avoid unacceptably small margins.

Doyle and Stein in [26] present a procedure for asymptotically recovering the LQ robustness properties when an observer is used. The procedure uses fictitious noise (in a special direction) to drive the filter poles to transmission zeros or infinity and, thus, the plant-observer-controller dynamics asymptotically approach those of the full state feedback case.

[†]This work represents the culmination of joint research by Jim Lewis, Norm Lehtomaki, and Wing Hong Lee at the Laboratory for Information and Decision Systems, Massachusetts Institute of Technology.

A legitimate question to ask, and one that arose in a practical application of a filter design, is, "Can an observer based optimal control scheme exhibit more robustness than its full state feedback counterpart?" More succinctly stated, "Can LQG beat LQ?"

The answer, as will be demonstrated via a simple two state single input single output example, is yes, observer based systems can be more robust than full state feedback. Classical control theorists will not be surprised to learn that, for this example, the added robustness has been achieved at the expense of system response, that is the cutoff frequency has been decreased. It is not clear, however, whether - for some other example - a more robust filter may be designed without decreasing the full state feedback cutoff frequency. This is one of many areas requiring further research.

II. Example

The example chosen here is the plant and controller used in [26],

Plant:

$$\dot{\underline{x}} = \underline{A}\,\underline{x} + \underline{B}\,\underline{u} \tag{G.1}$$

$$\underline{y} = \underline{C}\,\underline{x} \tag{G.2}$$

$$\underline{A} = \begin{bmatrix} 0 & 1 \\ -3 & -4 \end{bmatrix} \quad \underline{B} = \begin{bmatrix} 0 \\ 1 \end{bmatrix} \quad \underline{C} = \begin{bmatrix} 2 & 1 \end{bmatrix}$$

Controller:

$$\underline{u} = -\underline{G}\,\hat{\underline{x}}$$

$$\underline{G} = [50 \quad 10] \tag{G.3}$$

where $\underline{G}$ is the linear quadratic optimal gain resulting from the performance index,

$$J = \int_0^\infty (\underline{x}^T \underline{Q}\,\underline{x} + u^2)dt \tag{G.4}$$

$$\underline{G} = \underline{R}^{-1}\underline{B}^T\underline{P} \tag{G.5}$$

and $\underline{P}$ is given by the unique positive definite solution to the Riccati equation,

$$\underline{P}\,\underline{A} + \underline{A}^T\underline{P} + \underline{Q} - \underline{P}\,\underline{B}\,\underline{R}^{-1}\underline{B}^T\underline{P} = 0$$

$$R = 1 \qquad \underline{Q} = \begin{bmatrix} 2800 & 80\sqrt{35} \\ 80\sqrt{35} & 80 \end{bmatrix}$$

The open loop plant transfer function becomes,

$$\frac{\underline{Y}}{\underline{u}}(s) = \underline{C}(s\underline{I}-\underline{A})^{-1}\,\underline{B} = \frac{s+2}{(s+1)(s+3)} \tag{G.6}$$

The full state feedback case results in a forward path gain (see Figure G.1) of,

$$\frac{u^*}{u_{LQ}}(s) = \underline{G}(s\underline{I}-\underline{A})^{-1}\underline{B} = \frac{10s+50}{(s+1)(s+3)} \tag{G.7}$$

and a closed loop transfer function of,

$$\frac{y}{r}(s) = \underline{C}(s\underline{I}-\underline{A}+\underline{B}\,\underline{G})^{-1}\underline{B} = \frac{s+2}{s^2+2\zeta\omega_n s+\omega_n^2} \tag{G.8}$$

$$\zeta = 7/\sqrt{53} \simeq 0.962$$

$$\omega_n = \sqrt{53} \simeq 7.28$$

It is easily seen from the evaluation of equation (G.7) that this full state feedback case has a theoretically infinite gain and reduction margin and a phase margin of 86°.

Figure 2 illustrates the state reconstructor concept. The observer gain, H, is assumed to be a Kalman-Bucy gain and optimal with respect to some state process noise, Ξ and measurement noise Θ. For this single output system normalizing Θ to unity yields,

$$\underline{H} = \begin{bmatrix} h_1 \\ h_2 \end{bmatrix} = \underline{\Sigma}\,\underline{C}^T$$

where $\underline{\Sigma}$ is defined by the Riccati equation,

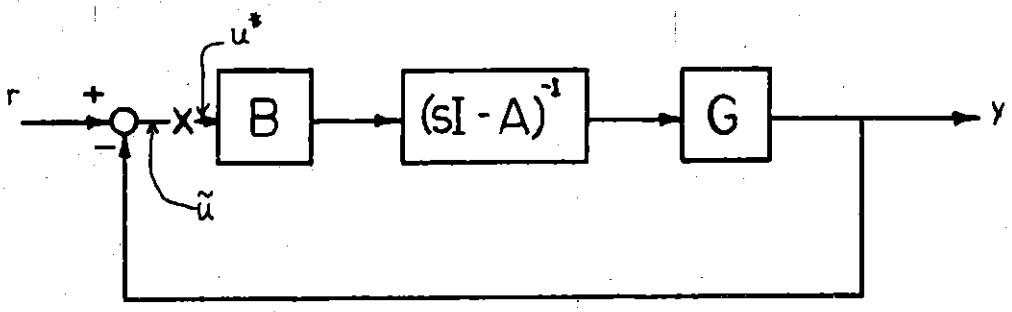

FIGURE 1

FULL STATE FEEDBACK
FORWARD PATH

$$\underline{A}\,\underline{\Sigma} + \underline{\Sigma}\,\underline{A}^T + \underline{\Xi} - \underline{\Sigma}\,\underline{C}^T\underline{C}\,\underline{\Sigma} = 0 \qquad \text{(G.10)}$$

Using this definition for $\underline{H}$ the forward path gain for the plant-observer-controller system becomes (see Figure G.2),

$$\frac{\underline{u}^*}{\underline{u}}_{LQG}(s) = \left(\frac{s+2}{(s+1)(s+3)}\right) = \left(\frac{(50h_1+10h_2)s + (170h_1+50h_2)}{s^2 + (2h_1+14+h_2)s + (53+2h_2-25h_1)}\right) \qquad \text{(G.11)}$$

The problem now is one of choosing h_1 and h_2 such that LQG, equation (G.11), is more robust than LQ, equation (G.7), and $\underline{H}$ is optimal for some process noise, $\underline{\Xi}$.

A matter of no small import is apparent by inspection of the LQG and LQ foward path gains. The linear quadratic controller exhibits a theoretical one pole roll off (the phase approaches 90° at high frequency), a characteristic of LQ controllers. The introduction of an observer in this example, LQG, results in a two pole roll off and as a consequence will always exhibit worse margins, in a singular value sense, at sufficiently high frequency. As a final comment the theoretical one pole LQ roll off is just that, theoretical, since it violates the well known condition [33],

$$\int_0^\infty \ell n\,|1 + g(j\omega)|\,d\omega = 0 \qquad \text{(G.12)}$$

thus the LQ forward path gain must be in error at "high" frequencies. For this reason the robustness at and below the cutoff frequency is of

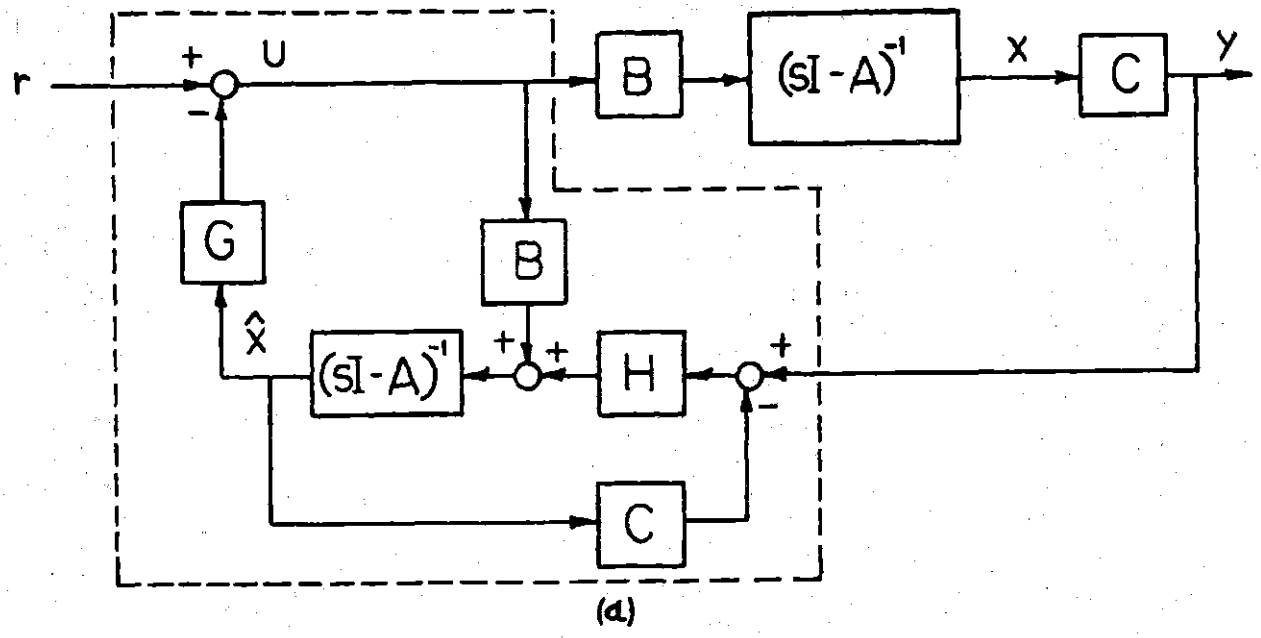

(a)

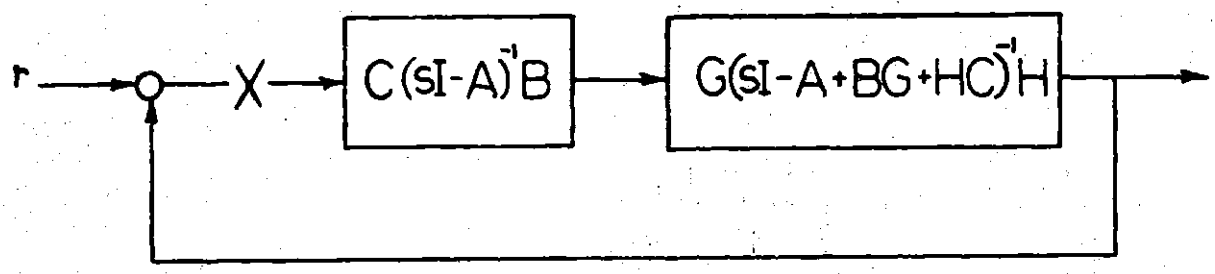

(b)

FIGURE 2

(a) PLANT-OBSERVER-CONTROLLER

(b) FORWARD PATH GAIN

primary concern and the classical concepts of gain, reduction, and phase margin will be used as a measure of robustness for this single input system.

III. Selection of the Observer Gain

The optimality condition on h_1 and h_2 can be met by considering the fundamental equation of optimal systems [28] (readily derived from (G.9) and (G.10)),

$$\left|1 + \underline{C}(j\omega\underline{I}-\underline{A})^{-1}\,\underline{H}\right| \geq 1 \qquad \forall\omega \tag{G.13}$$

Defining a rational polynomial

$$1 + \underline{C}(j\omega\underline{I}-\underline{A})^{-1}\,\underline{H} = \frac{p(j\omega)}{q(j\omega)} \tag{G.14}$$

then (G.13) becomes,

$$\frac{p(j\omega)p(-j\omega) - q(j\omega)q(-j\omega)}{q(j\omega)q(-j\omega)} \geq 0 \tag{G.15}$$

For the example under consideration this reduces to,

$$(4h_1^2+4h_1h_2+h_2^2+6h_1+4h_2)\omega^2 + (25h_1^2+20h_1h_2+4h_2^2+30h_1+12h_2) \geq 0 \qquad \forall\omega \tag{G.16}$$

Therefore,

$$4h_1^2+4h_1h_2+h_2^2+6h_1+4h_2 \geq 0 \tag{G.17}$$

$$25h_1^2+20h_1h_2+4h_2^2+30h_1+12h_2 \geq 0 \qquad (G.18)$$

In addition the closed loop filter must be stable, which for the two state case becomes,

$$tr\{\underline{A}-\underline{H}\ \underline{C}\} < 0 \quad = \quad 2h_1+h_2+4 > 0 \qquad (G.19)$$

and

$$det\{\underline{A}-\underline{H}\ \underline{C}\} > 0 \quad = \quad 5h_1+2h_2+3 > 0 \qquad (G.20)$$

A desirable property, though not a requirement, is to have the observer-controller combination stable,

$$tr\{\underline{A}-\underline{H}\ \underline{C}-\underline{B}\ \underline{G}\} < 0 \quad = \quad 2h_1+h_2+14 > 0 \qquad (G.21)$$

and

$$det\{\underline{A}-\underline{H}\ \underline{C}-\underline{B}\ \underline{G}\} > 0 \quad = \quad -25h_1+2h_2+53 > 0 \qquad (G.22)$$

Figure 3 graphically illustrates the h_1, h_2 constraints imposed by equations (G.17)-(G.22). It is now a simple matter to write a computer program which finds the region in the constrained h_1, h_2 plane where the LQG controller (equation (G.11)) has better margins than its LQ counterpart (equation (G.7)). This region is depicted in Figure G.4 where the system cutoff frequency has been indicated along the periphery to illustrate a relative measure of system response. From this figure it is clear that there exists a wide range of optimal

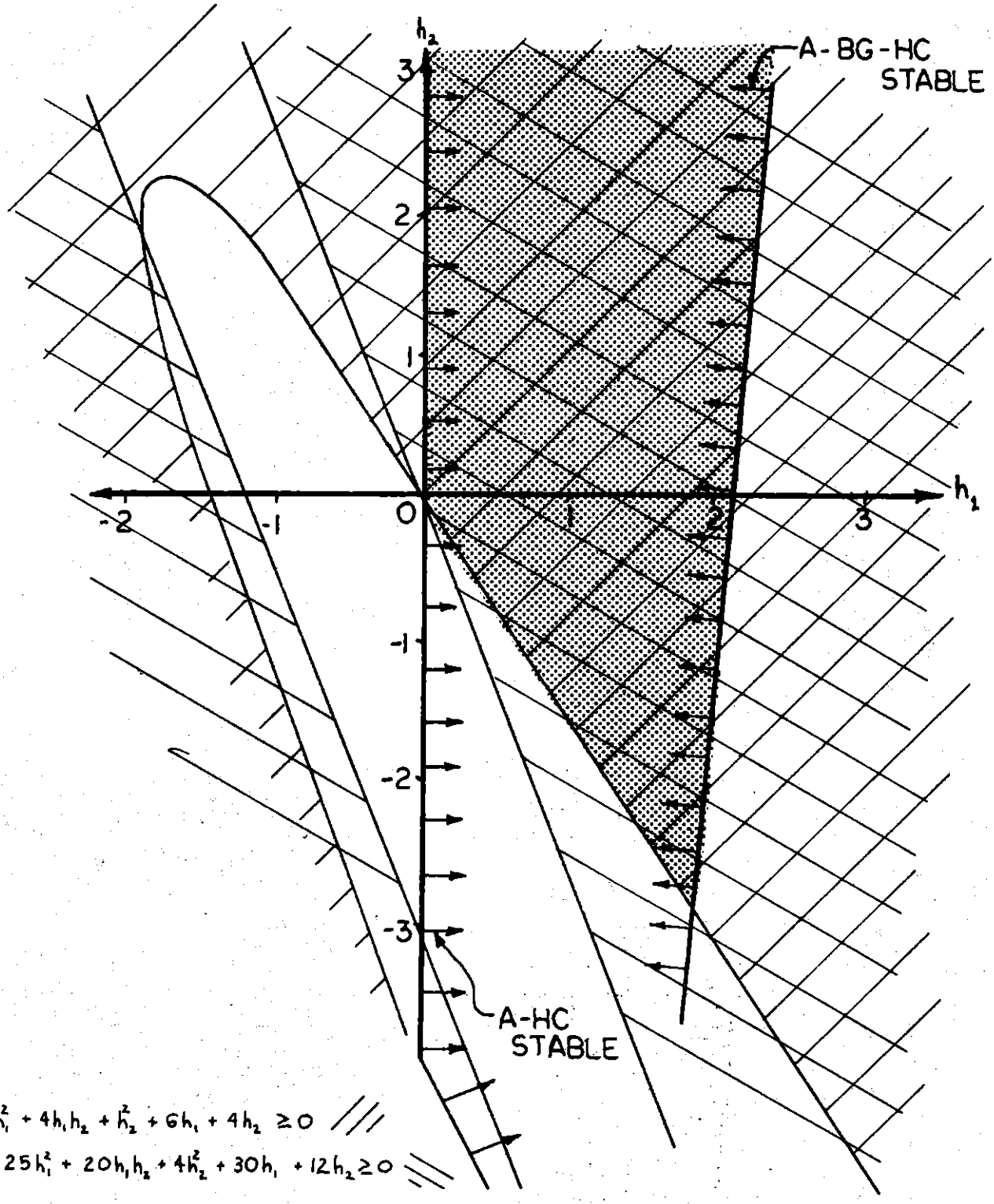

FIGURE 3
ALLOWABLE FILTER GAINS

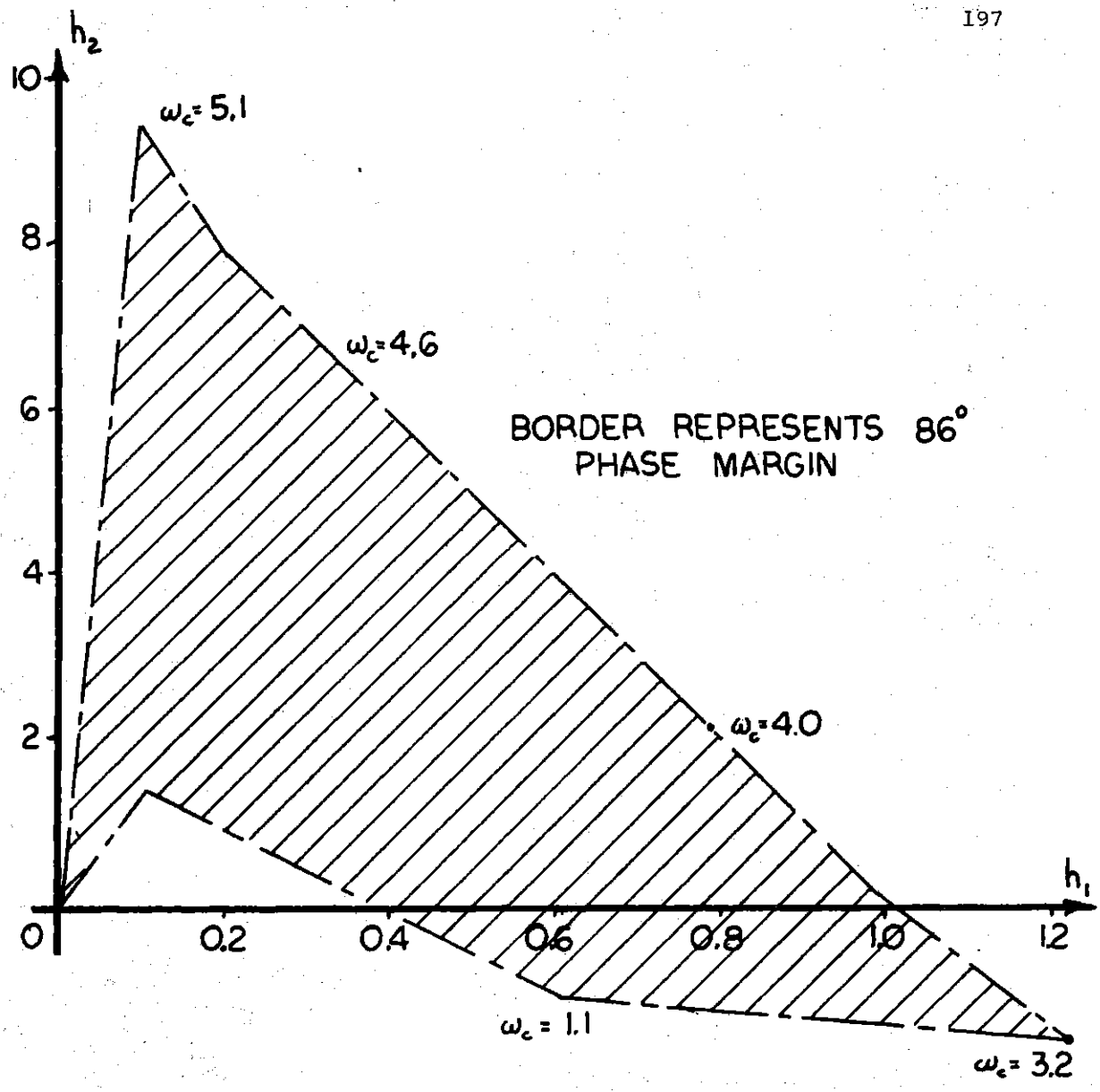

FIGURE 4
REGION OF ALLOWABLE GAINS
TO IMPROVE MARGINS

gains exhibiting improved margins relative to LQ. Further, a choice of h_1=0.1, h_2=9.5 results in a cutoff frequency, ω_c, around 5 radians/second (LQ has $\omega_c \simeq$ 11radians/second), which is the best LQG can do while still meeting the 86° phase margin constraint.

For completeness Nyquist and Bode plots are included for h_1=0.7, h_2=1.0. A noise matrix which yields this gain from (G.9) and (G.10) can be determined as,

$$\underline{\Xi} = \begin{bmatrix} 0.823334 & 0 \\ 0 & 10.-667 \end{bmatrix}$$

$$\underline{\Sigma} = \begin{bmatrix} 0.43333 & -0.166667 \\ -0.166667 & 1.33333 \end{bmatrix}$$

$$\underline{H} = \underline{\Sigma}\,\underline{C}^T = \begin{bmatrix} 0.700 \\ 1.000 \end{bmatrix}$$

IV. Conclusions

This appendix details a simple two state single input single output example where a wide range of optimal observer based controllers can be designed which improve the system robustness properties around the cutoff frequency. For this example the improvement over LQ was achieved

at the expense of response speed, though this may not be a general property of robust observer systems. Further research is needed to determine if this simple example can be extended to an algorithmic procedure which will, in some sense capture the response-robustness tradeoff.

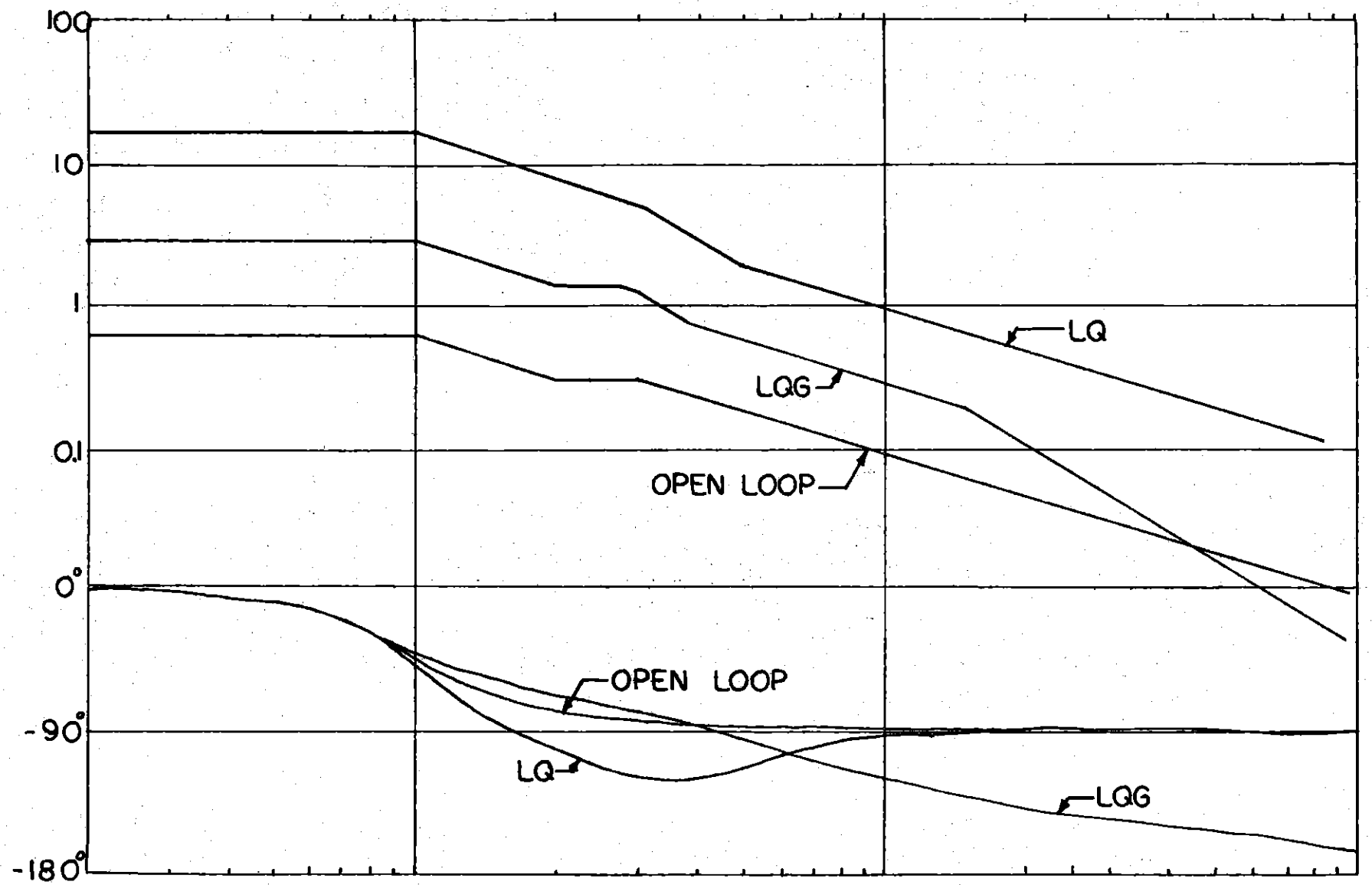

FIGURE 5
BODE PLOT

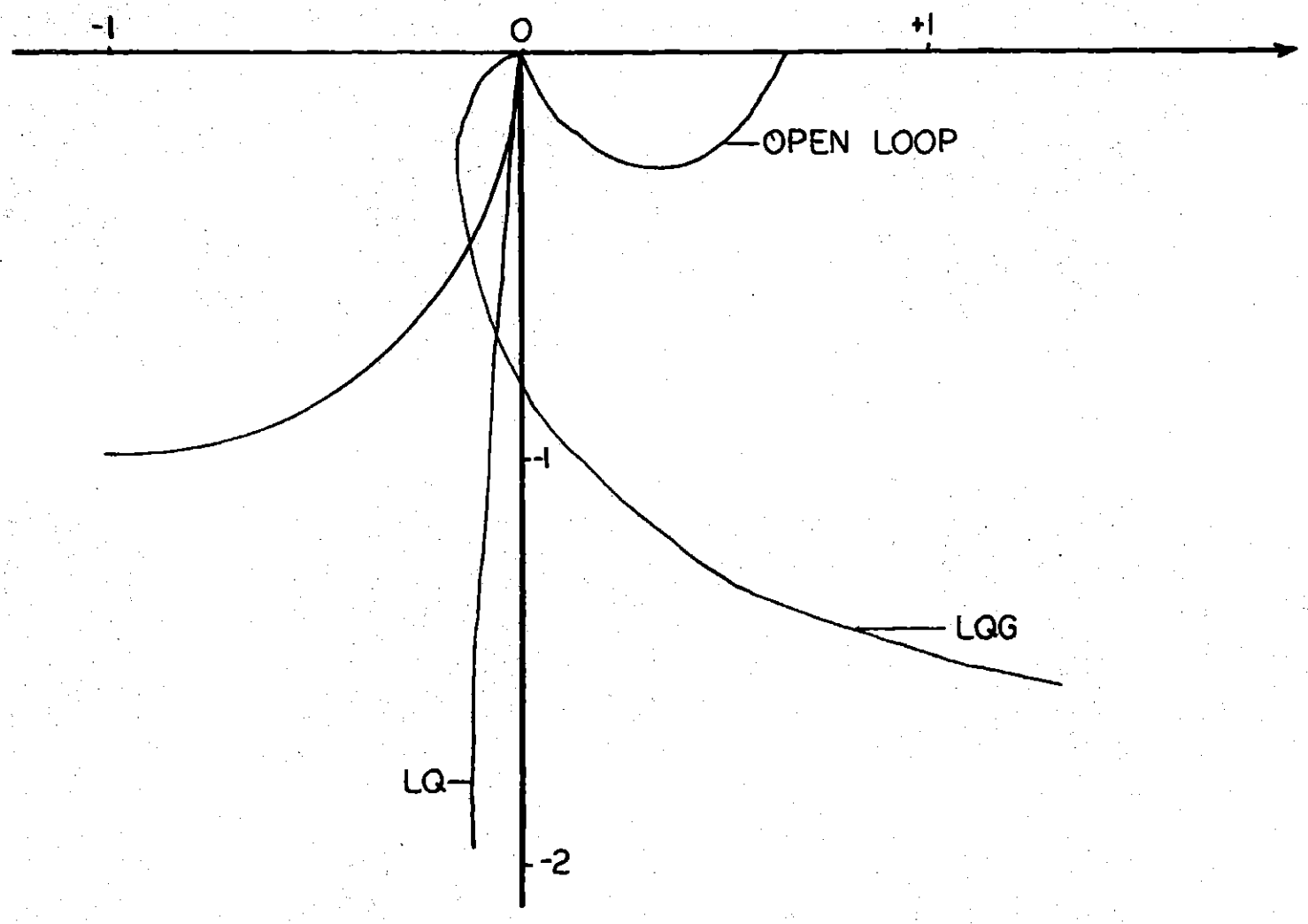

FIGURE 6
NYQUIST DIAGRAM

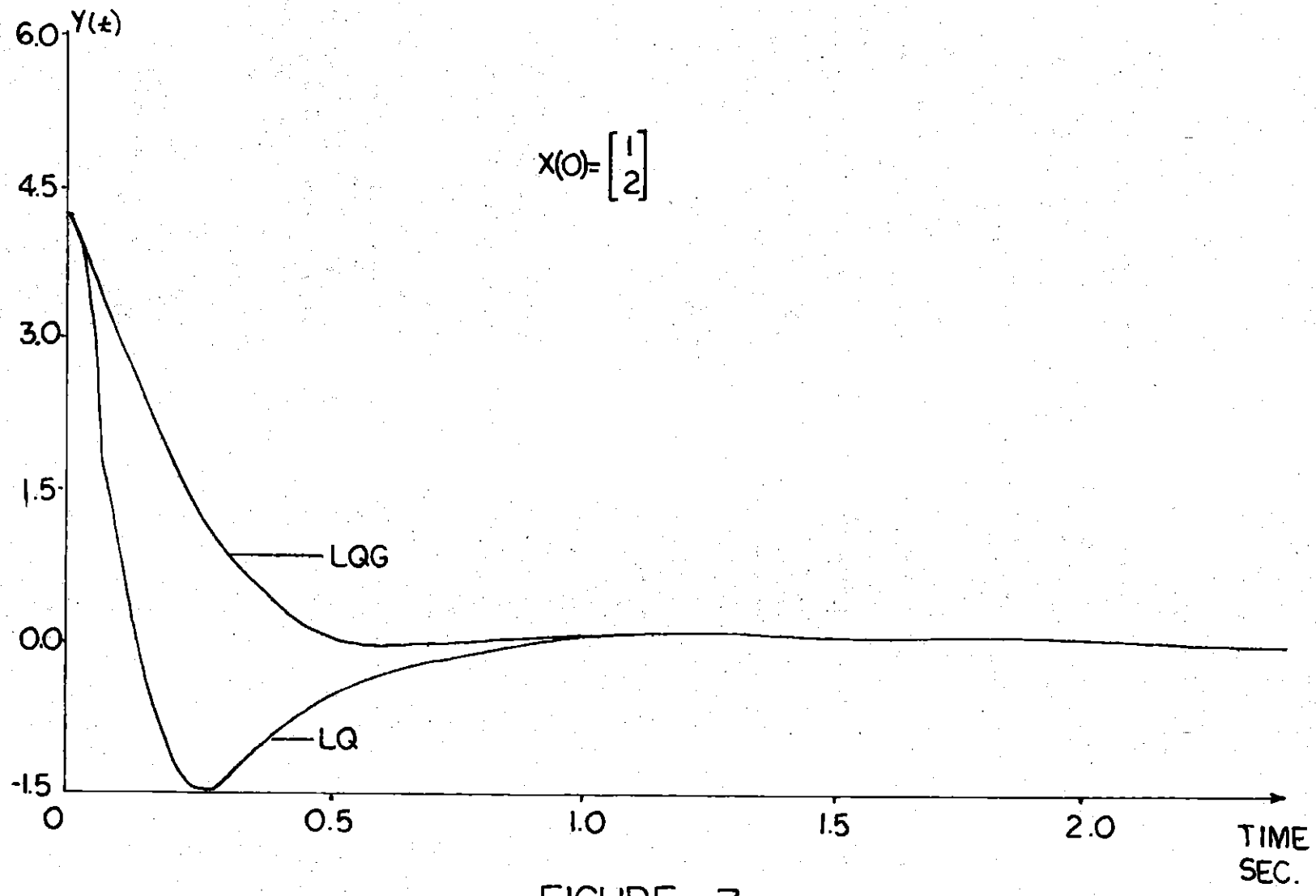

FIGURE 7
TRANSIENT RESPONSE

APPENDIX H

NOTATION

NOTATION

In this thesis the following conventions have been adopted.

A dot over a variable indicates time derivative as in,

$$\dot{m} = \frac{dm}{dt}$$

An underscore and lower case represents a vector ($\underline{x}$). Upper case with underscoring is used to denote matrices. Bibliographic references are indicated in brackets and only one bibliography is included for the entire thesis. The numerical bibliographic order is of no particular significance. Equation numbers are referenced in parenthesis and are consecutive beginning separately with each chapter; (2.3) signifies the third equation in Chapter II.

The following abbreviations and symbols are used consistently throughout this text.

LQ	linear quadratic
LQG	linear quadratic gaussian
kph	kilometers per hour
mph	miles per hour
$\lambda(A)$	eigenvalues of A
$\bar{\sigma}(A)$	maximum singular value of A
$\underline{\sigma}(A)$	minimum singular value of A

$\underline{x}$ vector of engine states (18)

$\underline{u}$ vector of engine inputs (4)

$\underline{y}$ vector of engine outputs (7)

$\underline{u}^*$ LQ control

$\underline{\tilde{u}}$ Nominal control

$$\underline{u} = \begin{bmatrix} \alpha_c \\ E_c \\ F_c \\ S_c \end{bmatrix}$$

α_c throttle command

E_c EGR command

F_c fuel command

S_c spark advance command

$$\underline{y} = \begin{bmatrix} T_b \\ N \\ P_m \\ \alpha_p \\ E_p \\ T_f \\ P_f \end{bmatrix}$$

T_b brake torque

N engine speed

P_m manifold pressure

α_p throttle position

E_p EGR position

T_f filtered torque

P_f filtered manifold pressure

D engine displacement

DF dilution factor $(\dot{m}_{air} + \dot{m}_{EGR})/\dot{m}_{fuel}$

k ratio of specific heats for manifold mixture

P_e	exhaust pressure
P_0	ambient pressure
P_{in}	power in to the engine system
P_{out}	power out of the engine system
Q	higher heating value of fuel
Q	state weighting matrix (clear from context)
r	compression ratio
R	ideal gas constant
R	input weighting matrix (clear from context)
T_e	exhaust temperature
T_m	manifold temperature
T_0	ambient temperature
V_f	characteristic liquid fuel velocity
V_m	intake manifold volume
z_0	characteristic manifold length
k_i	linear model steady state gains
α_i	linear model dynamics (parameters)
Δ	0.020 second sampling interval
α_r	throttle request
$\hat{\underline{x}}$	Kalman filter state estimates

δ	perturbation
ρ_m	manifold mixture density
η	volumetric efficiency
η^*	wide open throttle
η_e	engine efficiency
τ	engine sampling time delay

SELECTED BIBLIOGRAPHY

1. R. Stein, The American Automobile, Random House, New York, 1975.

2. J.F. Cassidy, "Comments on the Engine Control Problem", Electronics Department, GM Research Laboratories, Publication, GMR-2260, October, 1976.

3. J.F. Cassidy, M. Athans, W.H. Lee, "On the Design of Electronic Automotive Engine Controls Using Linear Quadratic Control Theory," Electronics Department, GM Research Laboratories, Report ET-180, December, 1978, (to appear in IEEE Trans. on Auto. Control, 1980).

4. D.J. Dobner, "A Mathematical Engine Model for Development of Dynamic Engine Control", GMR Report EG-159, April, 1979.

5. A.R. Dohner, "Optimal Control Solution of the Automotive Emission-Constrained Minimum Fuel Problem," GM Research Laboratories, Publication, GMR-2751, June, 1978.

6. P.A. Hazell, J.O. Flower, "Discrete Modelling of Spark-Ignition Engines for Control Purposes", International Journal on Control, Vol. 13, No. 4, 625-632, 1971.

7. M.H. Rubin, "Optimal Configuration of a Class of Irreversible Heat Engines. I and II", Physical Review, Vol. 19, No. 3, March, 1979.

8. H.S. Rao, A.I. Cohen, J.A. Tennant, K.L. VanVoorhies, "Engine Control Optimization Via Nonlinear Programming", SAE paper 790177, 1979.

9. J.F. Cassidy, "A Computerized On-Line Approach to Calculating Optimum Engine Calibrations", Electronics Department, GM Research Laboratories, Publication GMR-2286, December, 1976.

10. M. Athans, "The Role of Modern Control Theory for Automotive Engine Control", Laboratory for Information and Decision Systems, MIT, Report ESL-P-836.

11. J.F. Cassidy, "Optimum Engine Control Calibration Studies Via Nonlinear Programming", Electronics Department, GM Research Laboratories, Report ET-165, August, 1978.

12. J.F. Cassidy, "A State Variable Model for Engine Control Studies", Electronics Department, GM Research Laboratories, Report ET-180, December, 1978.

13. L.S. Vora, "Computerized Five Parameter Engine Mapping", Electronics Department, GM Research Laboratories, Publication GMR-22-91-R, February, 1977.

14. A.J. Kotwicki, "A Model for the Effect of Gear Ratio Upon the Frequency Response of the Coupled Automobile-Engine System", Electronics Department, GM Research Laboratories, Report to appear, 1980.

15. J.B. Lewis, J.F. Cassidy, "An Improved State Variable Model for Engine Control Studies", Electronics Department, GM Research Laboratories, Report , March, 1980.

16. M. Tanaka, E. Durbin, "Transient Response of a Carburetor", SAE paper 770046, 1977.

17. J.A. Tennant, R.A. Glacomazzi, J.D. Powell, H.S. Rao, "Development and Validation of Engine Models Via Automated Dynamometer Test", SAE paper 790178, 1979.

18. R.D. Fruechte, A. Kade, "Transfer Function Modelling of a Gasoline Engine and Engine Actuators," Electrical Engineering Department, GM Research Laboratories, Research Memorandum, 4-10-78.

19. G. Stein, N.R. Sandell, Classical and Modern Methods for Control System Design, Notes for subject 6.232, Department of Electrical Engineering and Computer Science, MIT, February, 1980.

20. N.R. Sandell, "Robust Stability of Linear Dynamic Systems with Application to Singular Perturbation Theory," Laboratory for Information and Decision Systems, MIT, Report P-837, August, 1978.

21. G. Stein, "Robust Stability of Linear Systems: Engineering Motivation", Laboratory for Information and Decision Systems, MIT, Report P-901, April, 1979.

22. A.J. Laub, "Robust Stability of Linear Systems - Some Computational Considerations", Laboratory for Information and Decision Systems, MIT, Report R-904, May, 1979.

23. N.R. Sandell, ed. Recent Developments in the Robustness Theory of Multivariable Systems, Laboratory for Information and Decision Systems, MIT, Report R-954, August, 1979.

24. M.G. Safonov, Robustness and Stability Aspects of Stochastic Multivariable Feedback System Design, Laboratory for Information and Decision Systems, MIT, Report R-763.

25. J.C. Doyle, "Robustness Properties of LQG Regulators", IEEE Trans. on Auto. Control, Vol. AC-23, August, 1978.

26. J.C. Doyle and G. Stein, "Robustness with Observers, IEEE Trans. on Auto. Control, Vol. AC-24, August, 1979.

27. M. Safonov and M. Athans, "Gain and Phase Margins for Multiloop LQG Regulators," IEEE Trans. on Auto. Control, Vol. AC-22, April, 1977.

28. R.E. Kalman, "When is a Linear System Optimal?", Trans. ASME Ser. D: J. Basic Eng., Vol. 86, pp. 51-60, 1964.

29. C.H. Harvey and G. Stein, "Quadratic Weights for Asymptotic Regulator Properties", IEEE Trans. on Auto. Control, Vol. AC-23, June, 1978.

30. G. Stein, "Generalized Quadratic Weights for Asymptotic Regulator Properties", IEEE Trans. on Auto. Control, Vol. AC-24, August, 1979.

31. P. Dorato, A.H. Levis, "Optimal Linear Regulators: The Discrete Time Case", IEEE Trans. on Auto. Control, Vol. AC-16, December, 1971.

32. W.H. Lee, M. Athans, D. Castanon, F. Bacchioloni, "Linear Tracking Systems with Applications to Aircraft Control System Design", Laboratory for Information and Decision Systems, MIT, Report R-720, January, 1977.

33. I.M. Horowitz and U. Shaked, "Superiority of Transfer Function over State Variable Methods", IEEE Trans. on Auto. Control, Vol. AC-20, February, 1975.

34. M. Athans and P.L. Falb, Optimal Control, McGraw Hill Book Co., New York, 1966.

35. A.E. Bryson and Y.C. Ho, Applied Optimal Control, Blaisdell, Waltham, Mass., 1969.

36. R. Bellman, Dynamic Programming, Princeton University Press, Princeton, N.J., 1957

37. Jan C. Willems, The Analysis of Feedback Systems, The MIT Press, Cambridge, Mass., 1971.

38. A.H. Jazwinski, Stochastic Processes and Filtering Theory, Academic Press, New York, 1970.

39. H. Kwakernaak and R. Sivan, Linear Optimal Control Systems, J. Wiley and Sons, New York, 1972.

40. B.D.O. Anderson and J.B. Moore, Linear Optimal Control, Prentice Hall, Englewood Cliffs, N.J., 1971.

41. K.J. Astrom, Introduction to Stochastic Control Theory, Academic Press, New York, 1970.

42. A.V. Oppenheim and R.W. Schafer, Digital Signal Processing, Prentice Hall, Englewood Cliffs, N.J., 1975.

43. C.F. Taylor, The Internal Combustion Engine in Theory and Practice, MIT Press, Cambridge, Mass., 1960, 1968.

44. E.M. Estes, quoted in the Boston "Herald American", November 19, 1978.

45. B.C. Kuo, Digital Control Systems, SRL Publishing Company, Champaign, Illinois, 1977.

46. M. Athans, "The Role and Use of the Stochastic Linear-Quadratic-Gaussian Problem in Control System Design", IEEE Trans. on Auto. Control, Vol. AC-16, December, 1971.